MODELING TWO-PHASE PIPE FLOW IN LIQUID LOADING GAS WELLS USING THE CONCEPT OF CHARACTERISTIC VELOCITY

A Dissertation

by

ARDHI HAKIM LUMBAN GAOL

Submitted to the Office of Graduate and Professional Studies of
Texas A&M University
in partial fulfillment of the requirements for the degree of

DOCTOR OF PHILOSOPHY

Chair of Committee,	Peter P. Valkó
Co-Chair of Committee,	Abu Rashid Hasan
Committee Members,	Hamn-Ching Chen
	Kan Wu
Head of Department,	Alfred D. Hill

August 2016

Major Subject: Petroleum Engineering

ABSTRACT

This work focuses on situations of particular significance in natural gas producing wells, when a certain condition brings about drastic liquid content increase, leading to a rich group of phenomena in the field, known as "liquid loading". Under circumstances believed to precede liquid loading, the still steady-state and stable liquid holdup may be several folds larger than the inlet volumetric fraction of the liquid due to partial flow reversal. This leads to increased resistance in the pathway of the produced gas, triggering instability in the coupled well-reservoir system and ultimately causing the end of the natural flow of gas from the reservoir to the surface.

In contrast to the standard models of liquid loading that relate the “onset of liquid loading” to the concept of “critical gas velocity,” we present a new wellbore model that is able to track the most important liquid loading symptom, namely the long-term gradual increase of overall wellbore liquid content and the progression of the strongly related bottomhole pressure.

The new empirical correlation was developed based on the multiphase upward flow measurement in a long vertical pipe. The model is shown to have capability in reproducing various published experimental and vertical gas well data sets with a reasonable accuracy. Additionally, we applied the new wellbore formulation in deviated gas wells affected by both liquid loading situations as well as artificial lift systems.

The new model is a flow-pattern-dependent correlation, hence, convenient to be used for simultaneous multi-well calculations. The derivation is straightforward, while

still able to capture the physics of two-phase conditions. The results indicate that the new wellbore model is suitable to be used in analyzing and diagnosing liquid loading culmination processes. An increased was observed in the liquid content and corresponding flowing bottomhole pressure before gas production became interrupted. Additionally, the new correlation provides a more realistic contribution from each pressure gradient component.

DEDICATION

To my wife, Laskary, for her unconditional love;

To my precious daughters, Abigail and Alexandra, for being my joy;

To my parents and parents-in-law, for their prayers.

ACKNOWLEDGEMENTS

This thesis would not have been possible without the support of many people. I would like to express many thanks with deepest sincerity to my advisor, Dr. Peter Valkó, for his tremendous guidance, understanding, patience, and continuous support throughout the course of this work. I have been incredibly fortunate to have the immense benefit of his broad knowledge.

I would like to acknowledge the support and help of Dr. Rashid Hasan for co-supervising this work and providing valuable comments and suggestions. Also, I would like to thank Dr. Hamn-Ching Chen and Dr. Kan Wu, for taking the time as committee members.

Special thanks go to Pedro Cavalcanti de Sousa and Dr. Paulo Waltrich for the technical help and invaluable discussions. I would also like to thank John Maldonado for all the help and support in my research.

I am thankful to all my friends and Permias TAMU for making my time in College Station a great experience.

NOMENCLATURE

D	Pipe diameter, m
dp/dz	Pressure gradient, Pa/m
f	Friction factor, dimensionless
g	Acceleration because of gravitation, m^2/s
h_l	Liquid holdup, dimensionless
N	Number of well segments, dimensionless
p	Pressure, Pa [psi]
Re	Reynolds number, dimensionless
S	Water salinity, percent
t	Time, day
T	Temperature, ^oF
u_c	Characteristic velocity, m/s
u*	Non-dimensional velocity, dimensionless
x	Gas mass fraction, dimensionless
z	Axial position, m
α	Void fraction, dimensionless
γ	Specific gravity, dimensionless
μ	Viscosity, cp
ρ	Density, kg/m^3
θ	Angle of inclination to the horizontal, radian

σ	Interfacial tension, N/m

Subscripts

A	Acceleration
calc	Calculated
exp	Experiment
F	Friction
G	Gravitation
g	Gas
k	Phase
l	Liquid
res	Reservoir
s	Superficial
th	Tubing head
tp	Two-phase
wf	Well flowing

TABLE OF CONTENTS

LIST OF FIGURES

Page

Page

LIST OF TABLES

Page

CHAPTER I

INTRODUCTION

Statement of the Problem

Recent advances in engineering practices in tight and shale gas field developments enable operators to produce natural gas aggressively. The liquid amount produced to the surface from these wells, either water or condensate, is relatively modest. But even a relatively modest amount of liquid can be detrimental, if it starts to accumulate in the wellbore. In general, at the early stage of production, the higher gas influx from the reservoir is sufficient to carry the liquid out of the well. At some later period in the life of the well, however, the liquid-content in the wellbore will start to increase. Whether the liquid is in dispersed form along the well length or is occupying the bottom of the vertical section as a "column" does not matter, the consequence is the same: the flowing bottomhole pressure increases. In addition to the loss of production rate, the accompanying erratic behavior of the coupled well-reservoir system may cause operational problems and eventually may lead to the end of the natural flow of gas. Liquid loading as the consequence of either production decline or some mechanical failure (or a combination of these factors) brings about productivity penalty and/or increase of operational expenses. As producing unconventional gas plays mature, there is an increased interest in characterizing, modeling and mitigating liquid loading.

The standard models of liquid loading in gas wells relate the "onset of liquid loading" to the concept of "critical gas velocity". As a mechanistic multiphase-flow

concept, the critical gas velocity would be the smallest velocity of the upward flowing gas still providing enough drag to rule out liquid accumulation in the wellbore. The richness of the related phenomena in the gas field, however, comes from the interaction of multiphase-flow in the well and in the reservoir. The concept of critical gas velocity (or rate) that is widely implemented in the industry is in fact misleading, because steady-state upward flow of a gas-liquid mixture can happen at arbitrary low gas velocities, if the inlet boundary condition is constant-rate type. In addition, the actual transient liquid accumulation processes are virtually impossible to reproduce under laboratory conditions. Therefore, transforming laboratory observations directly into onset prediction models – however often it is done – has not lead to major breakthrough in comparison to what the pioneering "critical gas rate" models could already offer.

In unconventional gas plays, enormous number of wells must be drilled and completed overtime to counter the nature of steep production declines. Therefore, well monitoring becomes more challenging than ever and highly practical model is much needed. The ultimate goal of this work is to devise a diagnostic tool by which production engineers can leverage day-to-day production data to effectively forecast and detect gradual increase of liquid content inside the wellbore way before liquid loading phenomena become obvious. The development of such a model also requires comprehensive understanding of multiphase flow system via experimental study in a large facility that is equipped with better measurement techniques.

Objectives

The primary objectives of this work are summarized as follows:

1. Modify the existing experimental facility by implementing a more appropriate liquid holdup measurement technique.
2. Conduct series of experimental runs in which pressure and liquid holdup under a stable two-phase flow are recorded.
3. Investigate the performance of various liquid holdup prediction methods in the presence of partial flow reversal or in the vicinity of liquid loading condition.
4. Investigate the existing frictional pressure drop models to be used in combination with the proposed wellbore liquid content model to determine overall pressure gradient.
5. Develop and validate a new wellbore liquid content model that well-suited to be used in real wells under the influence of liquid loading culmination process.
6. Implement the new wellbore model to investigate the gradual increase of liquid-content and the corresponding flowing bottomhole pressure in the wellbore.

Importance

The onset prediction of liquid loading utilizing solely critical gas velocity concept seems to be out of reach at the present. The liquid loading phenomena is increasingly viewed as a dynamic condition where the interaction between wellbore and reservoir triggers instability and hence cyclical production impairments. However, the coupled simulation of wellbore and reservoir systems is hardly to be performed simultaneously for

many wells because of the significantly small time frame. Therefore, the traditional critical gas velocity correlation is still more favorable due to its applicability.

Despite the improvements in solving coupling wellbore reservoir problem, the ultimate difficulty lies on the lack of wellbore model that has a better predictive capability under the presence of liquid loading situations. Therefore, a simple wellbore model yet satisfactorily captures important physics of a two-phase system is much needed.

For production engineers, the new wellbore model is suitable to be used in day to day basis for monitoring production of both vertical and deviated wells. The wellbore model is expected to provide recognizable signs of liquid loading occurrence in the future (including gradual increase of liquid content and flowing bottomhole pressure). Therefore, necessary remediation actions to prevent further development of liquid loading symptoms can be performed in a timely manner. The new model can also be used in liquid loading modeling effort. Instead of artificially involving critical velocity in determining flow conditions or directions in the wellbore, the new model is truly a wellbore model that delivers all necessary two-phase parameters point to overall pressure loss along the tubing.

Structure of the Dissertation

Chapter II provides details of existing hypothesizes and models commonly leveraged in petroleum industry to predict the occurrence of liquid loading. This chapter also describes the pitfall of most models in capturing the essential feature of liquid loading symptom, which literally is the proliferation of wellbore liquid content. The integrated

wellbore/reservoir models that seemingly deliver more realistic results are actually lack of appropriate wellbore model.

Chapter III presents a more appropriate approach in gathering liquid content data and other corresponding two-phase parameters from a state-of-the-art experimental facility. The experimental results are described in details to further accommodate wellbore model development.

Chapter IV prescribes a new wellbore liquid content correlation. The steps taken in deriving the new model is explained thoroughly. The new model was initially targeted to be in a simple form, referring to an annular void fraction model of Cioncolini and Thome (2012) or a flow-pattern dependent model of Gray (1974). The performances of several well-known correlations in reproducing our measurement results are also presented. Additionally, some existing frictional pressure drop models were investigated and the one with acceptable accuracy and higher degree of applicability was selected. The new model (consisting of a liquid content model and a compatible frictional pressure drop model) is generalized to handle real problems, including vertical and deviated wells.

Chapter V describes the process to validate the new model against both experimental and field data sets. First, the model is compared against several experimental data sets available in the literature. The data sets cover wider ranges of flow-loop dimension, gas and liquid flow rates, as well as the measured holdup. The predictive capability of several existing correlations are also presented alongside the proposed model. Second, field data sets consist of vertical wells whereby liquid loading was not reported

are selected. The new model then used to predict the flowing bottomhole pressure in comparison with other widely accepted models in the petroleum industry.

Chapter VI presents the application of the new wellbore model in predicting the progression of liquid content inside the tubing, way before liquid loading symptoms become obvious. First, we applied our model to reproduce the measured values of flowing bottomhole pressure of 22 gas wells in comparison with the model of Beggs and Brill (1973) and Gray (1974). Then, two wells representing "low producer" and "high producer" were selected to illustrate the applicability of our model. The increasing liquid content before shut-in periods due to liquid loading was identified to be influential in determining the overall pressure gradient hence the flowing bottomhole pressure.

Chapter VII gives a summary of this study and suggests future directions in modeling liquid loading in specific and multiphase flow in general.

CHAPTER II

LITERATURE REVIEW

Introduction

Gas producing wells are experiencing persistent production decline during their lifetime. The decreasing gas production is subject to the nature of reservoir depletion. However, a greater than expected production decline often follows the already justified reservoir pressure depletion, especially when multiphase mixture in the wellbore has relatively high liquid to gas ratio that exceeds permissible liquid content limit in the well. Gas production profile deviates from stable to unstable indicated by erratic and oscillating behaviors of surface measurements of pressure and flow rate. This phenomena, namely "liquid loading", is induced by dynamic interaction between multiphase flow in the reservoir and multiphase flow in the wellbore. The production impairment situation is also not sustainable and may ultimately lead to the end life of the well if appropriate prevention or remediation actions are not delivered in timely manner.

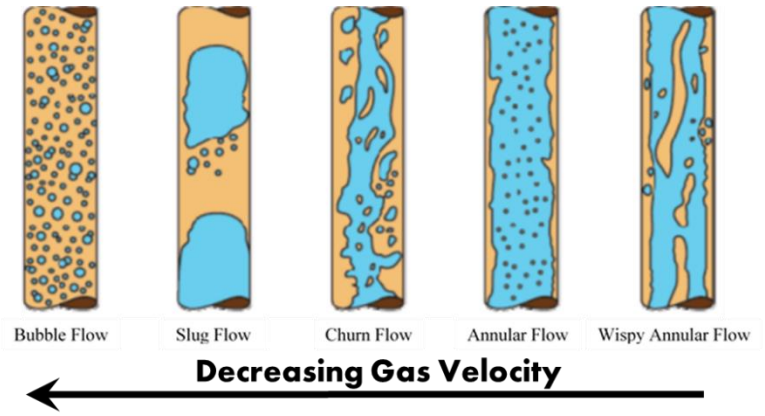

Fig. 2.1—Flow regimes in vertical upward two phase flow according to Hewitt (2012).

Two-phase liquid holdup has always been linked to the prevailing flow regimes in the wellbore. One possible classification of possible flow regimes is shown on **Fig. 2.1** according to Hewitt (2012). In a gas producing well various flow patterns may exist along the wellbore. In general, gas well with high initial production will first experience annular flow where liquid film flows upwards adjacent to the tube wall and gas flows in the center carrying liquid droplets. The forces exerted by the moving gas core cause the upward movement of liquid film that is against gravity. As gas production rate declines further, several flow regimes can co-exist depending on the variation of in-situ conditions along the production tubing. For instance, the flow regime near the bottom of the wellbore can be the slug flow while near the wellhead is being annular flow. This observation is of importance especially in analyzing the occurrence of liquid loading and in modeling effort to better characterize liquid loading culmination process.

In the two-phase system, gas phase acts as the primary driver of the upward mixture flow, continuously provides drag forces to accelerate the liquid upward. Gas rises at the center of the tube much faster than liquid because of two reasons: i) the density difference between phases and ii) the non-uniform velocity distribution existing even in single-phase gas flow. Liquid phase can be in the form of droplets residing in the gas core, film covering the tube wall, and liquid slug appearing in an intermittent fashion. In the context of mechanistic multiphase flow models, liquid loading is commonly correlated to the inability of the gas to provide the necessary amount of drag to force the liquid out of the wellbore.

During the culmination process of liquid loading, the amount of liquid content in the wellbore is progressively increasing while the gas rate is decreasing. The impact to the flowing bottomhole pressure is significant, if the overall pressure drop along the wellbore is dominated by the gravitational component. The increased flowing bottomhole pressure affects the gas and liquid influxes from the reservoir, triggering instability of the inlet boundary conditions.

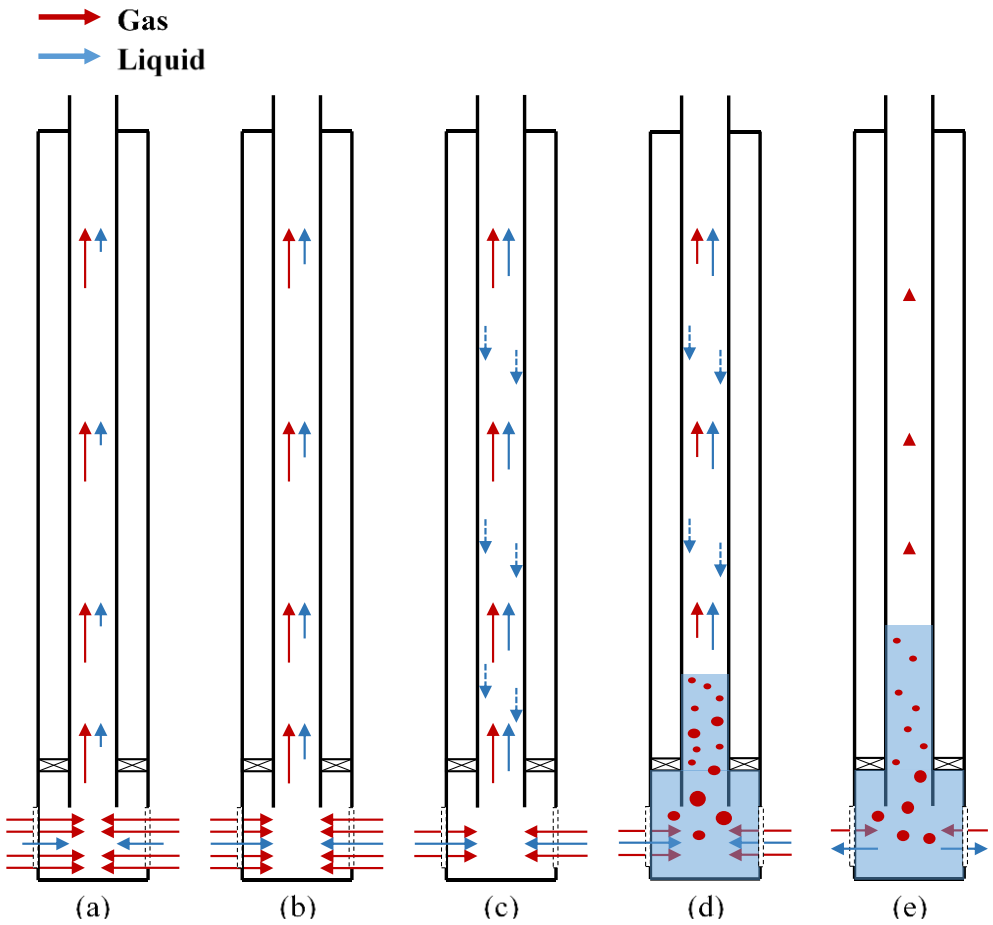

Fig. 2.2—Liquid loading illustration in a gas well. (a) Early production with high gas rate and clearly annular flow; (b) Early production with high gas rate and clearly annular flow despite very high liquid flow rate due to fracturing fluid flowback (in the case of unconventional wells); (c) Annular to churn flow transition with partial liquid film reversal and higher wellbore liquid content; (d) Various flow regimes take place along the tubing, partial flow reversal at top part of the tubing, highest liquid content at the bottom; (e) *Metastable* condition.

A simplified illustration of the liquid loading process is shown in **Fig. 2.2**. At the early production stage, high gas mass influx from the reservoir to the wellbore be in effect. The relatively small amount of liquid is also co-produced. In the case of unconventional

gas plays (shale and tight plays), very high initial liquid production can last for days or weeks indicating fracturing fluid flow-back. In general, the well is able to cope with this condition if the reservoir pressure is adequate to outmatch the backpressure from the wellbore. As reservoir pressure and gas production decline, the flow pattern shifts from annular to churn flow. Waltrich (2012) observed the oscillatory motion of liquid film pointing to the presence of churn flow, where partial flow reversal of liquid film occurs. This condition contributes to a higher wellbore liquid content. The liquid content also becomes greater as additional liquid enters the wellbore or more liquid formed as the result of gas condensation process. In addition, various flow patterns will also exist in the well, and hence significant variation of local liquid content along the. Highest and lowest liquid content are typically located at the bottom of the well and near the wellhead, respectively, depending on the wellbore geometry.

The increasing liquid content leads to a higher flowing bottomhole pressure and penalizes drawdown between the reservoir and wellbore. It will significantly reduce gas influx and may create production instability. Indeed, the well can still be producing for a long period of time under significantly reduced rate. This condition is known as *metastable* condition. Dousi et al. (2006) correlated this condition to the equilibrium between the amount of liquid flowing downward and the liquid re-injected into the formation. However, at later stage the well may die if backpressure outmatches near-wellbore pressure by significant margin given the proliferated liquid content in the well.

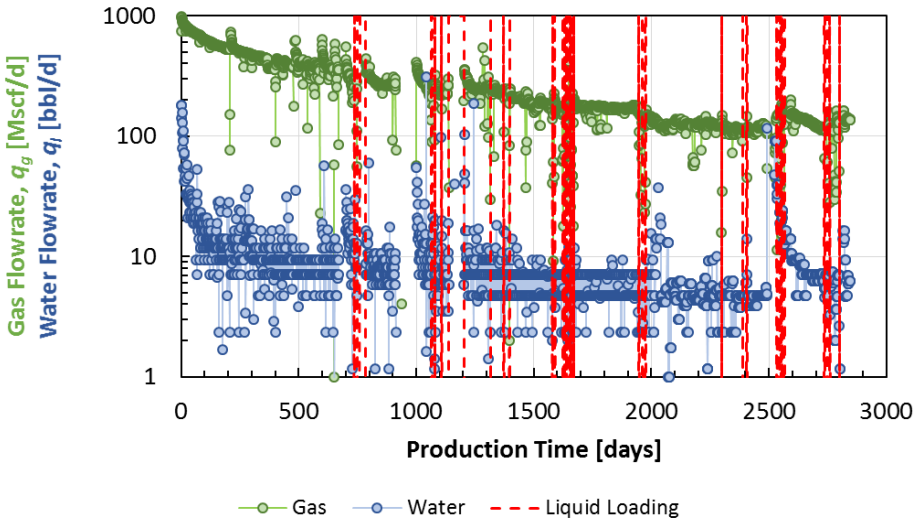

Fig. 2.3—Surface measurement results of gas and water production rates and observable liquid loading sequences of a gas well.

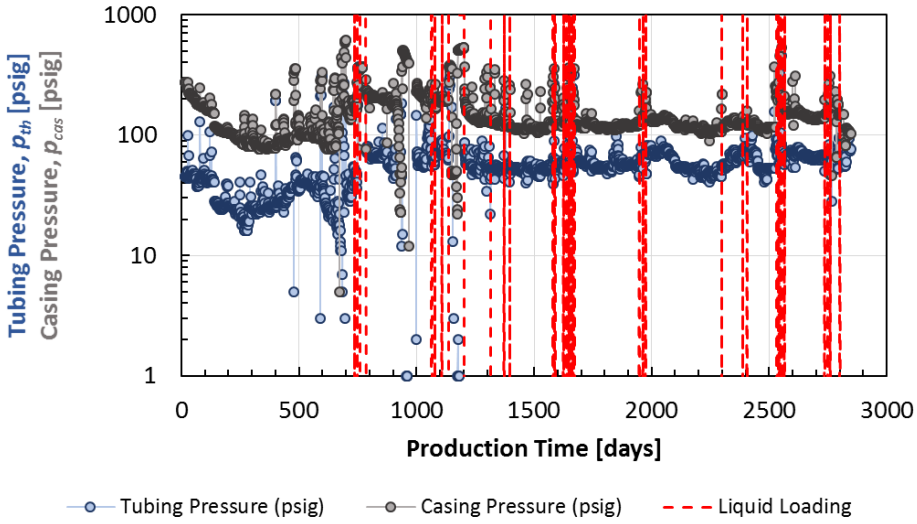

Fig. 2.4—Surface measurement of tubing and casing pressures and observable liquid loading sequences of a gas well.

The liquid loading symptoms are commonly observed by analyzing surface measurement results. The symptoms include erratic production profile, steeper production profile, divergence in tubing and casing pressures, and the existence of sluggish flow represented by very large pressure surge observable from high frequency acoustic measuring device (Lea et al. 2003). The typical production and surface pressures profiles of a gas well experiencing cyclical liquid loading sequences are illustrated by **Figs. 2.3** and **2.4**.

Liquid loading issue is considered to be more important at the present where natural gas price is fluctuating at its multi-year low. Liquid loading problems may significantly increase unanticipated production cost. In addition, as producing unconventional gas plays mature, there is an increased interest in characterizing, modeling, and mitigating liquid loading.

The Concept of Critical Gas Velocity in Predicting the Onset of Liquid Loading

The seminal work of Turner et al. (1969) postulated that there is a critical gas velocity below which liquid loading sets on. Then they provided two models. The first model states that the gas velocity has to exceed the free fall terminal velocity of the droplet to assure removal of the liquid from the wellbore. The second model which had been initially described by Dukler (1960) and Hewitt (1961) points to minimum gas velocity necessary to move the liquid film upward at the pipe wall. Using the two points of view, Turner et al. (1969) derived two possible functional forms for the critical gas velocity, one based on the falling droplet and one based on the falling film concepts. Then they analyzed

wellhead data available from 106 gas producing wells and suggested a critical velocity correlation based on the falling droplet concept. The second functional form (based on the film reversal concept) was found to be less effective to describe the particular dataset. The success of the Turner et al. (1969) correlation have been interpreted by some authors as proof of the criticality of the falling droplet concept.

The Turner et al. (1969) correlation in consistent unit is expressed as,

$$u_{crit,\,\text{Turner}} = 5.46\left[\frac{\sigma\left(\rho_l - \rho_g\right)}{\rho_g^2}\right]^{0.25} \tag{2.1}$$

where ρ_g and ρ_l are the gas and liquid densities, respectively, and σ is the interfacial tension. The coefficient of **Eq. 2.1** represents the increase of 20% of its original value to match their database and to ensure the effectiveness of liquid unloading process. In the rest of this chapter, the Turner et al. (1969) approach will be referred to as the Turner model.

Various modification of the Turner model have been proposed to better match numerous sets of field data. Coleman et al. (1991) underlined the importance of wellbore diameter and pressure variation to the onset of liquid loading. Based on their dataset, they proposed that the 20% adjustment of Turner correlation is not necessary. However, Nosseir et al. (2000) quite contradictorily came with an answer for the necessity of the adjustment made by Turner. It is applied to better match Turner dataset due to different prevailing flow regimes leading to drag coefficient variation.

Guo et al. (2006) introduced kinetic-based model to determine the critical velocity that is generally higher than the critical velocity of Turner. They also indicated the variable controling liquid loading is of pivotal at the bottomhole location rather than at the wellhead. Consequently, Sutton et al. (2010) suggested to evaluate the Turner's critical velocity at downhole conditions if the wellhead pressure is less than 1000 psia.

Zhou and Yuan (2010) proposed an empirical model which takes into account the effect of liquid holdup. They pointed out that critical rate should be increasing if the liquid holdup is above the threshold value. This actually shed light into our hypothesis that the alleviation of wellbore liquid content should drive liquid loading symptoms. However, Zhou and Yuan (2010) formulated liquid holdup using an assumption of homogeneous two-phase flow where the slip between phases is neglected. Additionally, the liquid holdup only represented the secondary factor controlling the mechanism of liquid loading, while critical rate of Turner was still considered as the primary factor.

Shi et al. (2016) emphasized liquid loading situation in multi-fractured horizontal wells. They underlined the liquid droplet deformation as a function of its size. Liquid droplet shape and size were investigated through series of two-phase experimental study with various pipe inclination angles. The height of the droplet was presented as a strong function of the width. Most of the time the height was observed significantly less than the width. As the original Turner correlation only considers spherical shape (that is the ratio of height to width equals to one), therefore, an empirical formulation was proposed to be embedded in the original Turner correlation to take into account various droplet shapes.

In addition, the formulation was expanded to accommodate calculation in deviated as well as horizontal pipes.

Turner's family of correlations implicitly assume liquid loading caused by dispersed phase. However, van't Westende et al. (2007) found that the droplet diameter postulated by Turner et al. (1969) is unphysical and direct evidence of falling droplets concept is not available. They observed that most of the time the droplets move upward. Their experimental results indicate that during the annular-churn transition the liquid-film becomes unstable because of the reduced interfacial shear from the gas side, and liquid-film reversal occurs. Indeed, the boundaries between flow patterns can be unpredictable because they may depend on the minor features of the flow, such as the entrance conditions and disturbance caused by non-uniform pipe roughness. Therefore, predicting the onset of liquid loading based solely on flow pattern boundaries is inadequate to provide a distinctive line between "loaded" and "not loaded", but more poorly describing the transition zone.

Most recent experimental work in vertical or deviated pipes tends to support the importance of liquid-film reversal. Yuan et al. (2013) conducted two-phase experimental study in a 17.5-m long and 76.2-mm ID vertical and inclined pipes. They proposed the onset of liquid loading to be at the condition where minimum pressure gradient is reached. This particular condition coincides with the transition from fully co-current annular flow to partially co-current annular flow, or known as churn flow.

Nowadays, the tubing size and inclination are varied widely depending on the location of particular gas field. Bigger pipe is commonly used at deep offshore gas field

with very high production rate. Smaller, deviating, and/or horizontal pipe is used for producing gas from unconventional reservoir. Therefore, there is an increased interest in mitigating the effects of pipe size and inclination to the mechanics of liquid loading.

Li et al. (2014) developed a mechanistic model to calculate critical gas rate based on the observation of liquid film variation across the pipe circumference as a function of pipe inclination. Relatively similar model was also proposed by Luo et al. (2014). Later, Skopich et al. (2015) investigated the effect of pipe diameter on the initiation of liquid loading. They performed experimental study in 51-mm and 102-mm ID pipes. Critical flow rate was found higher for the smaller pipe.

Most of the modified correlations described above were also applied to Turner's original data. Some authors could then provide equally convincing modified Turner type correlations and correlations based on the falling film concept. It also shows that in the petroleum engineering literature both concepts are increasingly viewed as a mechanistic condition. In other words, it is taken at face value that at smaller gas velocities steady-state operation is not possible. In contrast, laboratory experiments are routinely done at orders of magnitude less gas velocities, and the liquid is still transported upward in steady-state. The particular steady-state is, however, very different from the higher gas velocity steady-states in one respect: the liquid holdup is very large compared to the inlet fraction of the liquid.

In addition, while both concepts are formulated in the language of multiphase flow, the authors use them only as starting point for developing a critical rate correlation, where the actual choice of the hypothesis to accept and the numerical constant are both decided

upon using data solely from actual gas producing wells (not from laboratory observations). In our opinion this underlines the fact that the terms "liquid loading" and "critical gas rate" cannot be considered narrowly as mechanistic multiphase flow concepts. Indeed, the richness of the related phenomena in the gas field comes from the interaction of multi-phase flow in the well and in the underlying porous media. The actual phenomena of interest during "liquid loading" are virtually impossible to reproduce under laboratory conditions. This fact contradicts the claims by most researchers on their ability in visualizing and analyzing liquid loading via experimental study.

The Integrated Wellbore-Reservoir Model

Because the actual liquid loading phenomena in the field evolves as the result of the dynamic interaction between reservoir and wellbore, dynamically applying quasi steady-state nodal analysis or establishing transient inflow-outflow coupling may provide more realistic results and deeper insight.

The model of Lea et al. (2003) utilizes the conventional concept of steady-state nodal analysis by analyzing the combined inflow performance from the reservoir (IPR) and wellbore flow performance. The intersection between two curves illustrated on **Fig. 2.5** indicating the operating flow rate of the well contributed by a certain pressure drop at the point of interest (the nodal point is typically located at the bottom of the well where reservoir and wellbore meets.) Lea et al. (2003) postulated that liquid loading should occur if the well undergoes unstable operating condition, where the operating point is to the left of minimum pressure of the wellbore performance curve. In opposition to that, stable

operating point at the right side of the minimum pressure indicates that liquid loading symptoms do not take place.

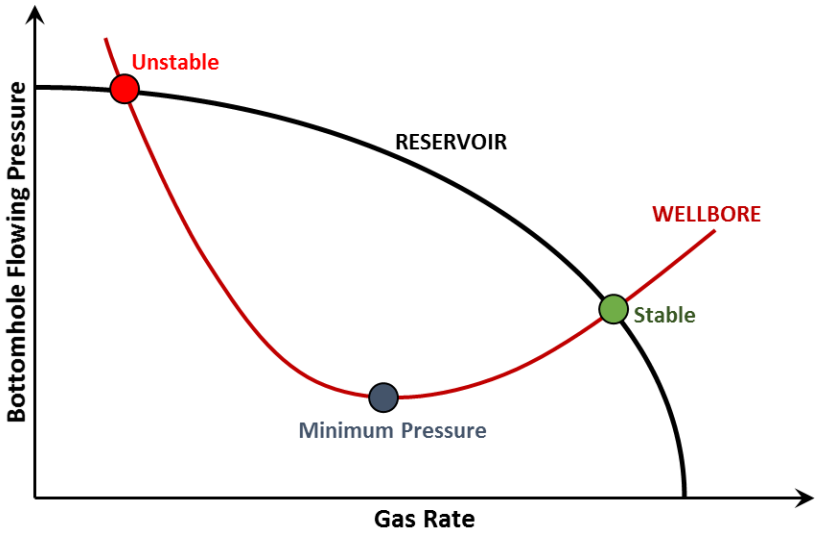

Fig. 2.5—Nodal analysis used to predict the onset of liquid loading (Lea and Nickens 2004).

The dynamic interaction between near wellbore reservoir and wellbore is also increasingly viewed as a transient feature. The rigorous model of liquid loading, therefore, must consider a very small timeframe because the boundary conditions (in this case is bottomhole conditions) are continuously changing. Even the smallest change will significantly affecting all other parameters involved in multiphase flow in the reservoir as well as multiphase flow in the wellbore.

Dousi et al. (2006) came up first with a numerical solution for coupling steady-state models of well and reservoir system. They investigated the occurrence of *metastable*

condition where gas wells experiencing reduced but stable gas flow rate that is less than the critical value of Turner model. This situation was correlated to the possibility of having different production and injection points at the bottom of the well. The liquid column inside the wellbore yields backpressure to the injection point and liquid flow to the reservoir is possible if the backpressure outmatches reservoir pressure. The height of the liquid column is controlled by the underlying gas flow rate (that is coming from the production point) driven by the drawdown between reservoir and wellbore at the corresponding production location. However, this dynamic height of liquid column is still primarily determined by Turner criterion, where it simply increases if the gas velocity is less than the critical velocity, or remains the same if gas velocity is higher than the critical velocity.

Numerous efforts to simulate the interaction between reservoir and wellbore were also performed by various authors (Chupin et al. 2007; Gool and Currie 2008; Hu et al. 2010; Veeken and Belfroid 2011; Limpasurat et al. 2015). The first group of these models still heavily relied on the Turner model to represent the flow situation in the wellbore. In effect, the Turner correlation was used to switch between steady-state upward flow of the liquid and no upward flow of the liquid. In other words, the critical velocity was considered as an actual mechanistic limit in flow simulation (in contrast to the original intention of Turner et al.)

The second group did not used the "critical velocity" concept. The study of Limpasurat et al. (2015) indicated the primary obstacle to successfully simulating liquid-loading phenomenon: the lack of tools to predict the actual liquid content in the wellbore.

The Necessity of New Liquid Content Model

Upward vertical gas-liquid flow behavior depends strongly on the in-situ volumetric fraction of the liquid phase. Due to gravity, the in-situ liquid volume fraction (h_l) is always larger than the inlet volume fraction (and hence often referred to simply as "liquid holdup".) Predicting holdup from a mechanistic model based strictly on first principles seems to be out of reach at present. However, a great number of empirical models have been proposed, often separately, for flow pattern, void fraction ($1 - h_l$), and frictional pressure drop, possessing an impressive combination of simplicity and predictive capability.

Cioncolini and Thome (2012) presented a new void fraction prediction method specifically for vertical annular two-phase flow. This method is simpler than most of the previously suggested correlations. It is based on a large data-bank of annular flow in circular tubes. The method provides reliable void fractions, covering macro-scale and micro-scale channels, as well as adiabatic and evaporating two-phase flow conditions. However, its suggested region of applicability is restricted in the sense that the flow cannot be affected by partial flow reversal.

As mentioned before that in annular flow part of the liquid travels as a film on the pipe walls with the rest being conveyed as droplets in the gas core. In "clear" annular flow the local velocity of liquid may vary with location, but its direction is always upward. For a fixed liquid rate, annular flow transits to churn flow as the gas rate is decreased. Levy (1999) describes annular flow near its transition to churn flow as unsteady, disturbed by flooding waves. However, in the words of Azzopardi (2008): "there is not a consensus

about the nature of churn flow." It is recognized that there are large structures often called "huge waves" present, periodically interrupting the continuity of the gas core and the wall covering liquid film. The huge waves carry most of the liquid upward, and between them the liquid film may move downward "thus giving the strong impression of oscillation". At even lower gas rates, the essentially uni-directional upward movement of the liquid is re-established when the flow regime transits to slug flow.

Within the oil and gas industry the annular to churn flow-pattern transition is of special significance because it leads to increased resistance in the path-way of the produced gas, triggering instability in the coupled well-reservoir system and ultimately causing the end of the natural flow of gas from the reservoir.

Liquid holdup despite its importance in characterizing multiphase flow is impractical to be measured from real gas wells. Therefore, production engineers commonly utilize the readily available correlations to quantify liquid holdup and hence the strongly related flowing bottomhole pressure. However, most existing liquid holdup correlations were generally derived from gas well data sets or experimental data sets gathered from limited length test section.

For the first case, liquid holdup is derived by accepting components defining total pressure gradient including gravitational, frictional, and accelerational pressure gradients. The frictional gradient is theoretically predicted by using standard flow correlations which consider flow condition (laminar-turbulent) as well as pipe roughness. Accelerational gradient most of the time can be neglected depending on the flow situation. Then, liquid holdup can be calculated. Deriving liquid holdup model using this concept seems to bring

a lot of uncertainties, and therefore, many researchers have offered various solutions via experimental studies. However, only a small fraction of oil and gas experimental facility in the world dedicated for this purpose. Additionally, most of these facilities are not equipped with necessary devices to measure holdup affected by partial flow reversal more accurately, or existing flow loops do not have enough dimension to allow multiphase flow to be fully developed beforehand.

As far as the more fundamental multiphase literature is considered, the co-current upward flow of gas and liquid already affected by partial flow reversal seems to be a grey area between annular flow studies and counter-current flow limitation studies. Traditionally, researchers either attempt to exclude such conditions when establishing void-fraction/holdup correlations as in the case of Cioncolini and Thome (2012) or focus on conditions allowing/excluding counter-current flow.

One of the difficulties regarding this grey area is associated with the fact that studying churn flow requires extremely long tubes Wallis (1969). Waltrich et al. (2013) observed continuing two-phase flow development as far from entrance as $L/D = 500$, especially for low liquid mass fluxes. These observations are in agreement with the experimental results reported by Kaji and Azzopardi (2010). Most existing liquid holdup prediction methods were derived from experimental measurements conducted in relatively short tubes ($L/D \ll 500$), so it is not surprising that some predictions might under/overestimate actual values by an order of magnitude in cases when partial flow reversal happens in the liquid.

Due to the rarity of measurements in long vertical tube and the restrictions on available correlations, it is still desirable to conduct experiments in the partial flow reversal affected region and develop new predictive methods. In addition, most recent experimental works illustrated that existing wellbore models have difficulties in reproducing observed liquid holdup in the vicinity of ”critical” conditions. Yuan et al. (2013) showed the TUFFP unified model (Zhang et al. 2003a, b) under-predicts liquid holdup and hence under-predicts the overall pressure gradient. Guner et al. (2015) observed that the existing liquid holdup prediction methods including the correlation of Beggs and Brill (1973), TUFFP unified model (Zhang et al. 2003a, b), as well as the commercial transient two-fluid model OLGA (Bendiksen et al. 1991) could reproduce experimental liquid-holdups only with very large errors. Skopich et al. (2015) also showed the discrepancy between measured liquid holdup and the mechanistic-model of Ansari et al. (1994).

Conclusion

Although time and effort have been invested to examine the underlying mechanism behind liquid loading, either experimentally or numerically, the availability of straight-forward and highly applicable diagnostic tools is limited. Therefore, the original formulation of Turner et al. (1969) is still the primary choice and in view of other uncertainties is still competitive in its predictive power. However, it is crucial to have a model that can help to interpret “warning signs” before the actual liquid-loading problem

becomes apparent. In this work we focus on the realistic modeling of the overall liquid content of the wellbore.

In our approach the concept of critical velocity is not used as a mechanistic limit between two types of behavior, because such sharp limit cannot be observed in the laboratory. Rather, we consider the Turner et al. (1969) correlation and its alternatives, as an appropriate scaling for gas velocity inside a holdup correlation. In this approach the primary interest is not in predicting the "onset" of a different dynamic behavior, rather to describe liquid holdup as a smoothly varying function of the flow conditions.

CHAPTER III

EXPERIMENTAL STUDY OF TWO-PHASE SYSTEM AFFECTED BY PARTIAL FLOW REVERSAL*

Introduction

The original aim of this study was to develop a new diagnostic tool to track the behavior of wellbore liquid content during liquid loading culmination process. The new model must have a higher degree of applicability in real gas well problems such that it can be used by production engineers in daily basis. Experimental study then has to be tailored accordingly in order to generate better data sets that can be used to derive an empirical correlation not only in the simplest form, but truly represents the actual phenomena.

This chapter provides details of the large scale flow loop utilized in this study which was originally designed by Fernandez et al. (2010) and developed by Waltrich (2012). The experimental facility (namely TowerLAB) accommodates one of the longest (tallest) flow loop in the world according to Fernandez et al. (2010).

* Part of this chapter is reprinted with permission from "Liquid holdup correlation for conditions affected by partial flow reversal" by Lumban-Gaol, A. and Valkó, P.P., 2014. *International Journal of Multiphase Flow*, 6, 149-159 Copyright 2014 by Elsevier.

The significant length to diameter ratio (L/D) of more than 500 was proven crucial in delivering fully developed flow. Indeed, the large L/D can also be attained by using shorter pipe with very small diameter. However, the pipe diameter which commonly used in gas field is always more preferred. Several researchers have also shown the importance of pipe diameter in determining the onset of liquid loading.

Experimental Flow Loop

The experimental apparatus consisted of air and water supply systems and tubular test section made of transparent PVC pipe with inside diameter (ID) of 48 mm and length of 42 m. The length is described as the distance between inlet and outlet locations. Therefore, the L/D of this flow loop is around 875. Schematic diagram of the experimental facility is shown in **Fig. 3.1**.

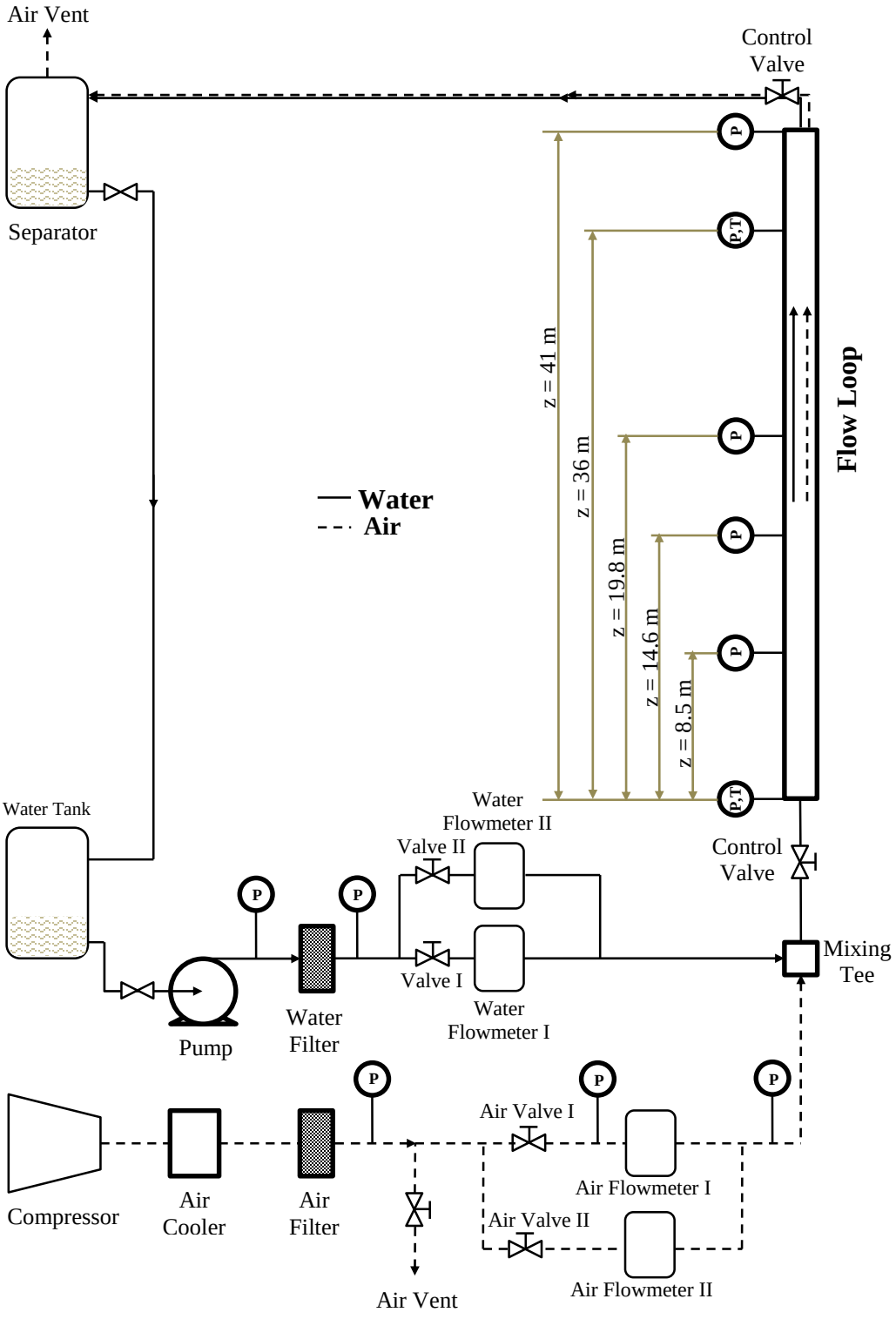

Fig. 3.1—Schematic diagram of 42-m long, 48-mm ID vertical flow loop.

Table 3.1—Comparison of flow loop dimensions.

	Fluids	D (mm)	L (m)	L/D	(1)
Present Study	Air – Water	48.6	42	864	SCV
Anderson and Mantzouranis (1960)	Air – Water	10.7	1.3	118	QCV
Hall-Taylor et al. (1963)	Air – Water	31.8	6.7	211	FT
Nguyen and Spedding (1977)	Air – Water	45.4	2.0	44	QCV
Oddie et al. (2003)	Air – Water	152.0	10.9	72	ND; CP; QCV
Kaji and Azzopardi (2010)	Air – Water	19.0	5.7	300	CP
Godbole et al. (2011)	Air – Water	12.7	2.2	173	QCV
Alamu (2012)	Air – Water	19.0	7	368	LD
Liu (2014)	Air – Water	40.0	6.0	150	QCV

(1) Holdup measuring technique: CP = capacitance probe; FT = annular film thickness; LD = laser diffraction; ND = nuclear densitometer; QCV = quick closing valve; SCV = simultaneously closing valve.

A comparison of the large-scale flow loop with several experimental facilities reported in some literatures is presented in **Table 3.1**, where L/D is the non-dimensional distance between inlet and outlet. The key advantage of our loop is the large L/D ratio, which enables capturing axial development of the flow regime. The main disadvantages are: limitations on maximum pressure and on the type of the liquid and gas. The maximum operating pressure is 1.4 MPa and only air/water flows can be studied in this flow loop.

The water is pumped from the water tank to the flow loop by utilizing centrifugal pump. Air is fed to the flow loop using a compressor which can deliver air mass flow rate up to 600 kg/hr. Two water flow meters (Coriolis mass flow meters) are provided to accommodate wide range of water rates. One of them is able to measure water mass rate as low as 10 kg/hr with reasonable accuracy. This particular device is important in resembling the actual phenomena in gas well where gas to liquid ratio is very high. Similarly, two air flow meters are also provided consisting of vortex and Coriolis flow meters.

Because the size of this flow loop, the absolute pressures were measured at several vertical locations, corresponding to z/D = 0, 189, 419, 671, 817. The variations of fluid properties and velocities along the tube then can be captured. Originally, local liquid holdup was measured at several tube locations relying on two-wire conductivity probes. We augmented the flow loop with the capability of measuring the overall holdup by the volumetric method, using simultaneously closing valves. The details of these two type of holdup measurements will be discussed later in this chapter.

All of our experiments were conducted in low pressure system. The outlet valve at the very top of the test section was left fully open, and thus, the outlet pressure was set at atmospheric condition. The underlying system pressure is extremely important in determining the holdup and pressure gradient. However, in this study the key emphasize is more on the holdup measurement and model development. Moreover, in chapter VI we will show the reliability of our model in predicting holdup and pressure loss for wider range of system pressure.

The facility also equipped with visualization system through four cameras located at different locations. The intention of using these cameras was to capture synchronized figures and videos to investigate the axial behavior of the two-phase flow. Additionally, state-of-the-art data acquisition and control system were also implemented enabling user to monitor and control all experimental parameters and to record signals from all sensors attached to the system with various sampling rates. Further details about the experimental description can be found in the dissertation of Waltrich (2012).

Liquid Holdup Measurement Technique

Initially, the concept of conductivity sensors (illustrated in **Fig. 3.2)** was implemented in TowerLAB to quantify the in-situ cross sectional liquid holdup. The sensors are located at three different locations. The two-wire conductivity probes read instantaneous electrical conductance proportional to the amount of liquid between the probes. Time averaging of the probe readings during steady-state period provides an approximation of the local film thickness. However, the amount of water travelling in the form of entrained liquid droplets is not measured directly, it is determined from an empirical correlation proposed by Barbosa Jr et al. (2002).

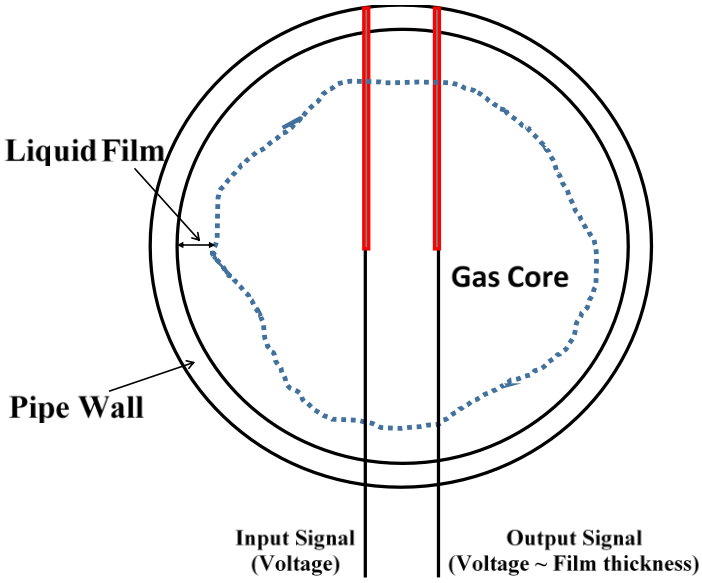

Fig. 3.2—Two-wire conductivity probes used to measure in-situ liquid holdup.

Waltrich et al. (2013) found that liquid holdup exhibited significant axial variation at all monitoring locations, especially for higher liquid mass fluxes. The fully developed churn flow was observed at the location where $z/D > 500$ for low liquid mass flux. In fact, we found that this axial variation of liquid holdup (or liquid content) for low liquid mass flux was also significant concerning the underlying implementation of holdup measurement technique.

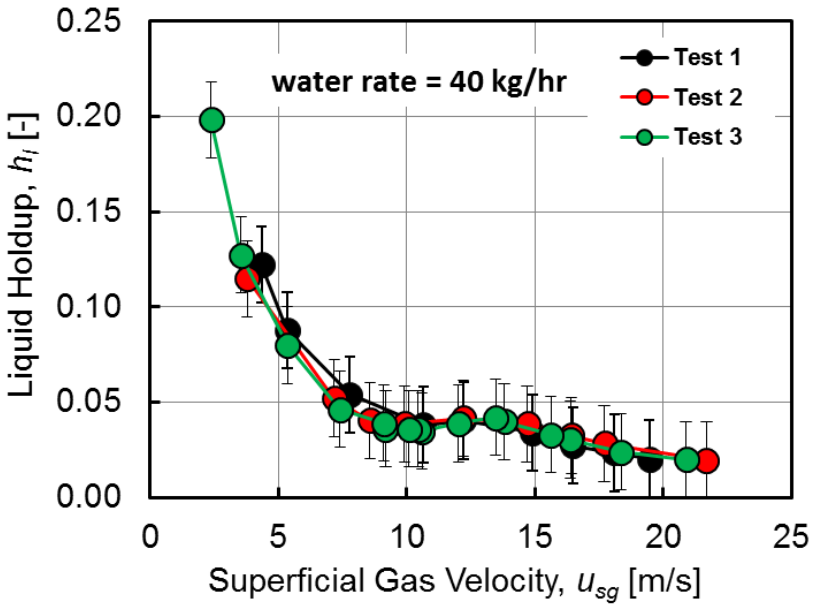

Fig. 3.3—Liquid holdup measured using conductivity probes.

We conducted preliminary experiments to exercise the consistency of holdup profile from conductivity probes by flowing only small water mass flow rate. **Fig. 3.3** shows the liquid holdup that is illustrated as a function of superficial gas velocity, u_{sg}.

This experiment was repeated three times to ensure the consistency of film thickness reading.

It can be seen that there are three regions characterizing the holdup profile. First, liquid holdup is increasing as gas rate decreases where $u_{sg} > 14$ m/s. Second, liquid holdup trend reverses when u_{sg} is between 10 and 14 m/s. Third, liquid holdup is sharply increasing as gas rate decreases after u_{sg} falls below 10 m/s. This observations contradict the original finding of Waltrich et al. (2013) where the trend of liquid holdup is monotonic considering the case of high liquid rate. Interestingly, for the particular small water flow rate we observed the transition between annular to churn flow occurred on u_{sg} between 10 and 14 m/s. Therefore, we hypothetically concluded that the non-monotonic holdup profile is attributed to the artifact of probes measurement, especially during thin liquid film establishment in combination with the presences of partial flow reversal and highly oscillating flow regime.

Several distinguishable sub-structures were visually observed using a high speed camera located at $z/D = 510$. As an example, we consider a typical churn flow situation. **Fig. 3.4** shows the underlying flow structures at different times where gas and liquid mass fluxes are 16 and 6 $kgm^{-2}s^{-1}$, respectively. Based on the probe-determined holdup, the periodically varying flow structure can be categorized corresponding to "low", "moderate", and "high" local liquid holdup. At the occurrence of "low" holdup, the interface between gas core and liquid film is clear. The liquid film is flowing downward.

Moreover, a small fraction of the liquid film breaks and some liquid gets entrained in the gas core.

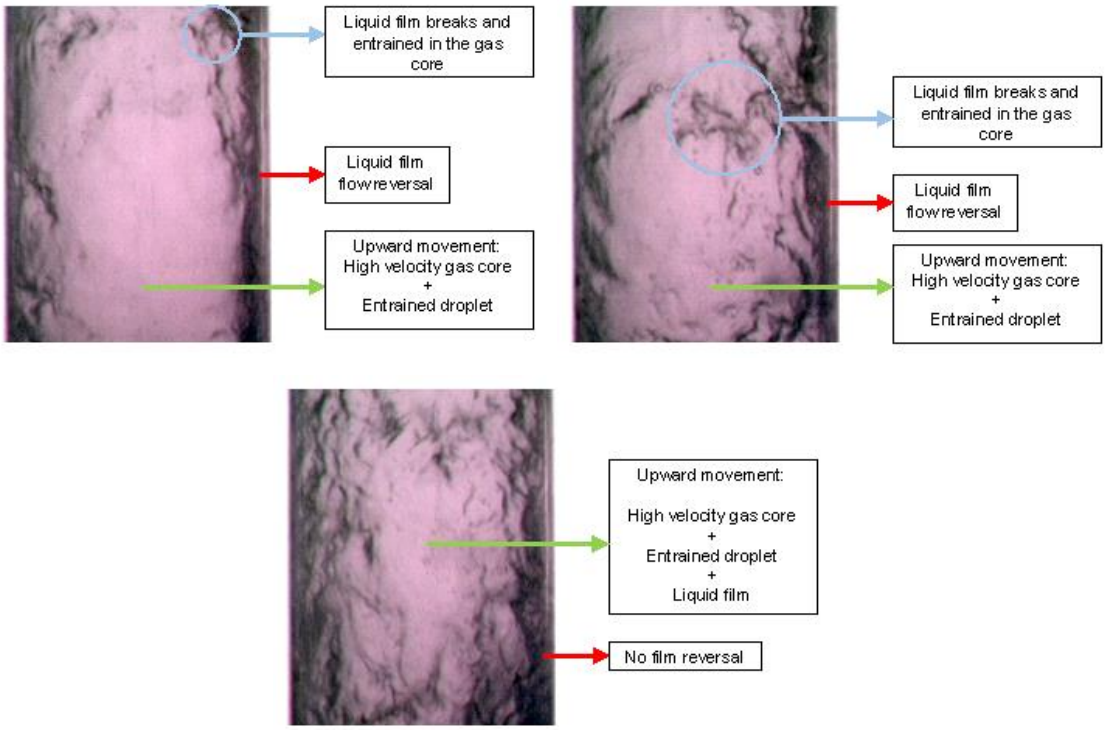

Fig. 3.4— Snapshot of high speed video camera to analyze flow structure at $\dot{m}_g = 16$ and $\dot{m}_w = 6$ kgm^{-2}s^{-1}, respectively. (a) low holdup region; (b) moderate holdup region after 0.86 s; and (c) high holdup region after 1.74 s.

Following in time, at the occurrence of "moderate" holdup, the interface is blurred but downward liquid motion is still observable near the wall. Finally, at "high" holdup occurrence, downward film motion cannot be detected and the interface cannot be located. The successive occurrence of these structures is illustrated in **Fig. 3.5** showing the film thickness at $z/D = 504$ when $\dot{m}_g = 16$ and $\dot{m}_w = 6$ kgm^{-2}s^{-1} and the flow regime can be

considered already "stabilized". The data was recorded at 40 Hz sampling frequency and smoothed by 8-point moving average. Considering a specific point in time, the fully developed local structures (low, medium and high holdup regions) usually co-exist and are periodically repeated along the tube.

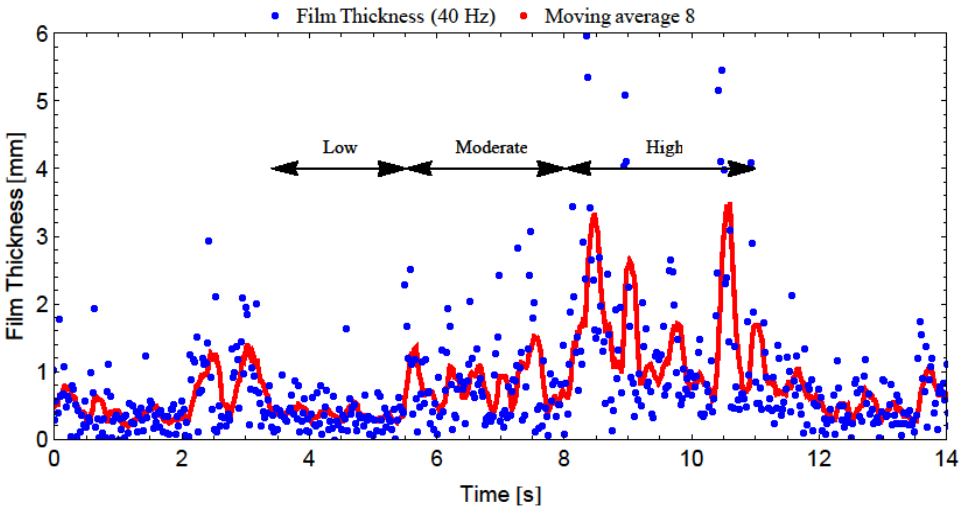

Fig. 3.5—Film thickness profile measured at $z/D = 510$ with gas and liquid mass fluxes of 16 and 6 $kgm^{-2}s^{-1}$, respectively.

The steady-state two-phase simulation using commercial software OLGA (Bendiksen et al. 1991) was also performed to provide additional analysis on axial holdup variation. The tubular conduit of 42-m was discretized into 200 segments where the flow rates and boundary conditions were set equivalent to experimental conditions. Axial holdup variation was continuously changing with time as illustrated in **Fig. 3.6**. However, the average holdup for the test section, $\overline{h_l}$, showed consistency. In contrast, measuring holdup by trapping liquid from a small section of the pipe, that is more commonly done,

provides inconsistent results (**Fig. 3.6** also illustrates holdup measurement between 20 to 25 m).

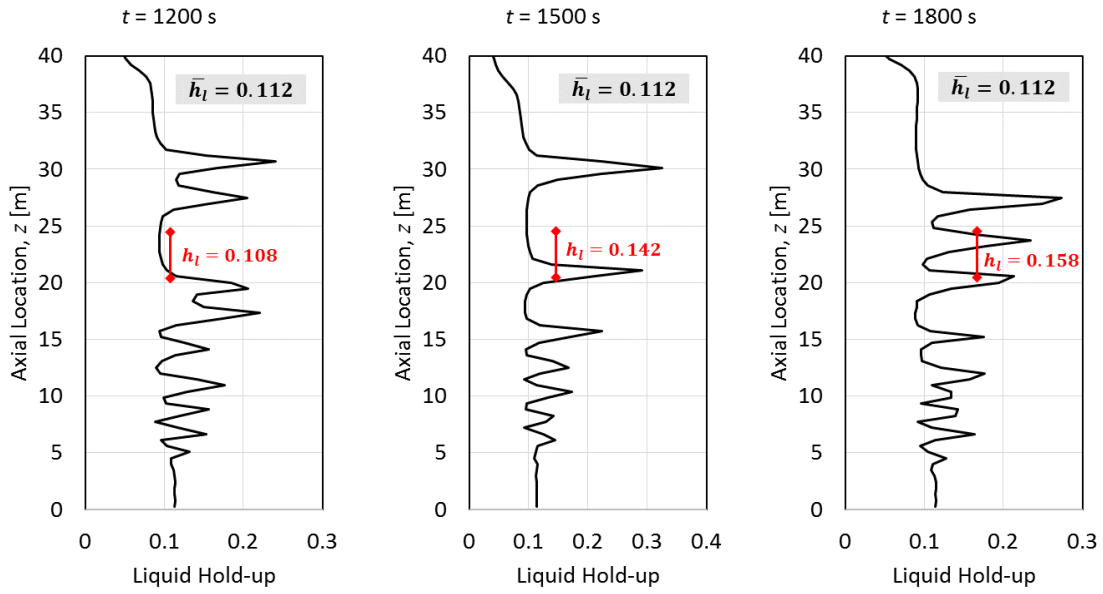

Fig. 3.6—Axial variation of liquid holdup at different times simulated using OLGA with gas and liquid mass fluxes of 16 and 6 $kgm^{-2}s^{-1}$, respectively.

Overall holdup measurement by trapping the liquid between inlet and outlet of the test section gives the spatial average holdup. Despite the underlying flow structure is characteristically dynamic, measuring holdup from the whole test section seems to boost the accuracy. This accuracy of the spatial average is better the larger is the ratio of equipment length to the maximum wavelength.

The additional capability of measuring shut-in holdup by trapping the fluid between two valves installed at the inlet and outlet of the test section has proved crucial in this study. The inlet and outlet valves can be closed within 2 to 4 seconds, depending

on the initial opening, where the distance between them is 42 m. A pressure transducer is positioned at the bottom providing the hydrostatic pressure and hence the height of the liquid column already in rest. The pressure measured holdup can be verified for those cases in which the water level reaches the transparent section of the pipe, confirming that the average liquid holdup measurement uncertainty is within ± 0.02 absolute unit. Oddie et al. (2003) also reported that in their experiments liquid holdup measured by probes gave less accurate results compared to the shut-in technique. However, Waltrich et al. (2013) emphasized that probes holdup measurement provides valuable insight into the axial development of the flow. Our observations coincide with both of the above opinions.

Measurement Results

The objective of the current experimental series was to establish a data set for the development of liquid holdup correlation within the vicinity of partial flow reversal. Therefore, we included flow reversal and no flow reversal conditions. The liquid holdup measurements were conducted systematically with gas and liquid mass fluxes ranging from 3.9 to 37.4 $kgm^{-2}s^{-1}$ and 4.5 to 60.7 $kgm^{-2}s^{-1}$, respectively. The gas and liquid mass flux intervals correspond to possible situations in natural gas producing wells where volumetric liquid rates are moderate or low, and (initial) volumetric gas rates are high, while mass fluxes are of the same order.

The corresponding liquid volumetric rates, q_g and q_l, ranging from 3 to 190 Mscf/D and 4.5 to 61 bbl/D, respectively. This corresponds to gas and liquid superficial velocities, u_{sg} and u_{sl}, 1.5 to 95 ft/s to 0.015 to 0.2 ft/s, respectively (phase superficial

velocity is equal to the phase volumetric flow rate divided by the total cross-sectional flow area). The measurement results are described in details in **APPENDIX A**. While at the actual gas well conditions, the in-situ pressure and gas velocity vary in significant magnitudes difference along the wellbore, it is shown in **Fig. 3.7** that our flow-loop provides adequate pressure and gas velocity variations.

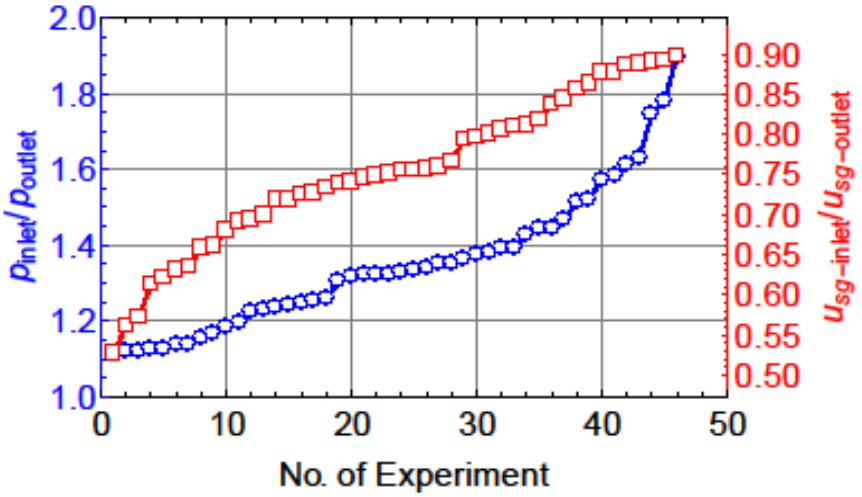

Fig. 3.7—Ratios of inlet to outlet pressure and superficial gas velocity for 46 measurements conducted in this study.

The comparison of the conditions in the present study with the experiment of Waltrich et al. (2013) is shown in **Fig. 3.8**. About 55% of liquid holdup data were measured with gas mass fluxes greater than liquid mass fluxes and more than 60% of experiments were performed around the visually observed annular-to-churn flow pattern transition.

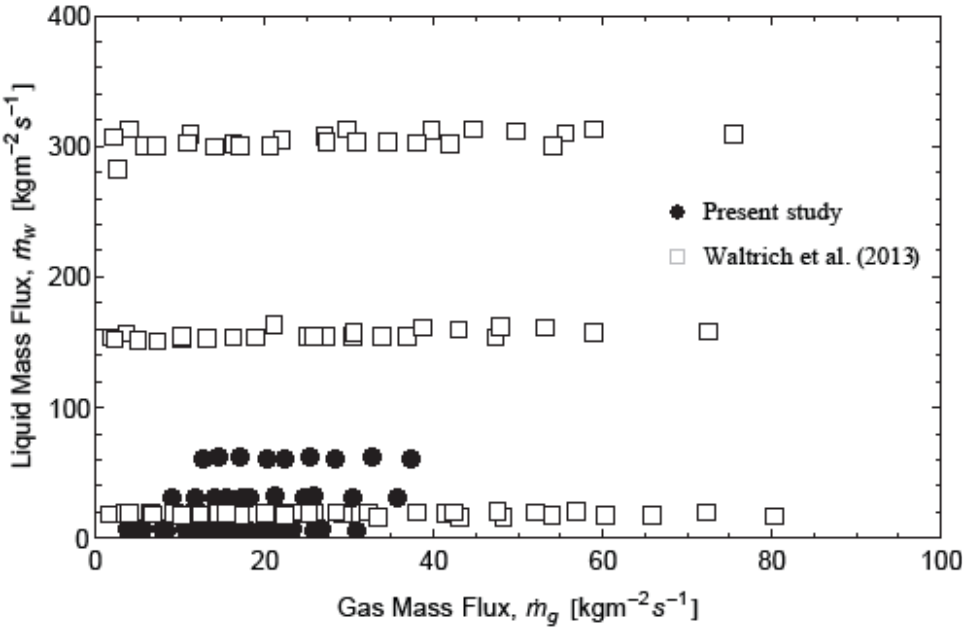

Fig. 3.8—Test matrix of gas and liquid mass fluxes.

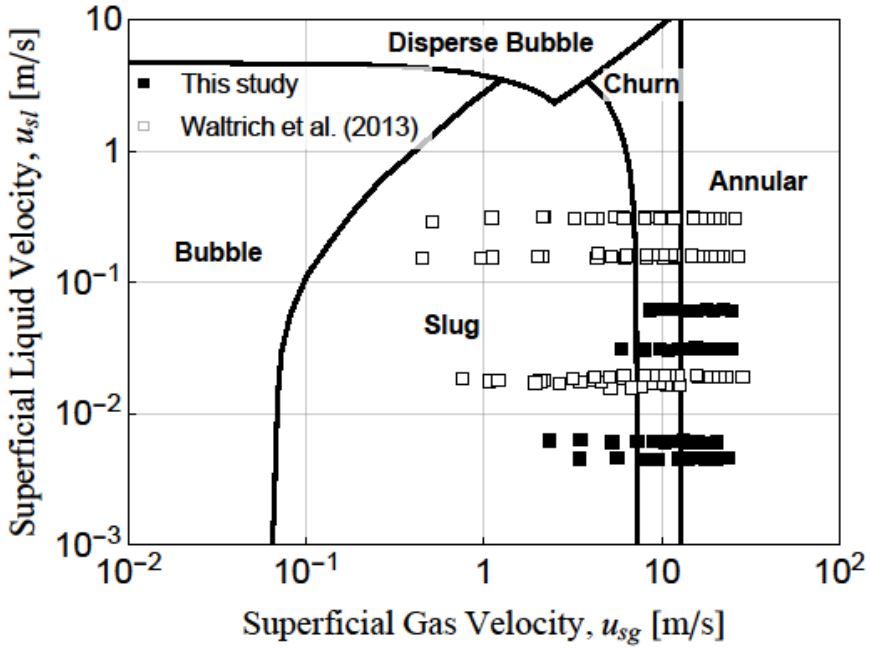

Fig. 3.9—Test matrix of superficial gas and liquid velocities in flow pattern map of Taitel et al. (1980).

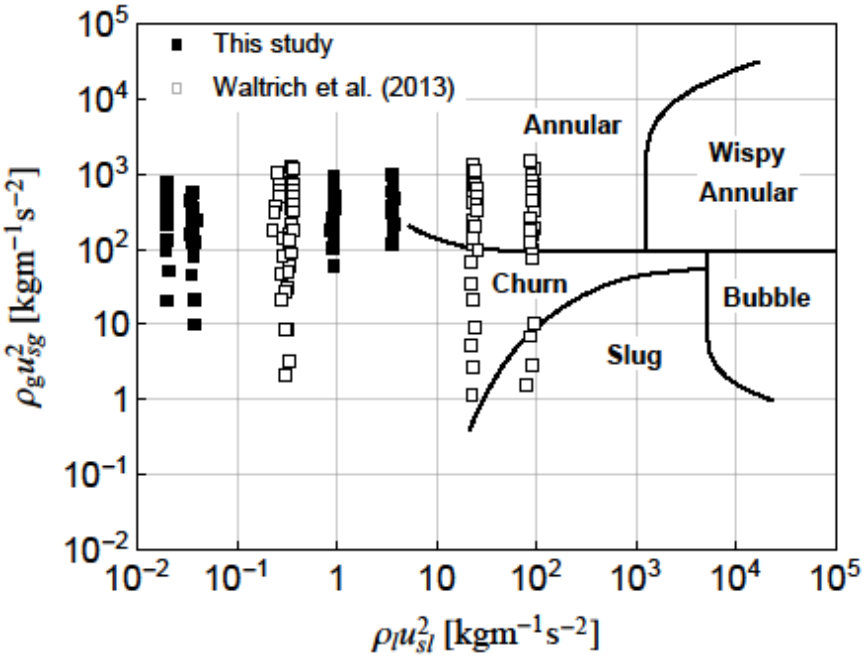

Fig. 3.10— Test matrix of gas and liquid momentum fluxes in flow pattern map of Hewitt and Roberts (1969).

Fig. 3.9 shows the superficial-velocity-based flow pattern map of Taitel et al. (1980), our experiments covered various flow regimes including annular, churn, and slug flows. Bubble flow was not the primary interest because its relevance to the onset of liquid loading is hypothetically limited compared to annular or churn flow regime. Meanwhile, more than 50% of the total experiment were conducted outside the momentum-flux-based flow pattern map defined by Hewitt and Roberts (1969) as indicated in **Fig. 3.10**.

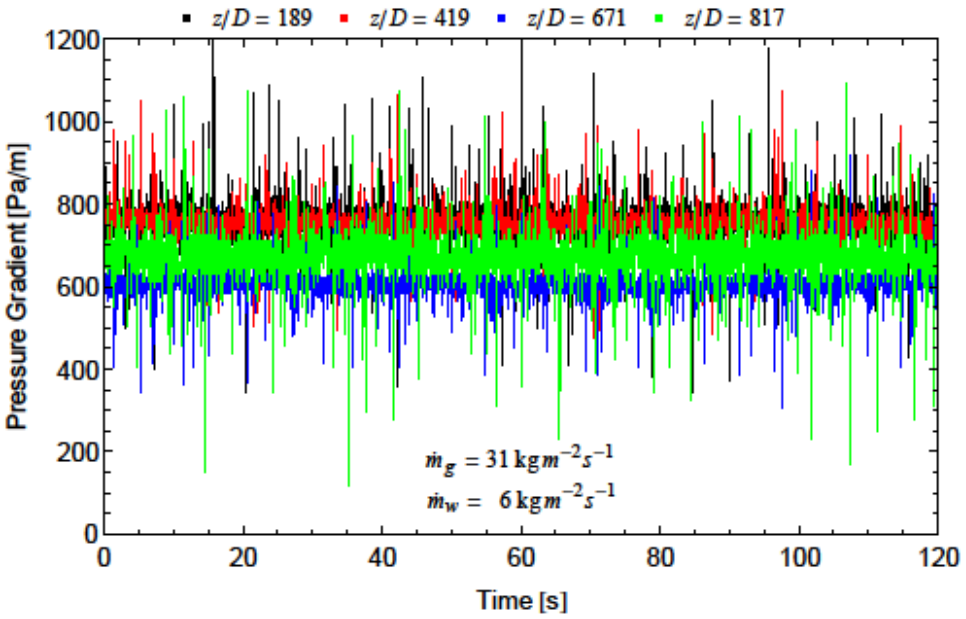

Fig. 3.11—Steady-state pressure gradient along the tube during experimental run.

Determination of the steady-state condition is illustrated on **Fig. 3.11**. We attempted to pick a situation when the amplitude of pressure gradient oscillations at several tube locations reached their minimum values simultaneously. The pressure gradient was determined from the difference of absolute pressures measured at two neighboring locations. While for the situation depicted on the figure the word "steady-state" is appropriate, because the observed quantities are constant except for some high frequency noise. In most of the experiments the term "stabilized-state" would be more appropriate, because lower frequency periodic phenomena were present. The lower frequency phenomena are characteristic features of churn flow and slug flow. Additionally, in some experiments we measured the water rate flowing out of the separator

and found it to be equivalent to the rate at the inlet. It can also be concluded that there was no water accumulated inside the tube during experimental runs.

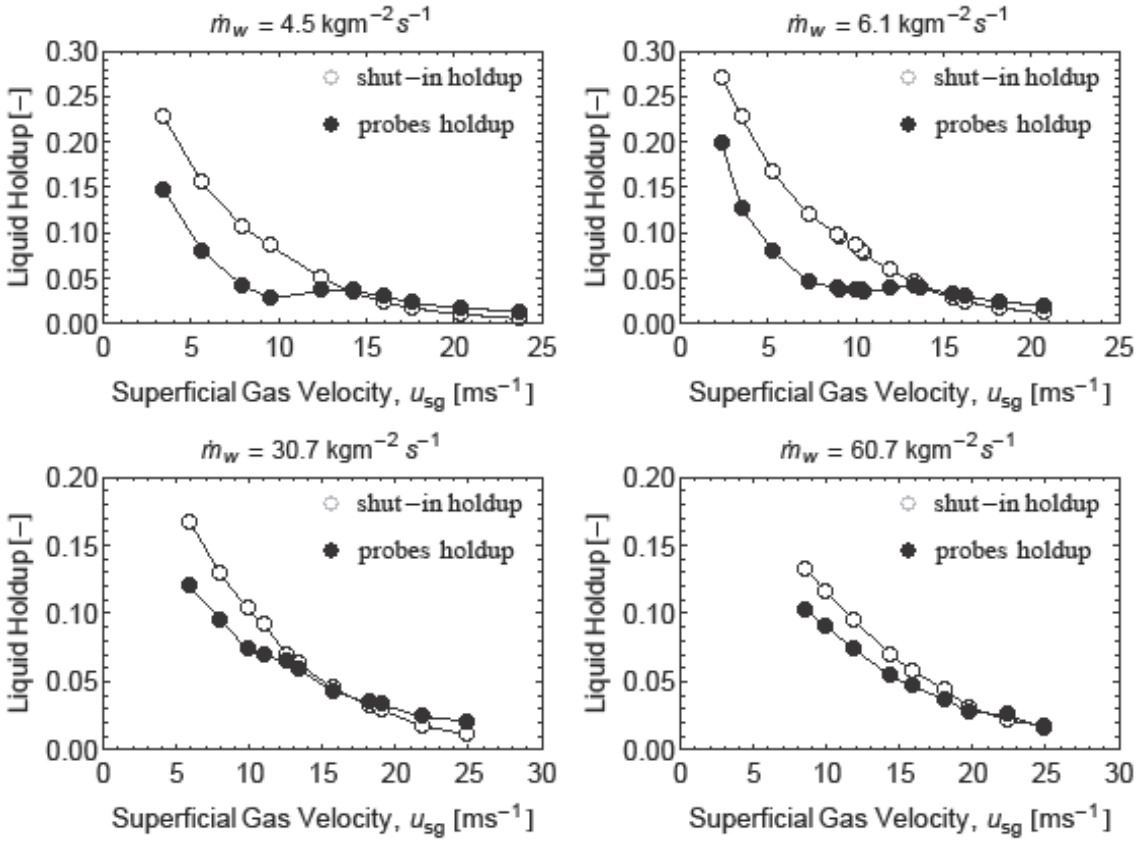

Fig. 3.12—Comparison of shut-in and probes holdup measurements at various gas and liquid flow rates.

By maintaining a constant water rate, steady-state liquid holdup was measured at several air rates. A total of 46 liquid holdup measurements were collected in this study. The experimental runs were conducted with average pressure between 110 and 150 kPa. The steady-state holdup results measured by both probes and shut-in techniques are shown in **Fig. 3.12**.

The holdup (overall, determined by shut-in) is increasing exponentially with the decreasing superficial gas velocity at a constant water rate. The probes holdup (obtained by averaging 3 local values along the tube) behaves similarly but with some inconsistency. The inconsistency occurred specifically at lower water fluxes (i.e. $\dot{m}_w = 4.5$ kgm^{-2}s^{-1} and $\dot{m}_w = 6.1$ kgm^{-2}s^{-1},) where only a thin liquid film was established along the pipe wall. While it is understood that the probes measurement underestimate the holdup (even after correction for entrained liquid droplets) when the water mass flux is moderate or low, it provides useful additional information. In fact the broken trends at superficial gas velocity, u_{sg} around 13 m/s for $\dot{m}_w = 4.5$ kgm^{-2}s^{-1} and $\dot{m}_w = 6.1$ kgm^{-2}s^{-1} on **Fig. 3.12** coincided with flow regime transition from annular to churn, that was also observable visually. This observation was in agreement with our preliminary experiments described in the previous section. At very low superficial gas velocities (u_{sg} < 5 m/s) a small decrease in superficial gas velocity triggers large increase in liquid holdup. In contrast, for u_{sg} > 20 m/s, liquid holdup is less sensitive to variations in the gas velocity.

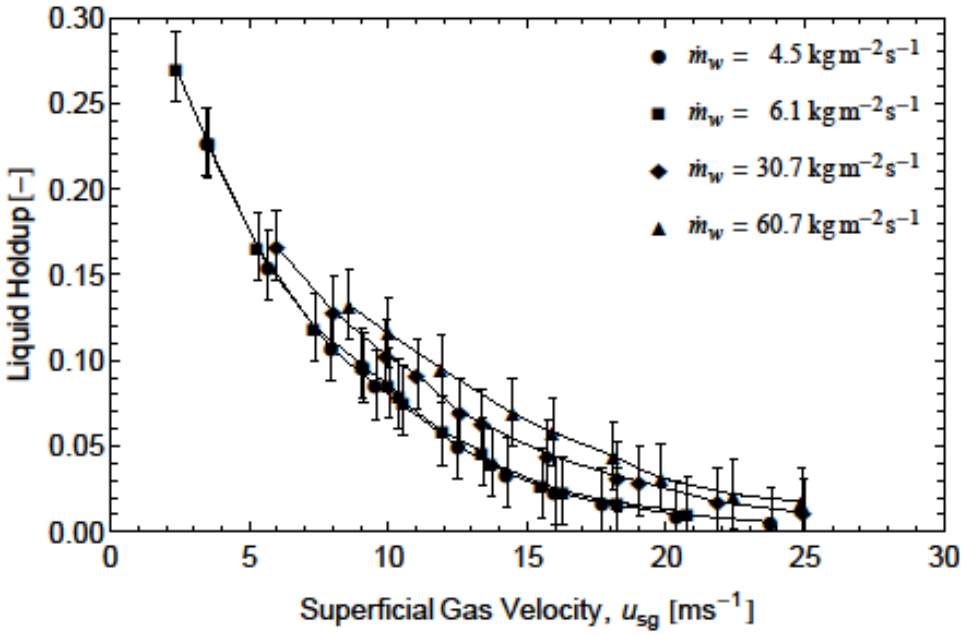

Fig. 3.13—Liquid holdup measurement results illustrated as a function of superficial gas velocity, u_{sg}.

As water mass flux increases, the liquid holdup versus superficial gas velocity curves shift vertically upward. **Fig. 3.13** shows that the curves shift consistently, without crossing each other, even for a relatively small change in water rate. In the following discussions, we will refer to the variation of holdup with superficial gas velocity as "primary" and with water mass flux as "secondary" effect. This grouping is justified both by the magnitude of the effects and by the characteristic shape of the corresponding curves.

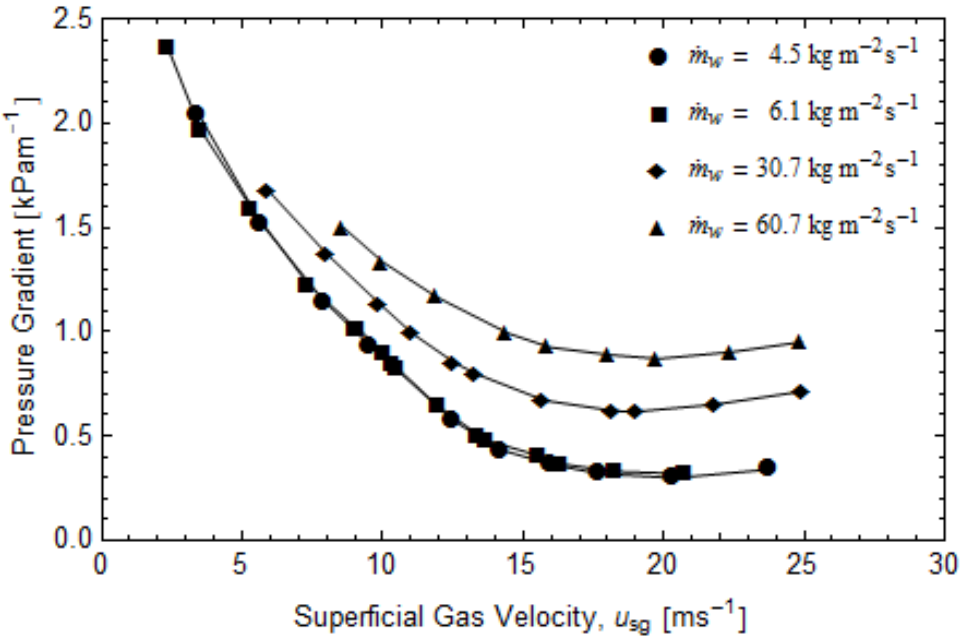

Fig. 3.14—Pressure gradient measurement results illustrated as a function of superficial gas velocity, u_{sg}.

The corresponding pressure gradient is shown in **Fig. 3.14**. In general, pressure gradient behavior is somewhat similar to liquid holdup where "jump conditions" during flow regime transitions do not exist. Only two types of flow are recognizable, namely frictional dominant and gravitational dominant. Minimum pressure gradient is located at u_{sg} between 15 and 20 m/s. To the right of this minimum point, the overall pressure loss is dominated by frictional component. To the left of the minimum point, gravitational forces start to dominate the system when liquid holdup inside the tube increases rapidly.

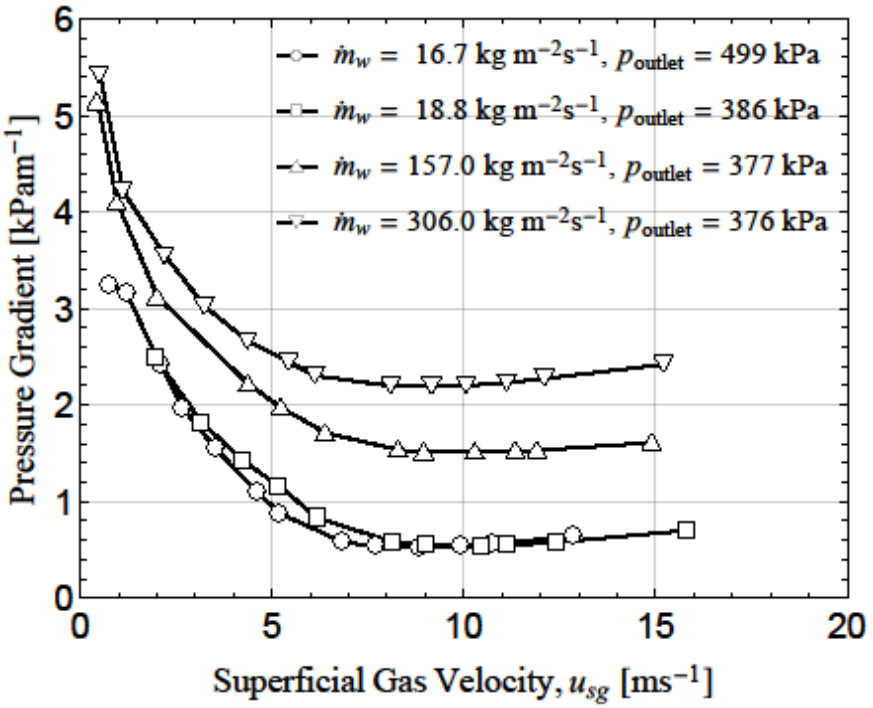

Fig. 3.15—Pressure gradient measurement results of Waltrich et al. (2013), illustrated as a function of superficial gas velocity, u_{sg}.

For a comparison, **Fig. 3.15** shows the pressure gradient measurement results of Waltrich et al. (2013) where the outlet pressure was controlled by limiting the valve opening. The outlet pressures were four times as high as the atmospheric condition is. It can be seen that the pressure gradient reached its minimum at u_{sg} between 7 and 12 m/s, depending on the outlet pressure. It differs from what we previously found where the outlet pressure was set to atmospheric. Some researchers correlated the onset of liquid loading to the minimum pressure gradient. Based on their experimental observations, they proposed some specific superficial gas velocities or gas rates as the thresholds indicating

the condition of “loading” or “no loading” in gas wells. As a matter of fact, this approach is misleading.

Conclusion

The modification of the initial experimental facility has been made to accommodate spatial-average holdup measurement. It is considerably more important than time-average holdup considering variations of local two-phase condition along the longer tube. The shut-in holdup method delivered more consistent results compared to indirect holdup measurement through conductivity probes. However, we found that the conductivity probes may generate reasonable measurement results if the liquid mass flux is high enough.

The time to attain stabilize condition varies significantly depending on the flow conditions, but the conformity between inlet and outlet flow rates as well as the observed stabilize-state of pressure gradient refer to steady condition.

The expected liquid accumulation at the bottom of the pipe did not take place during the experiment with very low gas rates, which were way below critical Turner velocity (or any other Turner type correlations.) Instead, we observed monotonically increasing holdup as gas rate decreases while water rate remained the same, despite the prevalence of various flow regimes. Similarly, pressure gradient as a function of gas rate has been represented as a smooth curve. These important information are set as the basis in constructing the new wellbore liquid content model.

A proposition of semi-mechanistic gas critical velocity determining the liquid loading situation is actually unrealistic. The actual liquid loading conditions can only be modeled by coupling the wellbore and reservoir systems. Therefore, this study focuses on developing a more appropriate wellbore model based on experimental observations such that it can be used to monitor the gradual increase of liquid content way before the onset of liquid loading or to predict the corresponding overall pressure gradient.

CHAPTER IV

WELLBORE MODEL DEVELOPMENT*

Introduction

The two-phase pressure gradient behaviors as functions of multiple variables such as fluid properties, fluid velocities, flow patterns, as well as liquid holdup have been studied many years. It has been re-investigated lately with the hope to gather a deeper insight into the liquid loading phenomena. From our perspective, the most essential matter is the methodology of observing and modeling the liquid holdup under various conditions. In the context of liquid loading, however, such meticulous experiments are hardly to be performed. The limitations include limited length of tubular conduit, significant low system pressure and most importantly, the absence of experimental reservoir.

The monotonic trend of liquid holdup that we observed during experimental study simplifies the hypothesis of liquid loading situation: the cause of liquid loading is natural production decline leading to consistent increase of wellbore liquid content and flowing bottomhole pressure. In this chapter, we leverage these observations diligently to construct an empirical correlation to be used in gas wells experiencing liquid loading.

* Part of this chapter is reprinted with permission from "Liquid holdup correlation for conditions affected by partial flow reversal" by Lumban-Gaol, A. and Valkó, P.P., 2014. *International Journal of Multiphase Flow*, 6, 149-159 Copyright 2014 by Elsevier.

Wellbore model suitable to be used under liquid loading conditions is actually not available at present. Additionally, most existing correlations have difficulties in reproducing both experimental and field data sets in which certain gas and liquid rates allegedly contribute to the occurrence of partial flow reversal or liquid loading.

Modeling Wellbore Liquid Content for Vertical Well

Waltrich et al. (2013) presented the time-averaged liquid holdup which was measured using conductivity probes. Their measurement results indicated liquid holdup is increasing exponentially as gas rate decreases, even when the two-phase flow system encounters flow regime transitions. However, in the previous chapter we showed that the measurement using conductivity probes delivered inconsistent results for lower liquid rates. Consequently, the spatially averaged holdup was considered as a necessity for developing a new holdup correlation. We observed the similar sharp (exponential) but continuous increase of the (overall) liquid-content as the gas rate decreased at a fixed liquid rate, regardless the prevailing flow-pattern. Indeed, the holdup vs gas velocity curves did not cross for various liquid rates and were relatively smoothly varying. Similar holdup trend was also observed by Yuan et al. (2013) and Liu (2014) as shown in **Fig. 4.1**.

These observations will be the basis of the empirical correlation development, specifically applicable at inlet conditions characterized by moderate inlet liquid fraction and not too large gas velocity. Those are the essential features for producing gas wells near to or already affected by liquid loading.

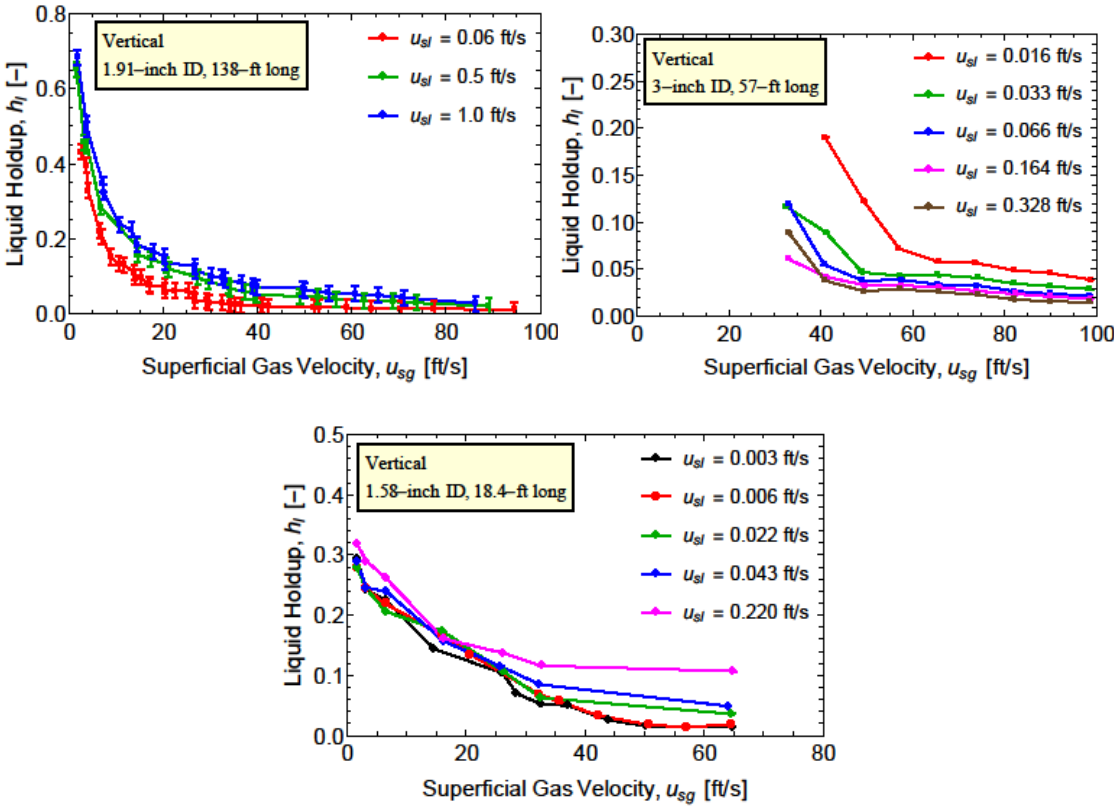

Fig. 4.1— Measured liquid holdup at various gas and liquid flow rates in vertical flow-loop presented by Waltrich et al. (2013) (top-left), Yuan et al. (2013) (top-right), Liu (2014) (bottom).

The new model does not need to consider separate conditions in the wellbore since all forms of liquid are directly taken into account in the holdup calculation. Therefore, we refer to wellbore liquid content term through the rest of this study. In the following discussions, we will refer to the variation of holdup with superficial gas velocity as "primary" and with water mass flux as "secondary" effect. This grouping is justified both by the magnitude of the effects and by the characteristic shape of the corresponding curves.

The smoothness and regularity of the shut-in holdup curves suggest that the liquid holdup behavior may not depend heavily on the particular flow regime and follow a simple

relationship. However, it is important to emphasize that frictional pressure loss is strongly affected by the type of the prevailing flow pattern.

The simplest way to represent the previously described primary effect resembling exponential dependency of holdup on superficial gas velocity is to use scaling. Wallis (1969) studied the phenomena of liquid film reversal where the experiment was set having different inlet locations for gas and water. Gas was injected through the bottom of the pipe while the inlet for liquid located at higher location. Therefore, the gas and liquid were not mixed below the liquid inlet location. By maintaining constant water rate, the gas rate was reduced sequentially until flow reversal was observed. Wallis (1969) then introduced non-dimensional gas and liquid velocities where the original intention was to help predicting the onset of flow reversal in real problems with similar inlet conditions. These non-dimensional velocities employ a balance between inertial and hydrostatic forces and written as follows:

$$u_g^* = \frac{u_{sg}}{u_{cg}} \tag{4.1}$$

$$u_l^* = \frac{u_{sl}}{u_{cl}} \tag{4.2}$$

where u_{sg} and u_{sl} are the gas and liquid superficial velocities which represent inertial forces, while u_{cg} and u_{cl} are the gas and liquid characteristic velocities representing gravitational forces.

The u_{cg} and u_{cl} are formulated as:

$$u_{cg} = \left[g D \left(\frac{\rho_l}{\rho_g} - 1 \right) \right]^{0.5} \tag{4.3}$$

$$u_{cl} = \left[g D \left(1 - \frac{\rho_g}{\rho_l} \right) \right]^{0.5} \tag{4.4}$$

where ρ_g and ρ_l are the gas and liquid densities, *D* is the tube diameter, and g is the acceleration due to gravity. In addition to these, additional forces which worth of consideration are including interfacial surface tension and viscous forces of both phases.

Therefore, it is convenient to rewrite both **Eqs. 4.3** and **4.4** in typical Turner formulation as indicated below:

$$u_{cg,\text{Turner}} = 5.46 \left[\frac{\sigma(\rho_l - \rho_g)}{\rho_g^2} \right]^{0.25} \tag{4.5}$$

$$u_{cl,\text{Turner}} = 5.46 \left[\frac{\sigma(\rho_l - \rho_g)}{\rho_l^2} \right]^{0.25} \tag{4.6}$$

For the sake of simplicity, we will use the u_{cg} and u_{cl} definitions of Wallis (1969) as the basis for deriving the new empirical liquid content correlation. Later in this chapter, the characteristic velocity based on Turner criterion will be shown to have similar capability as a scaling function to determine liquid content.

Counter-current flow limitation correlations use these concepts (hydrodynamics of inertial-gravitational of the liquid film) in a more general framework:

$$\sqrt{u_g^*} + m\sqrt{u_l^*} = C \;\; \rightarrow \;\; \text{Affected by flow reversal} \tag{4.7}$$

where m is a constant which lies between 0.8 and 1.0, and C between 0.7 and 1.0. While **Eq. 4.7** may also imply partial flow reversal due to decrease in u_l^*, for gas producing well related investigations u_g^* dominates compared to u_l^*. Therefore, the second term on the left hand side of **Eq. 4.7** can be neglected, and assuming C is equal to unity, we obtain:

$$\sqrt{u_g^*} < 1 \quad \rightarrow \quad \text{Affected by flow reversal} \tag{4.8}$$

Based on **Eq. 4.8**, 37 out of 46 liquid holdup data points are actually affected by flow reversal.

The liquid holdup behavior can be represented as a deviation from the primarily as a function of non-dimensional superficial gas velocity (see **Fig. 4.2**) with the secondary effect being liquid rate.

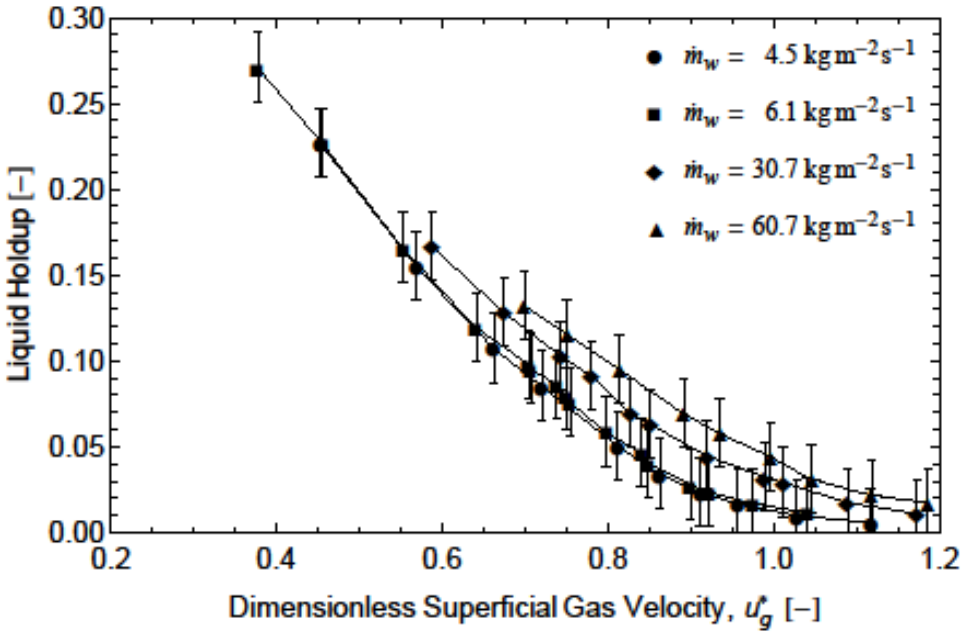

Fig. 4.2—Liquid holdup as a function of dimensionless superficial gas velocity, u_g^*.

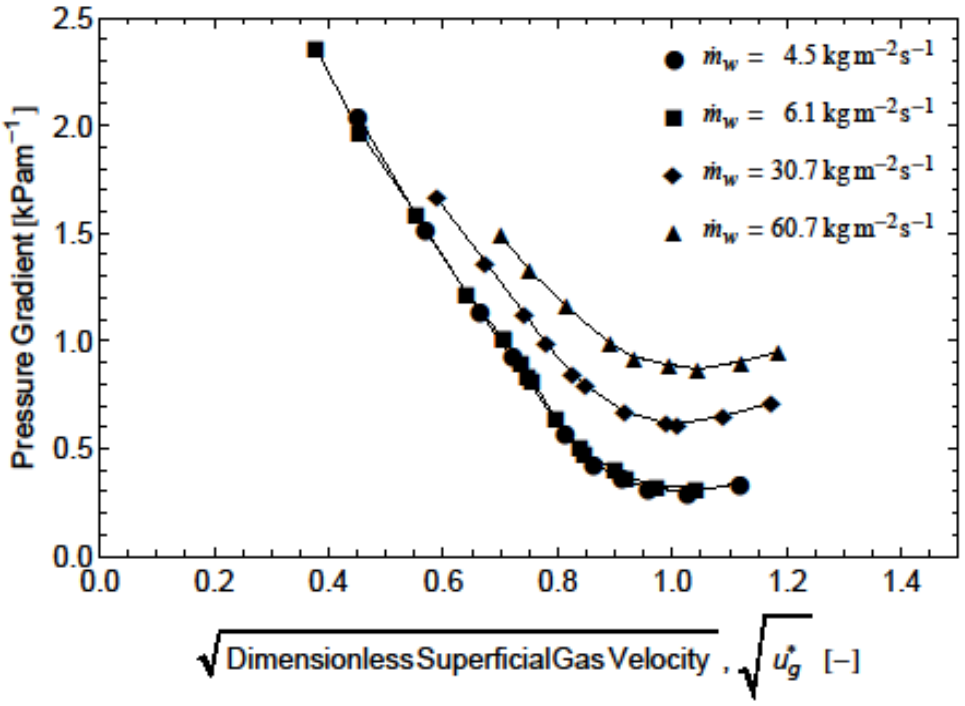

Fig. 4.3—Overall pressure gradient as a function of dimensionless superficial gas velocity, u_g^*, shows its minimums at $0.9 < \sqrt{u_g^*} < 1.1$

Zabaras et al. (1986) found that onset of flooding in counter-current flow is related to the minimum pressure drop point in the tube, when the wall shear stress approaches zero and interfacial shear stress is balanced by the gravitational forces. Accepting this basic insight, our experiments were conducted within one order of magnitude vicinity of $\sqrt{u_g^*} = 1$. Indeed, as shown in **Fig. 4.3**, the minimum average pressure gradient at any fixed water rate appears at $0.9 < \sqrt{u_g^*} < 1.1$. The region of transition between churn flow and annular flow was identified at the minimum pressure gradient. Partial film reversal was also observed below the minimum.

Gray (1974) developed a simplified liquid holdup correlation to be used in calculation involving gas wells producing some liquids, which expressed as:

$$h_{l,\,\text{Gray}} = 1 - \left(1 - \frac{u_{sl}}{u_{sg}}\right)(1 - \mathrm{e}^{f_l}) \tag{4.9}$$

where f_l is a factor involving various parameters including phases densities, interfacial tension, tubing size, and the effect of gravitational forces. However, this holdup correlation was not derived directly from experimental data.

With the ever growing interest in studying annular flow in various industries, recently Cioncolini and Thome (2012) came up with a new empirical correlation to predict annular void fraction. The method is simpler than most previously suggested correlations as it relies only on the density ratio and vapor quality (or gas mass fraction). However the correlation is not suggested to be used in flow patterns other than annular flow. This annular void fraction correlation is expressed as:

$$\alpha = \frac{hx^n}{1 + (h-1)x^n} \tag{4.10}$$

where variables h and n are expressed as functions of gas to liquid density ratio (ρ_g/ρ_l) and involving 4 fitting constant parameters.

From the two examples above, it can be concluded that a simple yet rigorous empirical holdup correlation is still the primary interest especially with the ever increasing number of gas producing wells.

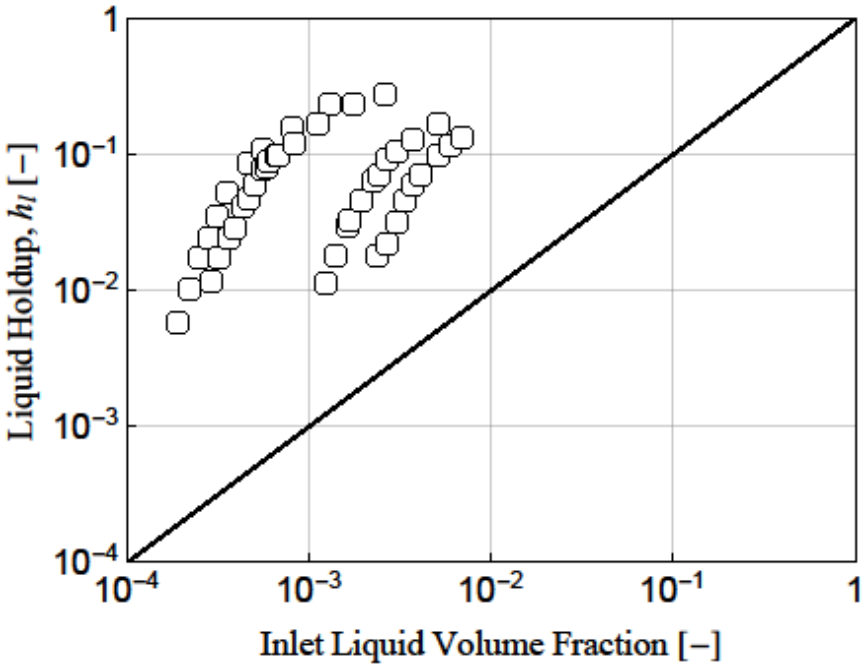

Fig. 4.4—Comparison between inlet liquid volume fraction and the corresponding liquid holdup.

It can be seen in **Fig. 4.4** that in upward gas-liquid flow the liquid holdup is more than the inlet liquid volume fraction, but less than unity. Therefore, the holdup can be written as

$$h_l = \frac{u_{sl}}{u_{sg} + u_{sl}} + \frac{u_{sg}}{u_{sg} + u_{sl}} f\left(u_g^*, x\right) \tag{4.11}$$

where the factor $f\left(u_g^*, x\right)$ is positive and less than unity. When the gravity effect is negligible (for instance at high pressures and sufficiently high gas rates) **Eq. 4.11** becomes the homogenous model with $f = 0$. The two variables of the f factor represent the primary and secondary effect, implying that they can be represented by the scaled gas velocity u_g^* and the gas mass fraction, x. Since f is positive and less than unity, it is convenient to

write it as e raised to a negative exponent. A particularly simple form of the exponent involves linear dependency on u_g^* and a "slight correction" by the liquid mass fraction:

$$f(u_g^*, x) = e^{-\left(1+au_g^*(1-x)^{-b}\right)} \tag{4.12}$$

where a and b are dimensional parameters to be determined from the experiments. We determined a, and b using the 46 holdup experiments available. By re-arranging **Eq. 4.11**, it can be cast into a straight line form. Shown in **Fig. 4.5** are the 46 observations and the least squares straight line fit that resulted in:

$$a = 2.12, \quad b = 0.25 \tag{4.13}$$

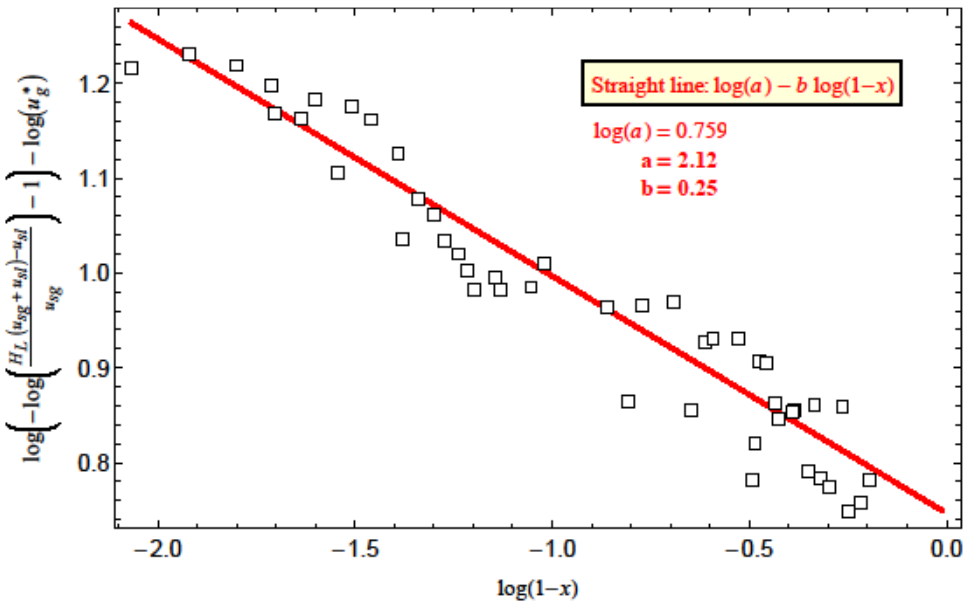

Fig. 4.5—Approximation of dimensionless parameters a and b in **Eq. 4.12** from a straight line fit of **Eq. 4.11** using 46 experimental results.

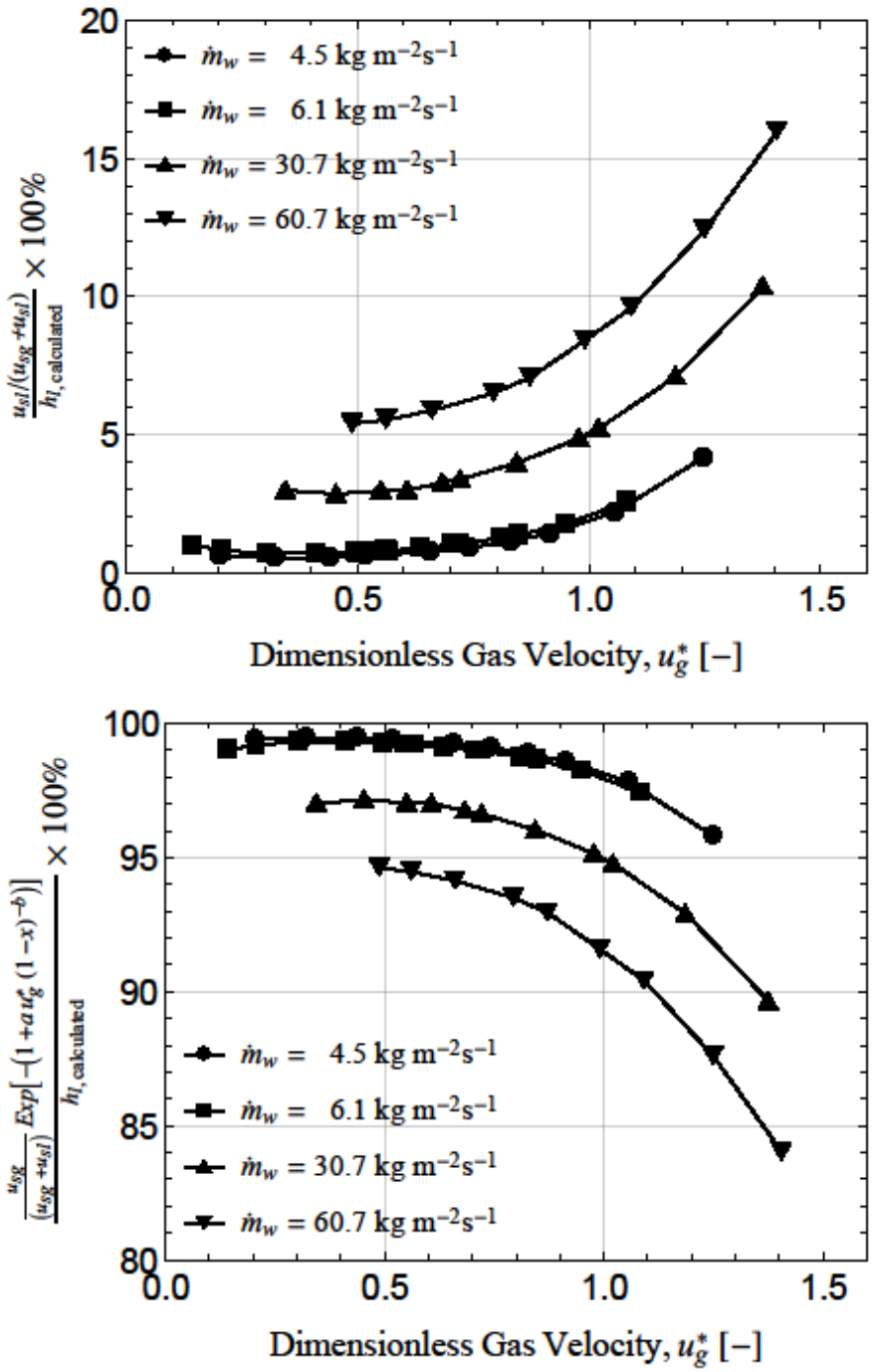

Fig. 4.6—Contributions of the first and second terms of **Eq. 4.11** to the calculated holdup, using experimental results of this study.

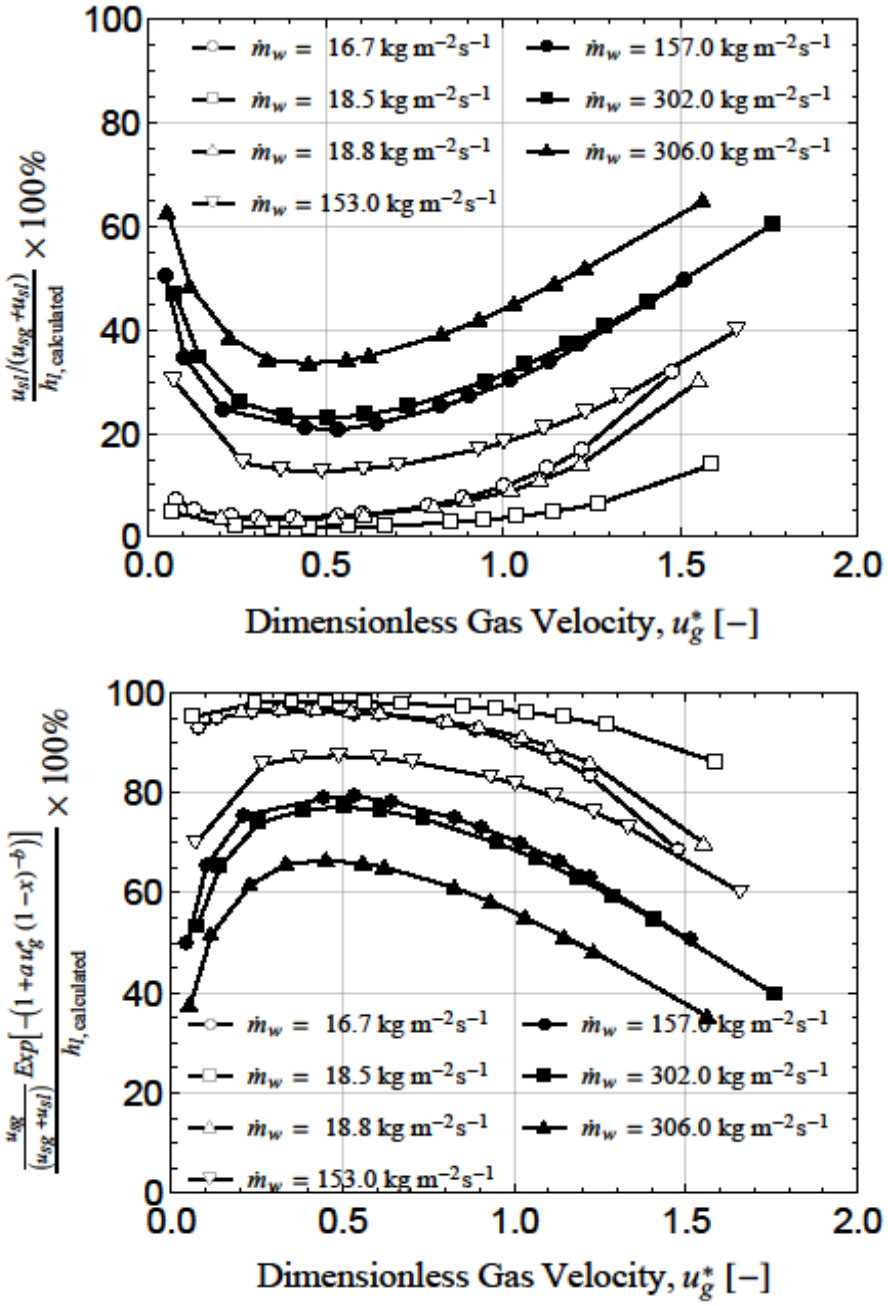

Fig. 4.7—Contributions of the first and second terms of **Eq. 4.11** to the calculated holdup, using experimental results of Waltrich et al. (2013).

It can be seen from **Figs. 4.6** and **4.7** that the effect of gas rate contributes significantly to the overall holdup. Interestingly, the effect of liquid rate is increasing exponentially as gas rate increases or decreases at the right and left sides of the minimum point. Homogeneous behavior then is truly taking place when gas and liquid travel at an equivalent velocity (or the slip ratio is equal to unity). This commonly occurs at the critical conditions, where the differences between properties of the gas and liquid are insignificant, which also depend upon mixture quality. It is characterized by the presence of bubbly flow (very low gas velocity) or mist flow (very high gas velocity).

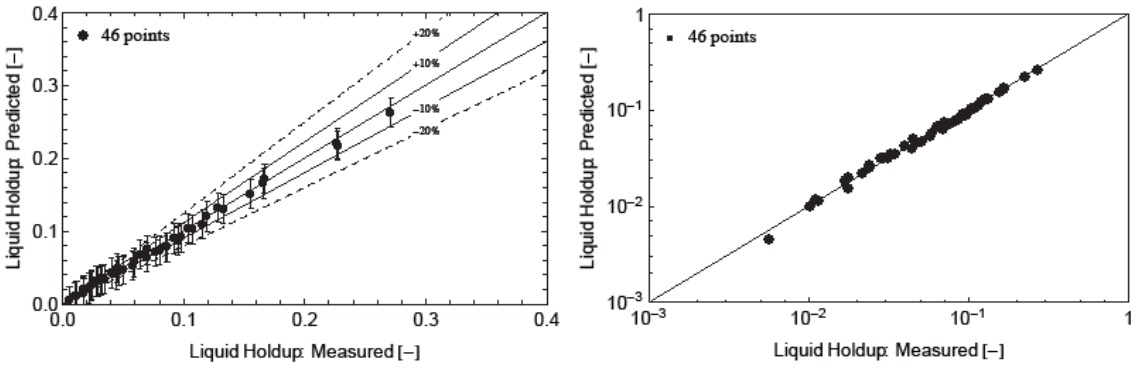

Fig. 4.8—Comparison of measured liquid holdup and calculated with the proposed model in linear and logarithmic scales.

The new liquid holdup correlation, consisting of **Eqs. 4.1**, **4.3**, **4.11**, **4.12**, and **4.13** requires only the knowledge of the tube diameter (D), the two volumetric flow rates and the two densities. Comparison of the measured liquid holdup with the predictions is presented in **Figs. 4.8** and **4.9**. The root mean squared percentage error (RMS) of the predictions is 7%. **Fig. 4.9** illustrates the capability of the proposed liquid holdup

correlation in reproducing measured liquid holdup consistently, by convincingly following the trend at each individual water rate. The predicted holdup values are within the measurement uncertainty, in spite of the surprisingly simple form of the model.

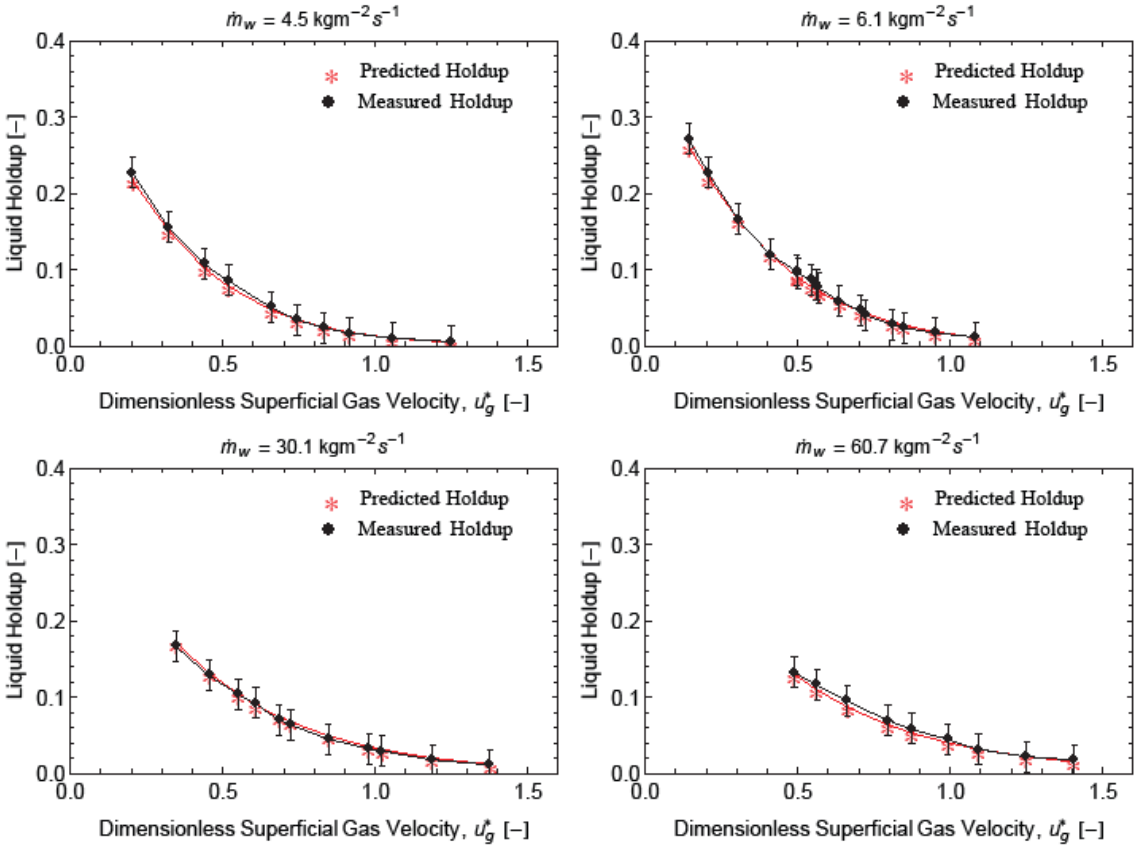

Fig. 4.9—Comparison of measured liquid holdup and calculated with the proposed model for various water mass fluxes.

As mentioned earlier, the actual form of **Eq. 4.3** can be replaced using the scaling of Turner criterion of **Eq. 4.5**. We repeat the fit of **Eqs. 4.11** and **4.12** and find that the best fit parameters change slightly to $a = 1.55;\ b = 0.25$ but the RMS percentage error

remains unchanged (7%) for our 46 experimental points. Hence, either scaling for u_g^* might be used together with **Eqs. 4.11** and **4.12** without affecting the accuracy of the liquid holdup prediction. However, we accepted the conclusion of Waltrich et al. (2013) that **Eq. 4.3** is more appropriate to be used for the conditions prevailing in our experimental setup. Therefore, the definition of u_g^* according to **Eq. 4.3** is used throughout this study.

Modeling Wellbore Liquid Content for Deviated Well

Multi-fractured-horizontal-wells have complex geometry and the deviation from vertical flow path is not negligible. The underlying effect of tubular deviation has been also studied across various industries. Fiedler and Auracher (2004) investigated the occurrence of liquid-film reversal in a small diameter inclined tube. They introduced the angle dependency factor to take account for the tube inclination, θ, where the effect of gravity fades and liquid film thickness becomes a more dominant factor controlling the film reversal mechanism as the tube deviates from vertical to horizontal position. Belfroid et al. (2008) applied this additional factor to the original critical gas velocity correlation of Turner et al. (1969) and presented its comparison with field data. In order to preserve the smoothness of the holdup correlation we incorporate all the effects of the deviations from vertical as a multiplier to the characteristic velocity. The resulting equation is as follow:

$$u_{cg,\,\text{Film}} = f(\theta) \times \left[\frac{g\,D\left(\rho_l - \rho_g\right)}{\rho_g}\right]^{0.5} \tag{4.14}$$

The $f(\theta)$ represents the effect of deviation angle (here θ is measured from the horizontal and should be greater than 0.) Adapting the term for angle correction of Belfroid et al. (2008), we have

$$f(\theta) = 1.35\,[\,\sin(1.7\,\theta)\,]^{0.38} \tag{4.15}$$

The function $f(\theta)$ is illustrated in **Fig. 4.10** where the maximum is found at pipe deviation angle of 53 degree. This minimum point contributes to the lowest possible value of u_g^* and results to the maximum holdup. This observation is in agreement with the observation of Beggs and Brill (1973) where they found that the liquid holdup passes its maximum value at deviation angle of approximately 50 degree.

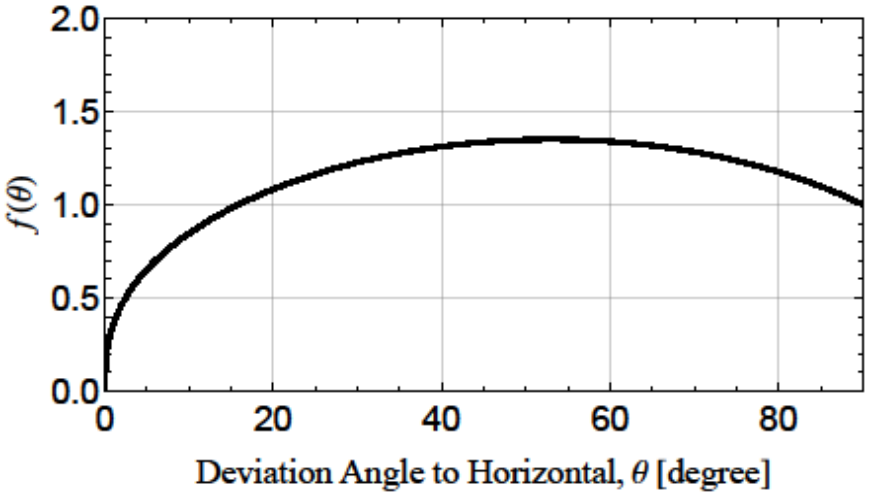

Fig. 4.10—Pipe angle correction function.

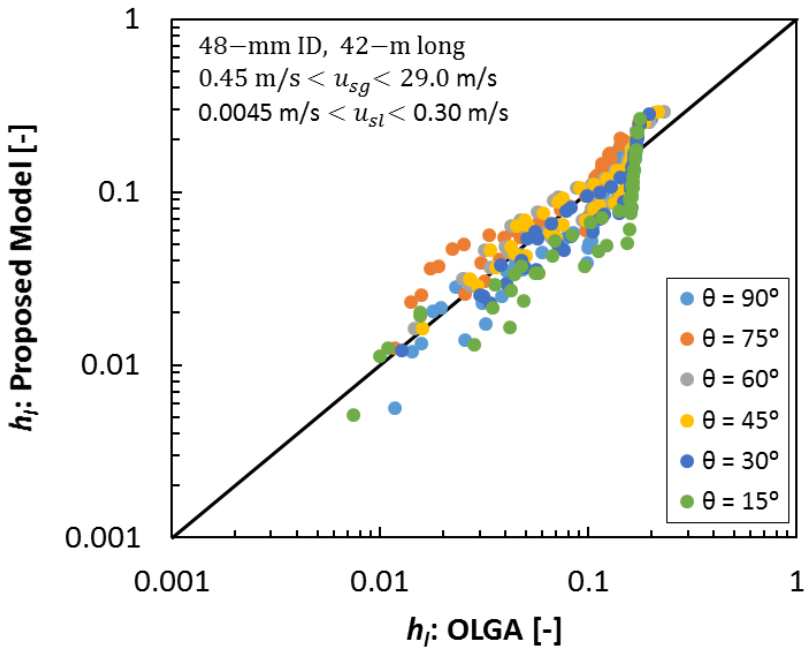

Fig. 4.11—Comparison of liquid hold-up predicted by OLGA to the suggested method with various pipe deviation angles.

While observed results of liquid holdup in deviated pipe from the larger-scale facility are not available, we performed numerical experimentations of two-phase flow for various tube deviations using OLGA model. The calculation results of **Eqs. 4.11** to **4.15** are compared with the prediction of OLGA, shown in **Fig. 4.11**. It can be observed that the proposed model has a fair agreement with OLGA while maintaining monotonic liquid holdup profile.

Pressure Drop Model

The steady-state two-phase pressure gradient is expressed as the sum of gravitational, frictional, and accelerational pressure gradients,

$$-\left(\frac{dp}{dz}\right)_{tp} = -\left[\left(\frac{dp}{dz}\right)_{G} + \left(\frac{dp}{dz}\right)_{F} + \left(\frac{dp}{dz}\right)_{A}\right] \tag{4.16}$$

The gravitational pressure drop accounts for the weight of the fluids in the two-phase mixture. The gravitational and accelerational pressure gradients can be expressed as,

$$-\left(\frac{dp}{dz}\right)_{G} = g\,\rho_{tp}\sin\theta \tag{4.17}$$

$$-\left(\frac{dp}{dz}\right)_{A} = \rho_{tp}u_{tp}\left(\frac{du_{tp}}{dz}\right) \tag{4.18}$$

where the two-phase velocity, $u_{tp} = u_{sg} + u_{sl}$. The two-phase mixture density is the total mass divided by the total volume, and hence it is irrelevant whether the liquid is in the form of droplet or film.

The homogenous frictional pressure gradient is commonly expressed as,

$$-\left(\frac{dp}{dz}\right)_{F} = 2f_{tp}\rho_{tp}u_{tp}^{2}/D \tag{4.19}$$

The two-phase Fanning friction factor, f_{tp}, depends on the laminar-turbulent characteristics of the system represented by the two-phase Reynolds number, $Re_{tp} = \rho_{tp}u_{tp}D/\mu_{tp}$, and in some cases the relative pipe roughness, ε. The two-phase mixture

viscosity, μ_{tp}, is commonly expressed in a similar way as the ρ_{tp}, such that, $\mu_{tp} = h_l\mu_l + (1 - h_l)\mu_g$. In most wellbore calculations the acceleration term can be neglected.

The **Eqs. 4.17** and **4.18** are well-known to reproduce gravitational and accelerational pressure drops in a way resembling the dependency on the liquid holdup. Several authors presented the experimental results of overall pressure gradient as a function of superficial gas velocity (Waltrich et al. 2013; Yuan et al. 2013; Li et al. 2014; Lumban-Gaol and Valkó 2014; Luo et al. 2014; Guner et al. 2015). Although the presented results may be in a magnitude difference, the trend follows that of the liquid holdup. As discussed earlier that the prevalence of a particular flow pattern does not affect the trend, and hence, the "jump conditions" are not needed. The overall pressure gradient is gradually decreasing as gas flow rate decreases when the frictional pressure gradient dominates the system. It reaches its minimum before the gravitational related forces start to be the dominant component.

We found that while most of the commonly used two-phase flow models may be able to predict the overall pressure gradient in an acceptable manner, the share of the individual pressure gradient components in the total is not always realistic especially in the vicinity of liquid loading conditions.

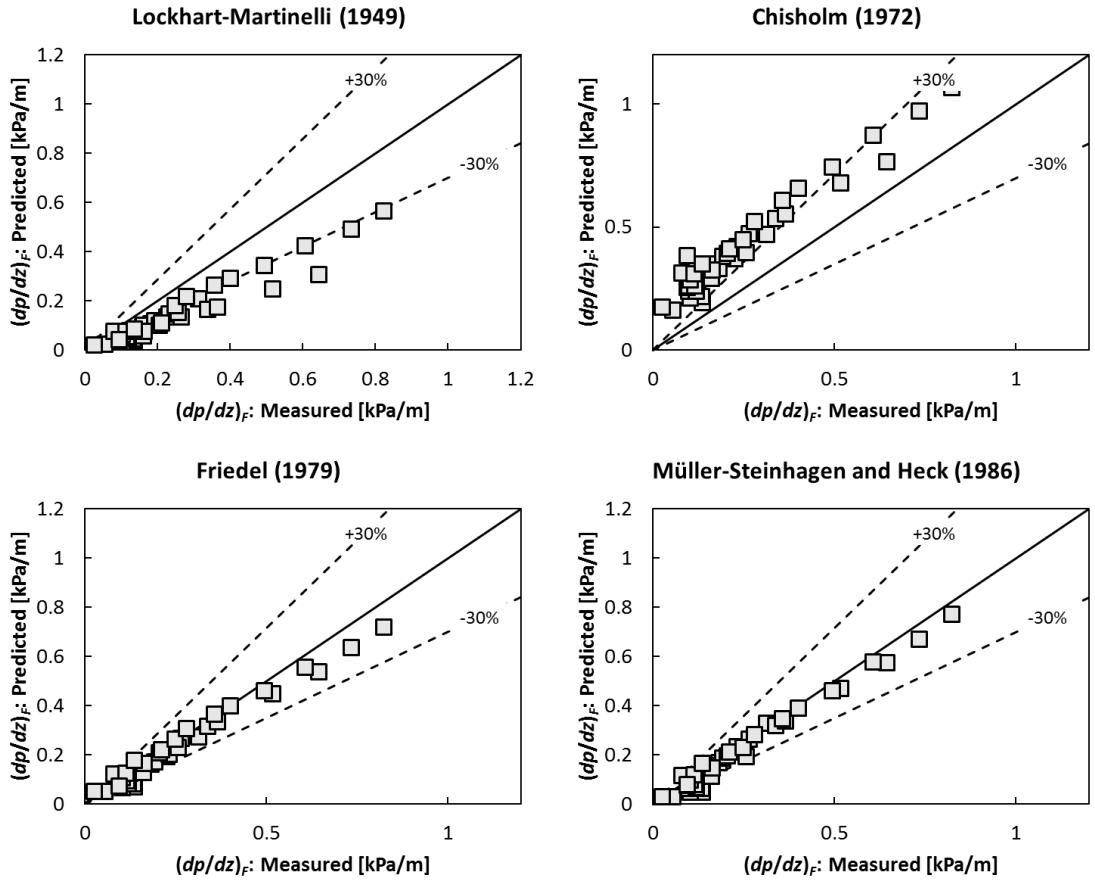

Fig. 4.12—Comparison of frictional pressure gradient predicted by various models with our measurement results.

In this study, we put special emphasize on the several existing frictional pressure gradient models, namely a group of separated flow models. The existing correlations presented here are based on the semi-empirical work of Lockhart and Martinelli (1949) and have been tested thoroughly against substantial experimental data. **Fig. 4.12** depicts a summary of the performances of select two-phase frictional pressure gradient models against our experimental results.

Table 4.1—Performance of selected frictional pressure gradient correlations.

	$RMS = \sqrt{\frac{1}{n}\sum_{1}^{n}\left(\frac{\Delta p_{F,exp} - \Delta p_{F,calc}}{\Delta p_{F,exp}}\right)^2} \times 100\%$
Lockhart and Martinelli (1949)	45.3
Chisholm (1973)	144.7
Friedel (1979)	22.1
Müller-Steinhagen and Heck (1986)	22.3

The statistical performance in the form of root mean squared percentage error (RMS) of the selected correlations is provided in the **Table 4.1**. It is shown that the correlations of Friedel (1979) and Müller-Steinhagen and Heck (1986) have acceptable accuracy compared to others. The Müller-Steinhagen and Heck (1986) correlation is more favorable because it was originally derived from a broader range of tubular diameter of 38 to 380 mm and significant amount of multiphase hydrocarbons flow data were used. The simplicity of the underlying correlation is also taken into consideration as most of the inputs are already pre-determined from the hold-up calculation.

The Müller-Steinhagen and Heck (1986) correlation is written as follow

$$-\left(\frac{dp}{dz}\right)_F = \left\{\left(\frac{dp}{dz}\right)_{F,l} + 2x\left[\left(\frac{dp}{dz}\right)_{F,g} - \left(\frac{dp}{dz}\right)_{F,l}\right]\right\}(1-x)^{1/3} + \left(\frac{dp}{dz}\right)_{F,g} x^3 \quad (4.20)$$

where $(dp/dz)_{F,g}$ and $(dp/dz)_{F,l}$ are the contributions from each phase to the overall frictional pressure gradient,

$$-\left(\frac{dp}{dz}\right)_{F,k} = \frac{2\, f_k\left(\rho_g u_{sg} + \rho_l u_{sl}\right)^2}{\rho_k D} \quad (4.21)$$

The subscript *k* denotes fluid phases, *l* and *g* for liquid and gas phases respectively. The friction factor, f_k is calculated with the Fanning friction model using the Reynolds number, $Re_k = \left(\rho_g u_{sg} + \rho_l u_{sl}\right)D/\mu_k$

$$\begin{gathered} f_k = 16\, Re_k^{-1} \text{ for } Re_k < 2000 \\ f_k = 0.079\, Re_k^{-0.25} \text{ for } 2000 \le Re_k < 20{,}000 \\ f_k = 0.046\, Re_k^{-0.2} \text{ for } Re_k \ge 20{,}000 \end{gathered} \quad (4.22)$$

Calculation Method for Long Pipes

The proposed combination of equations described above were originally derived from tubes with limited length to diameter ratios. In calculating the overall pressure loss along the gas production well, the ordinary differential equation of **Eq. 4.16** can be solved explicitly using Euler method. In this study, we discretize the tubing into N segments, when one segment length cannot exceed 42 m (the actual length of our experimental flow

path.) The tubing head conditions are selected as the initial value. The in-situ pressures are sequentially calculated from the tubing head to the end of tubing as follow

$$p_{i+1} = p_i + \Delta z \left(\frac{dp}{dz}\right)_{tp\ (i,\ i+1)} \tag{4.23}$$

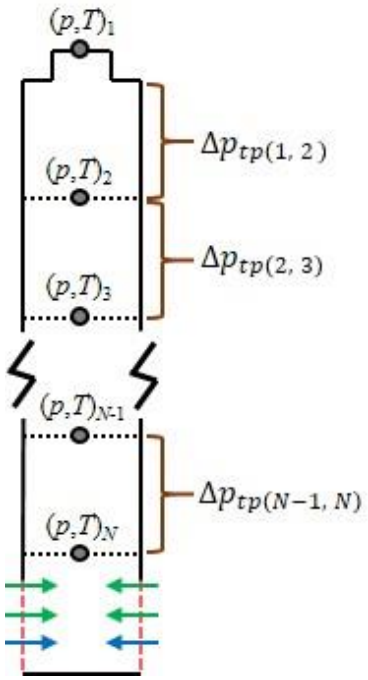

Fig. 4.13—Sequential flowing bottomhole pressure calculation from the tubing-head to the bottom of the well.

As illustrated in **Fig. 4.13**, i denotes the point at the start of each tubing segment where $i = 1$ is the tubing head location and $i = N$ is the bottomhole location. The two-phase pressure drop between locations i and $i + 1$, $(dp/dz)_{tp\ (i,\ i+1)}$, is calculated using fluid properties based on pressure, p, and temperature, T, at location i. The fluid properties are calculated using readily available correlations in the literatures described in **Appendix**

B. In summary, the overall pressure drop correlation requires only the knowledge of tube diameter, well deviation angle, phase volumetric flow rates, phase densities, and phase viscosities.

Conclusion

The new wellbore liquid content has been formulated based on the 46 steady-state and spatially-averaged holdup measurements conducted in a large scale experimental facility. The liquid content model takes into consideration the effects of partial flow reversal or liquid loading by embedding characteristic velocity into the correlation. Therefore, the new model does not distinguish sharp limit between "loading" and "not loading", rather, it is even more useable in monitoring the trends of overall liquid content and flowing bottomhole pressure.

The proposed liquid content model was paired with an existing frictional pressure gradient model which not only simple but also has capability in reproducing our 46 pressure gradient measurements within reasonable accuracy.

The overall wellbore model has been arranged such that observable surface parameters of gas wells are adequate for calculation. The inputs needed are limited to only gas and liquid flow rates, phase densities and viscosities, tubing size, and well geometry. Then, we can use a sequential calculation from wellhead to the bottom of the well to analyze the liquid content profile along the well over production time and to predict the corresponding flowing bottomhole pressure.

CHAPTER V

MODEL VERIFICATION*

Introduction

In this chapter, we consider first the performance of some previously recommended correlations in describing our 46 experiments. The existing correlations used as comparisons including flow-pattern-dependent of drift-flux type and some available well-known petroleum industry models. To avoid research bias, we consider both experimental and field data sets to be equally important. Therefore, the proposed model is validated against both type of data sets.

In general, flow-regime based models employ a specific equation for each individual flow pattern. Additionally, empirical constants may also differ from one flow type to another. Therefore, the liquid holdup as a function of gas rate may not form a smooth and continuous curve. In contrast, our model does not differentiate flow regimes despite they were visually distinguishable during experimental runs and observable through high frequency data analysis. Eventually, the complexity of forces acting in a particular flow pattern may be represented by a single parameter determining the overall pressure loss, which is liquid holdup. Therefore, it is crucial to further verify the new wellbore model

* Part of this chapter is reprinted with permission from "Liquid holdup correlation for conditions affected by partial flow reversal" by Lumban-Gaol, A. and Valkó, P.P., 2014. *International Journal of Multiphase Flow*, 6, 149-159 Copyright 2014 by Elsevier.

Table 5.1—Satisfactorily performing void fraction correlations according to Godbole et al. (2011).

Source	Correlation
Lockhart and Martinelli (1949)	$\alpha = \left[1 + 0.28\left(\frac{1-x}{x}\right)^{0.64}\left(\frac{\rho_g}{\rho_l}\right)^{0.36}\left(\frac{\mu_g}{\mu_l}\right)^{0.07}\right]$
Dix (1971)	$\alpha = \frac{u_{sg}}{C_0\left(u_{sg}+u_{sl}\right)+u_{gu}}$ $C_0 = \frac{u_{sg}}{u_{sg}+u_{sl}}\left[1+\left(u_{sl}/u_{sg}\right)^b\right]$ $b = \left(\rho_g/\rho_l\right)^{0.1}, \quad u_{gu} = 2.9\left(g\sigma\frac{\rho_l-\rho_g}{\rho_l^2}\right)^{0.25}$
Greskovich and Cooper (1975)	$\alpha = \frac{u_{sg}}{\left(u_{sg}+u_{sl}\right)+u_{gu}}$ $u_{gu} = 0.671\sqrt{gD}(\sin\theta)^{0.263}$
El-Boher et al. (1988)	$\alpha = \left[1 + 0.27\left(\frac{x}{1-x}\frac{\rho_l}{\rho_g}\right)^{-0.69}(Fr_{sl})^{-0.177}\left(\frac{\mu_l}{\mu_g}\right)^{0.378}\left(\frac{Re_{sl}}{We_{sl}}\right)^{0.067}\right]^{-1}$ $Fr_{sl} = \frac{u_{sl}^2}{gD}, Re_{sl} = \frac{\rho_l u_{sl} D}{\mu_l}, We_{sl} = \frac{\rho_l u_{sl}^2 D}{\sigma}$
Woldesemayat and Ghajar (2007a)	$\alpha = \frac{u_{sg}}{C_0\left(u_{sg}+u_{sl}\right)+u_{gu}}$ $C_0 = \frac{u_{sg}}{u_{sg}+u_{sl}}\left[1+\left(u_{sl}/u_{sg}\right)^b\right], b = \left(\rho_g/\rho_l\right)^{0.1}$ $u_{gu} = 2.9(1.22+1.22\sin\theta)^{p_{atm}/p_{sys}}\left[\frac{gD\sigma(1+\cos\theta)\left(\rho_l-\rho_g\right)}{\rho_l^2}\right]^{0.25}$

Performance Comparisons in Reproducing Our Experimental Data

Godbole et al. (2011) analyzed 52 void-fraction/holdup correlations and pointed to the one with the best predictive capability. The basis of their analysis was the holdup measurements using fast acting valves conducted on a 2.2-m long, 0.0127-m ID pipe ($L/D = 173$). Based on their observation, several void-fraction/holdup correlations including the ones presented in **Table 5.1** (represented as void fraction, α) are acceptable

to predict most of the experimental data. Most of the presented correlations are of the drift-flux type according to the classification of Levy (1999), and flow regimes independent. In general, the drift-flux model is expressed as a function of distribution parameter (C_0), drift velocity (u_{gu}), as well as gas and liquid superficial velocity:

$$\alpha = u_{sg}\left[C_0\left(u_{sg} + u_{sl}\right) + u_{gu}\right]^{-1} \tag{5.1}$$

The non-drift-flux correlations are represented as the contrast between gas and liquid viscosities (μ_g/μ_l) and dimensionless numbers of Froude (Fr_{sl}), Reynolds (Re_{sl}), and Webber (We_{sl}).

The 46-measured holdup points described in the previous chapter were reproduced using these approaches. The results shown in **Fig. 5.1** indicating reasonable agreement with the current experiments for lower holdup values, but all suggest systematic deviation for larger holdup values, where partial flow reversal has a strong effect.

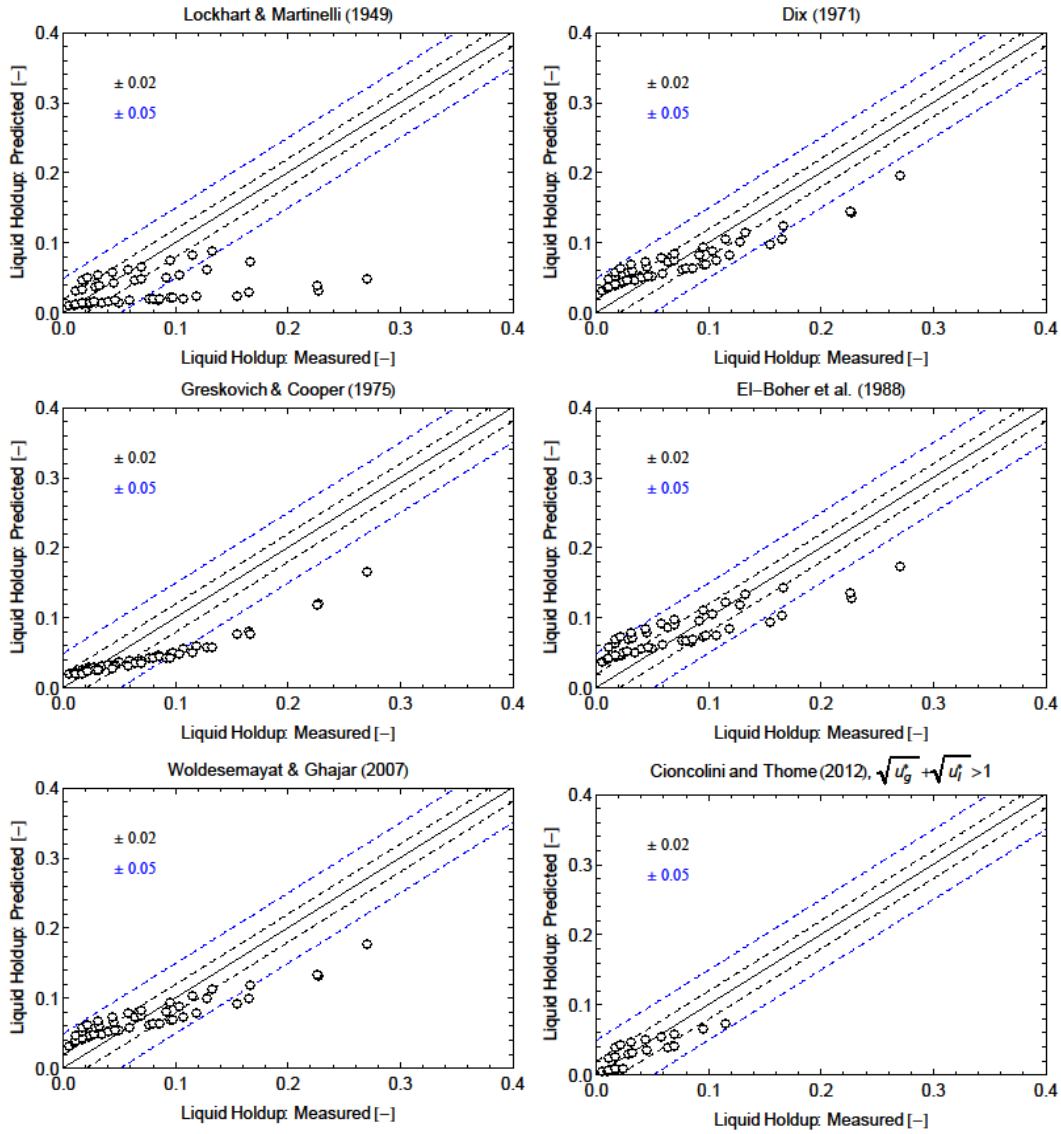

Fig. 5.1—Performance of various liquid holdup models against our measurement results.

It is worth noting that most of the existing experimental facilities were designed to measure liquid holdup instead of void fraction. However, because of the wide variety of industrial interest, researchers commonly derived void fraction correlation from liquid holdup data. Since in natural gas producing wells small difference in holdup has large

impact on flow mechanism, we present the comparison in the form of liquid holdup. Using void fraction or holdup should be interchangeable as far as only absolute units are used, but once relative deviations are involved the choice may affect the perception of goodness-of-fit.

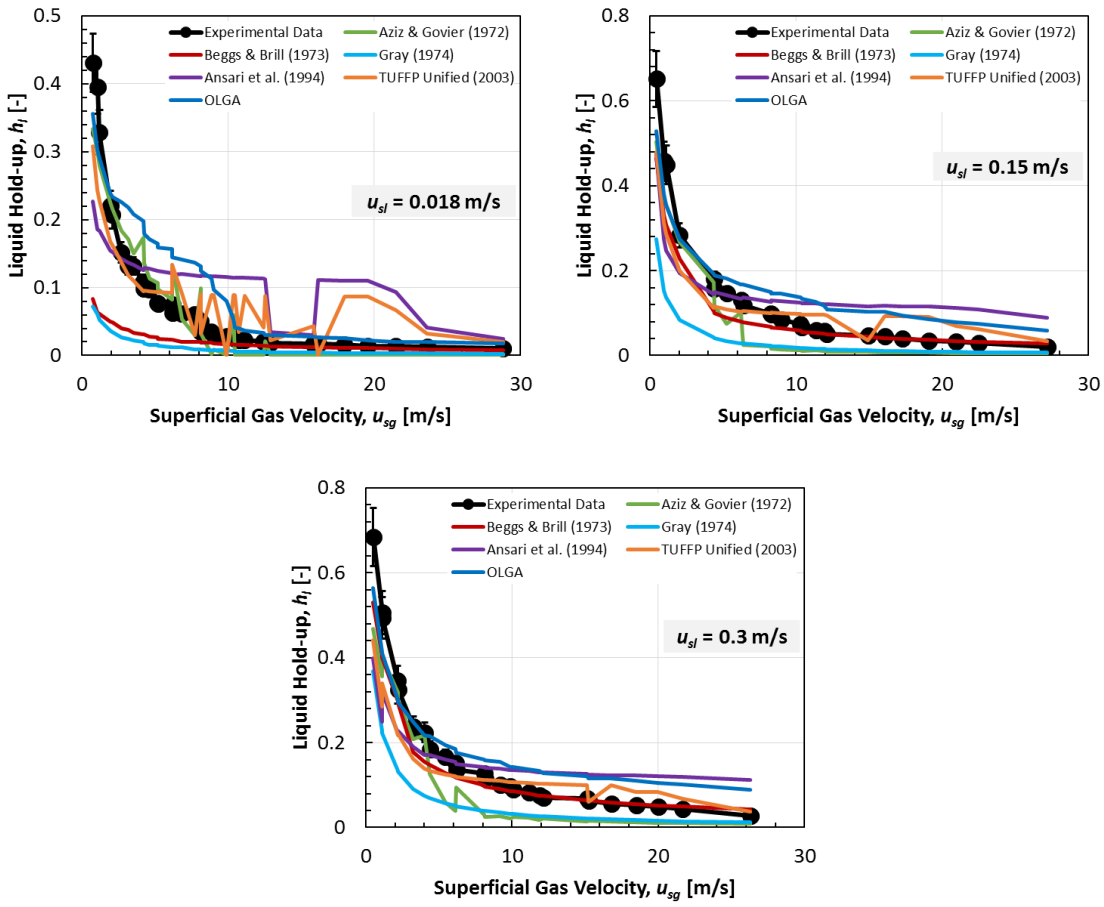

Fig. 5.2— Comparison of liquid holdup predicted by Beggs and Brill (1973), Gray (1974), Ansari et al. (1994), TUFFP unified model (Zhang et al. 2003a, b), and OLGA against the measurement results of Waltrich et al. (2013).

Liquid holdup through existing empirical and mechanistic models commonly used in petroleum industry may also be under/over-estimated depending on the various factors such as gas and liquid flow-rates. **Figs. 5.2 and 5.3** show the profiles of experimental and predicted holdup, h_l, as a function of superficial gas velocity, u_{sg}, with various superficial liquid velocities, u_{sl}. For higher liquid rates, both steady-state correlations as well as the two-fluid model (OLGA) provide a similar holdup trend. The actual holdup values can be slightly different, but corrections can still be made. However, the problem starts to appear at lower liquid flow-rates, where the flow-pattern based models result in hyper sensitivity to small changes of the inlet conditions.

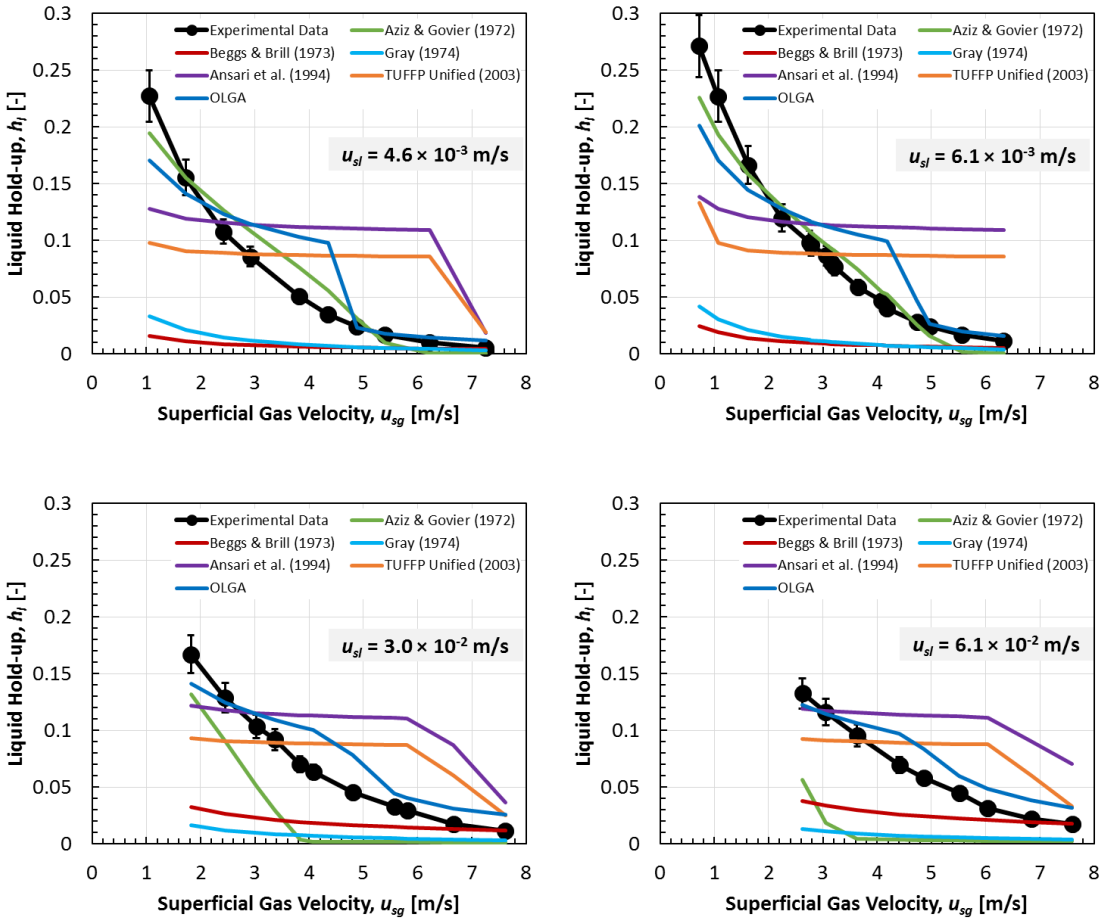

Fig. 5.3—Comparison of liquid holdup predicted by Beggs and Brill (1973), Gray (1974), Ansari et al. (1994), TUFFP unified model (Zhang et al. 2003a, b), and OLGA against our measurement results.

Fig. 5.4 also suggests the difficulties of existing petroleum engineering correlations in reproducing our holdup measurements. It can be seen that systemic deviation persists almost for all models. Most of the time, the existing models underestimate the holdup. This finding is of importance, considering underestimation of holdup leads to the underestimation of overall pressure drop inside the well.

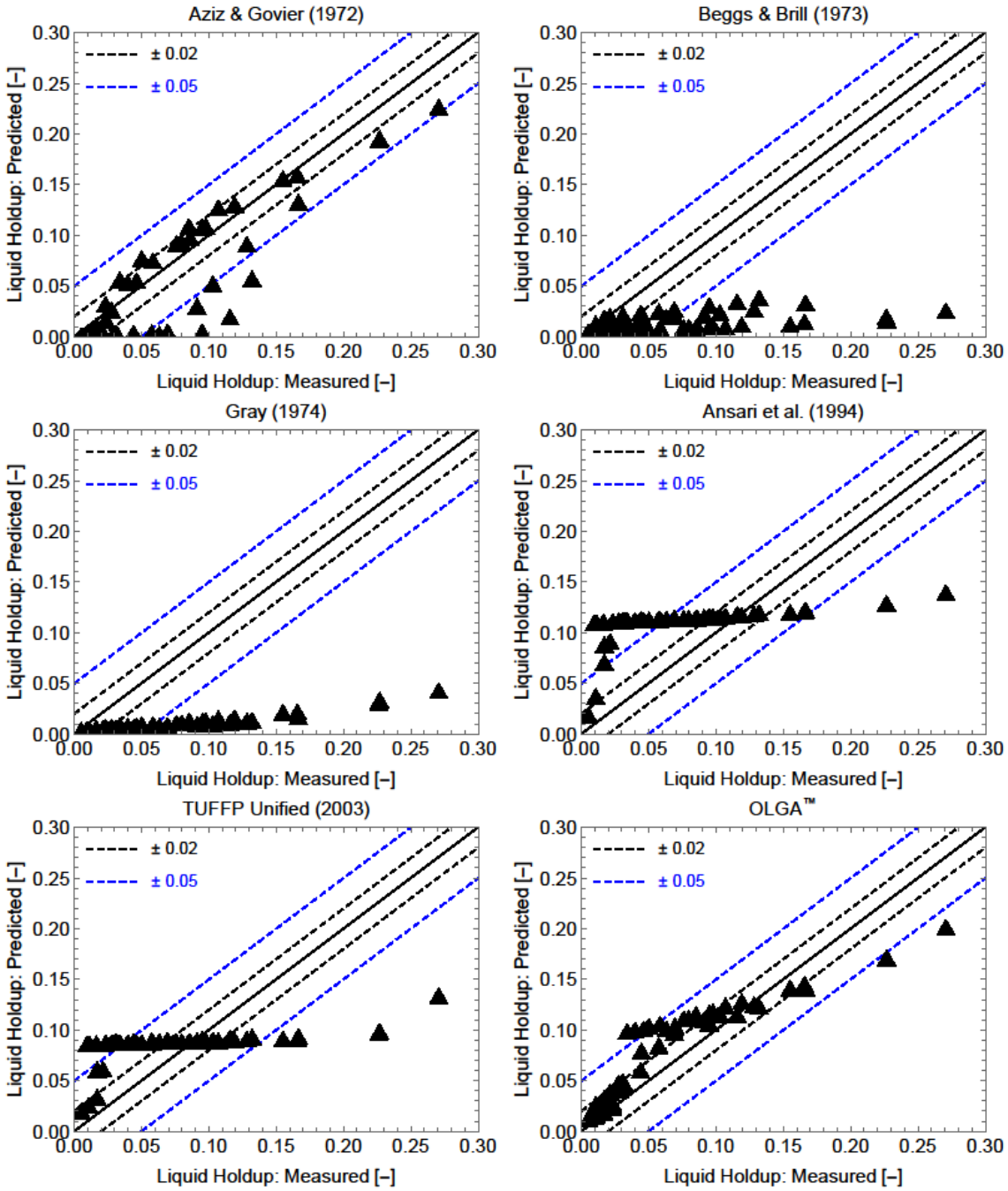

Fig. 5.4—Performance of various liquid holdup models commonly used in petroleum industry against our measurement results.

Table 5.2—Statistical comparison of satisfactorily performing correlations according to Godbole et al. (2011) based on 46-points included in **Appendix A**.

	$RMS\ error^a$ (%)	Percentage of data predicted within	
		± 0.02	± 0.05
Suggested model	7.2	100	100
Lockhart and Martinelli (1949)	69.7	37.0	67.4
Dix (1971)	119.0	37.0	89.1
Greskovich and Cooper (1975)	148.0	34.8	84.8
El-Boher et al. (1988)	58.8	45.7	71.7
Woldesemayat and Ghajar (2007b)	122.0	34.8	89.1
Cioncolini and Thome (2012)[b]	54.1	71.4	100

[a] $RMS\ error = \sqrt{\frac{1}{n}\sum_1^n \left(\frac{h_{l,exp} - h_{l,calc}}{h_{l,exp}}\right)^2} \times 100\%$

[b] Performed when flow conditions satisfy $\sqrt{u_g^*} + \sqrt{u_l^*} > 1$ and $h_l < 0.3$, 21 out of 46 points fall within this criterion.

The new prediction method explicitly taking into account the nearness of the $u_g^* \sim 1$ condition shows an improvement in holdup predictability. The statistical comparison between experimental and calculated holdup is shown in **Table 5.2 and Table 5.3**. The suggested model fits the present experimental data with RMS percentage error of 7% and 100% of the holdup points fall inside the ± 0.02 error band.

Table 5.3— Statistical comparison of correlations commonly used in petroleum industry based on 46-points included in **Appendix A**.

	$RMS\ error\ (\%)$	Percentage of data predicted within	
		± 0.02	± 0.05
Aziz and Govier (1972)	64.7	52.2	80.4
Beggs and Brill (1973)	73.5	30.4	52.2
Gray (1974)	83.4	23.9	45.7
Ansari et al. (1994)	275.0	19.6	47.8
TUFFP Unified (Zhang et al. 2003a, b)	200.0	32.6	63.0
OLGA	61.1	56.5	84.8

Of the various liquid holdup correlations commonly used in petroleum industry, it is not surprising that the OLGA model delivered more consistent results relatively to others. OLGA was originally developed as a two-fluid model where continuity and momentum equations are solved (Bendiksen et al. 1991). The gas and droplet flowing in the middle of the pipe is treated as a single fluid while liquid film is separated. Despite OLGA covers higher degree of two-phase flow complexity, the underlying frictional pressure drop still heavily relies on the flow regime determination. Therefore, we observed systemic deviation of OLGA model in comparison with our experimental results especially when the model confronted flow regime transition.

Validation Against Published Experimental Data Sets

For fairness, one has to admit that the model parameters (a, b) were obtained from the same 46 experiments, so some advantage is anticipated. Therefore, in the following we consider data not used in deriving the 2 model parameters.

Table 5.4—Experimental data used to verify the proposed liquid holdup correlation.

Author	Fluids	No. points	D (mm)	L/D	$\dot{m}$ (kgm^{-2}s^{-1})	x	u_g^*	h_l
Hall-Taylor et al. (1963)	Air-Water	18	31.8	211	33-64	0.40-0.80	0.86-2.19	0.02-0.05
Nguyen and Spedding (1977)	Air-Water	62	45.4	44	30-1060	0.07-0.93	0.31-3.46	0.01-0.17
Alamu and Azzopardi (2011)	Air-Water	36	19	368	66-194	0.10-0.47	1.08-3.46	0.01-0.06
Waltrich et al. (2013)	Air-Water	66	48.6	864	19-385	0.04-0.83	0.31-1.76	0.01-0.24
Liu (2014)	Air-Water	28	6	150	6-222	0.11-0.93	0.25-1.11	0.01-0.17

Published holdup data from various sources included in **Table 5.4** were used to check the performance of the proposed correlation. The reported experimental holdup data were selected based on the criterion that it should lie within one order of magnitude vicinity of u_g^*~1 and u_g^* is not less than 0.2 where fully developed slug flow is attained according to Owen (1986). Most of the underlying liquid holdup data were reported in the form of liquid holdup, void fraction or holdup ratio. In cases when only film thickness was available, the additionally required entrained liquid fraction was calculated using either the correlation of (Barbosa Jr et al. 2002), specifically designed for conditions near the annular to churn flow transition or of Azzopardi and Wren (2004) that covers wider flow conditions. A total of 265 measured holdup points (including our own 46 experimental

points) covering tube diameters between 6 to 49 mm were collected in this extended data set.

In addition to classifying the points in terms of "used in deriving the present model, or not" we also need to distinguish between "not affected" and "possibly affected" by partial flow reversal points. This is important for comparison with the so called minimum model of Cioncolini and Thome (2012). In the development of their correlation data were carefully filtered out if suspected to be affected by flow reversal, therefore it would be unfair to use their model for such points. Using the criterion proposed by Wallis (1969) , that is **Eq. 4.7** with the constants m and C set to unity, we find that, 191 out of the total 265 points can be considered "not affected" by flow reversal (representing "clearly annular flow").

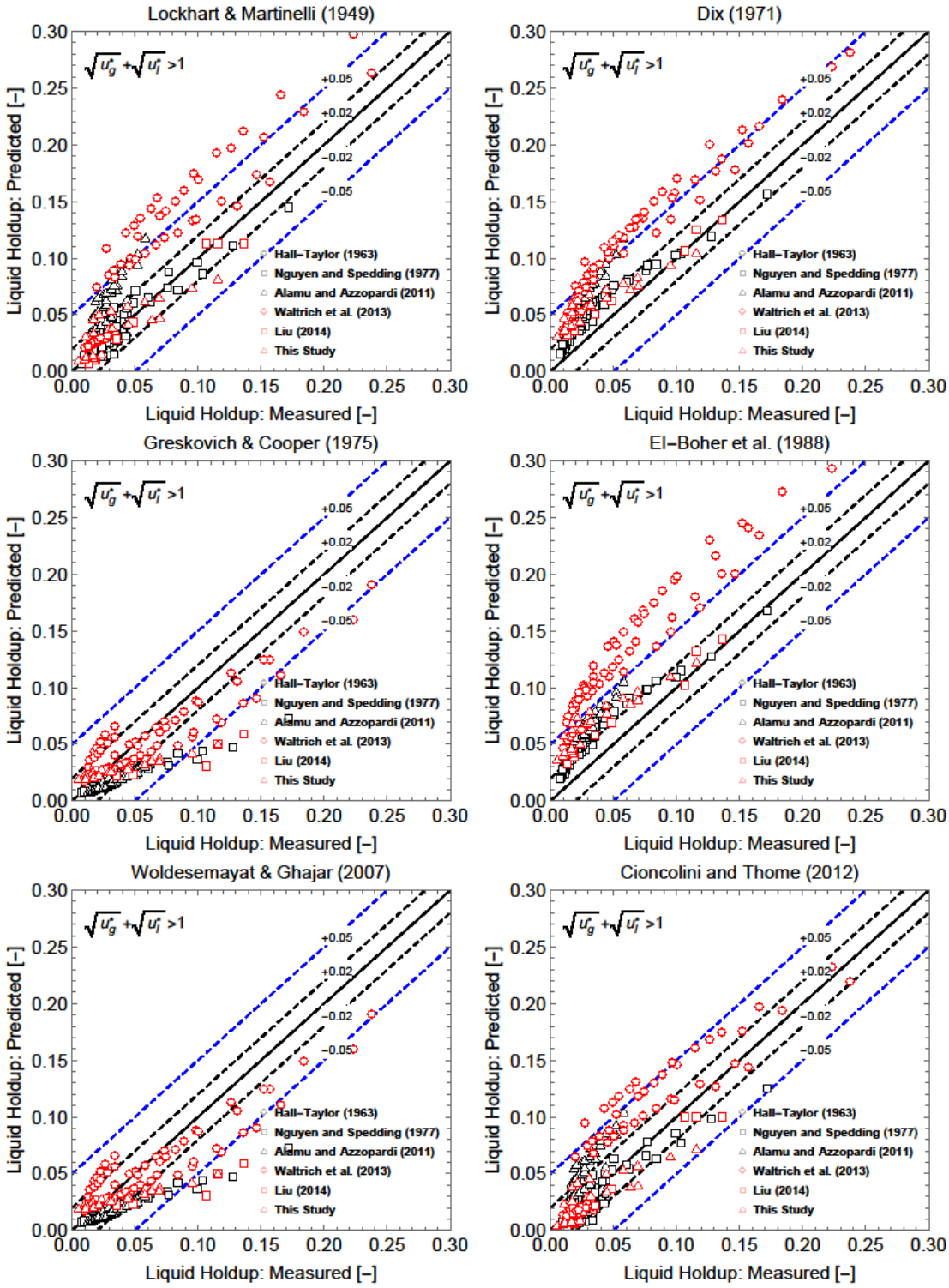

Fig. 5.5—Comparison of calculated liquid holdup using various methods in annular flow (not affected by flow reversal) where $\sqrt{u_g^*} + \sqrt{u_l^*} > 1$ (191-holdup points).

The comparison of measured and calculated liquid holdup for points in the extended data set exhibiting clearly annular flow is shown in **Figs. 5.5 and 5.6**. The prediction method of Cioncolini and Thome (2012) fits the data with an RMS percentage error of 67% and only 71 points out of 191 fall outside the ± 0.02 error band (defined in absolute units). The new method (see Chapter IV) describes the same points somewhat better, with root mean squared percentage error of 54% with only 45 points out of 191 falling outside the ± 0.02 error band. **Table 5.5** shows the statistical comparison between various prediction methods including the new proposed model.

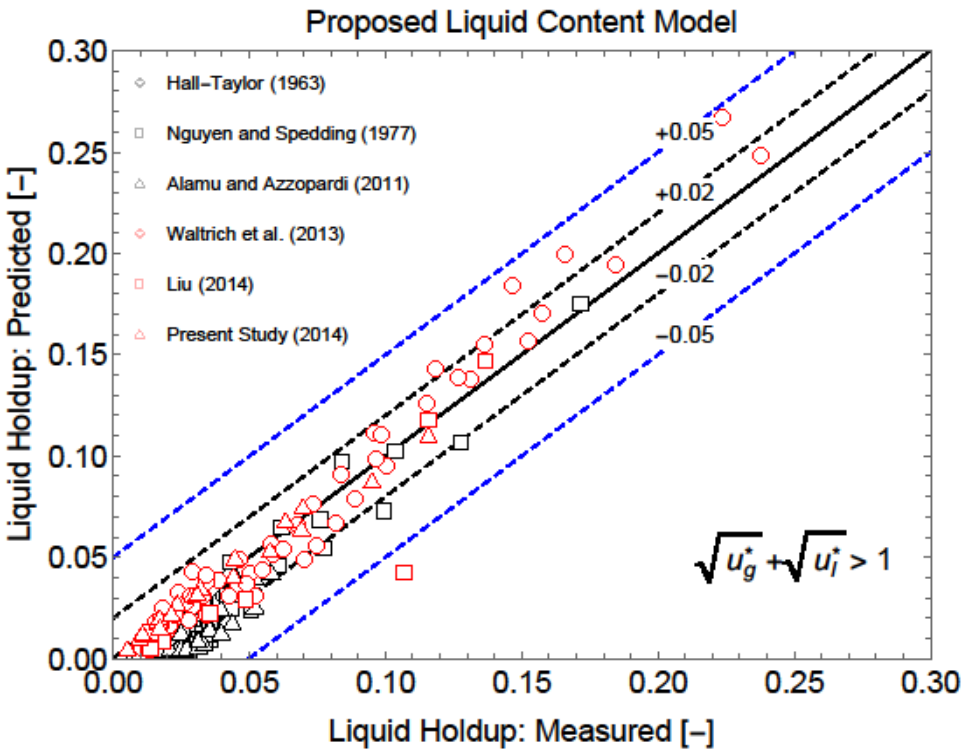

Fig. 5.6—Comparison of calculated liquid holdup using the suggested wellbore liquid content model in annular flow (not affected by flow reversal) where $\sqrt{u_g^*}+\sqrt{u_l^*}>1$ (191-holdup points).

Table 5.5—Statistical comparisons based on 191-points exhibiting annular flow (not affected by flow reversal) shown in **Figs. 5.5** and **5.6**, satisfying condition of $\sqrt{u_g^*} + \sqrt{u_l^*} > 1$.

	$RMS\ error\ (\%)$	Percentage of data predicted within	
		± 0.02	± 0.05
Suggested model (Chapter IV)	53.8	76.4	99.5
Lockhart and Martinelli (1949)	83.6	60.7	85.3
Dix (1971)	127.0	26.7	79.6
Greskovich and Cooper (1975)	51.4	72.8	93.2
El-Boher et al. (1988)	154.0	15.2	71.7
Woldesemayat and Ghajar (2007b)	112.0	36.6	90.1
Cioncolini and Thome (2012)	67.5	62.8	96.3

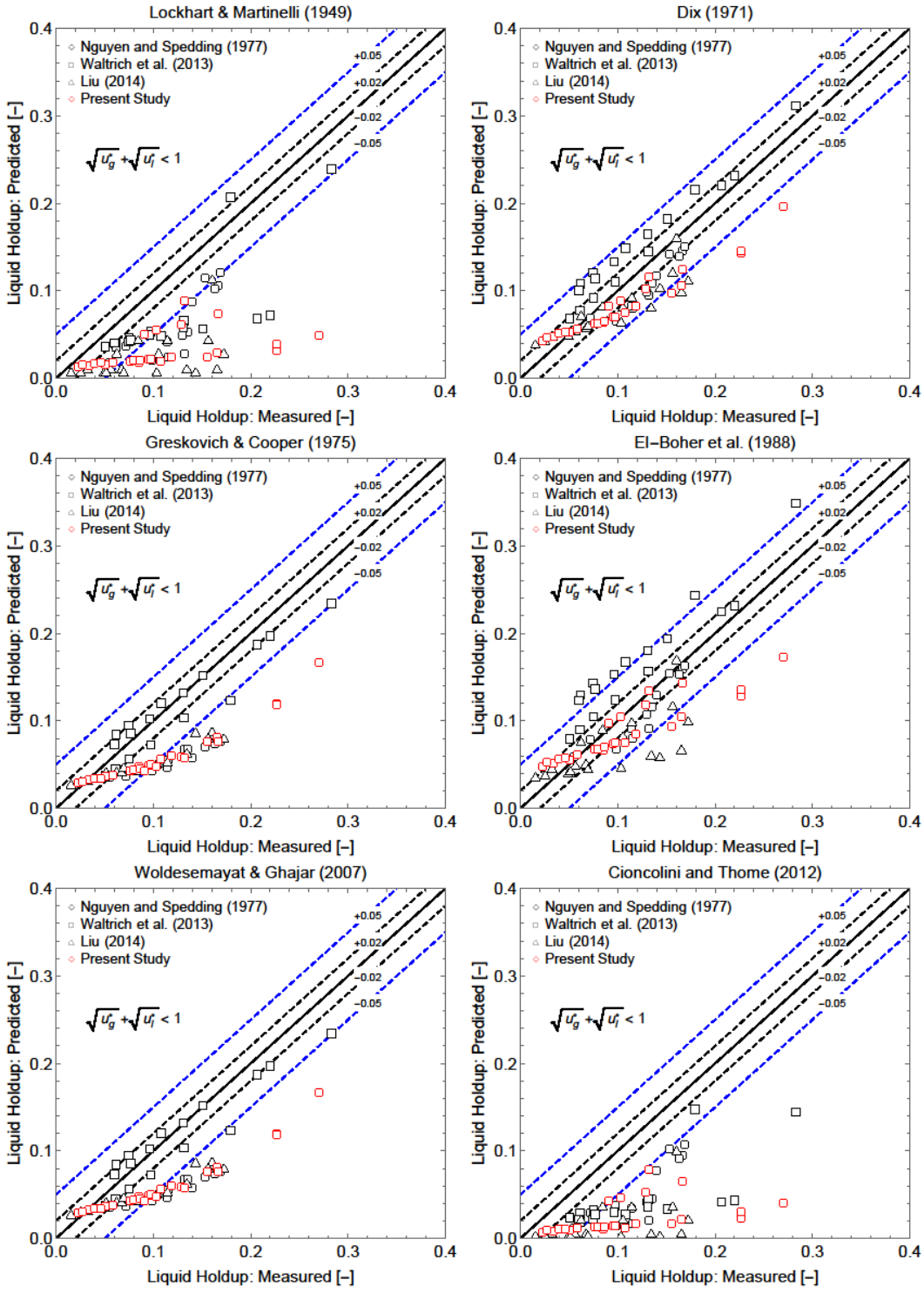

Fig. 5.7—Comparison of holdup data affected by flow reversal $\left(u_g^* > 0.2 \text{ and } \sqrt{u_g^*} + \sqrt{u_l^*} < 1\right)$ with calculated liquid holdup using various methods (74-holdup points).

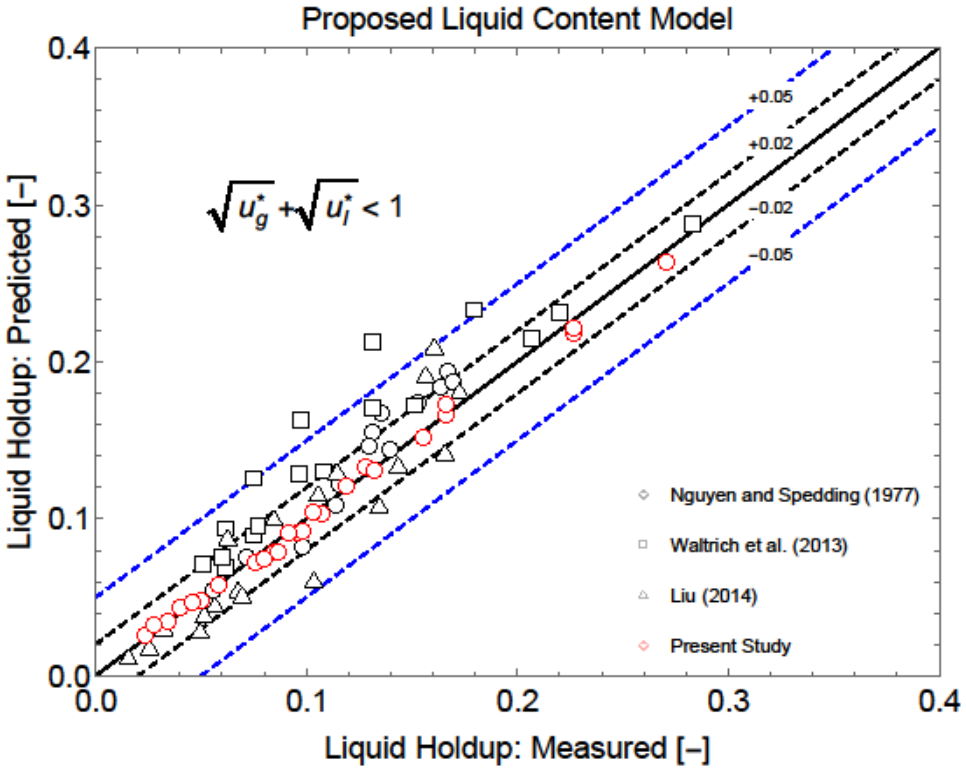

Fig. 5.8—Comparison of holdup data affected by flow reversal $\left(u_g^* > 0.2 \text{ and } \sqrt{u_g^*} + \sqrt{u_l^*} < 1\right)$ with calculated liquid holdup using the proposed liquid content model (74-holdup points).

The comparison of measured and calculated liquid holdup for points in the extended data set affected by flow reversal is shown in **Figs. 5.7** and **5.8**.

Table 5.6—Statistical comparisons based on 74-points affected by flow reversal (including 25 points out of 46 from present study) shown in **Figs. 5.7** and **5.8**, satisfying the conditions of $u_g^* > 0.2$ and $\sqrt{u_g^*} + \sqrt{u_l^*} < 1$.

	$RMS\ error$ (%)	Percentage of data predicted within	
		± 0.02	± 0.05
Suggested model (Chapter IV)	22.0	89.5	98.4
Lockhart and Martinelli (1949)	65.4	63.9	79.1
Dix (1971)	34.4	78.0	95.8
Greskovich and Cooper (1975)	41.8	72.8	83.2
El-Boher et al. (1988)	41.7	79.1	90.6
Woldesemayat and Ghajar (2007b)	33.2	79.1	93.7
Cioncolini and Thome (2012)	75.5	62.8	73.3

The statistical comparison between experimental data affected by flow reversal (74 out of 265 data points included in **Table 5.4** and **Appendix A**) and calculated holdup is shown in **Table 5.6**. In general, the suggested model fits the experimental data affected by flow reversal in a satisfactory manner: with 22% RMS percentage error, and 90% of the points falling inside the ± 0.02 error band. The latter fact is even more important, because the 22% RMS percentage error is unfavorably affected by a few near zero holdup observations. The results also verify the accuracy of the Cioncolini and Thome (2012) correlation beyond its recommended flow range, where low accuracy of holdup prediction is expected in the presence of flow reversal.

We conclude that when the flow is affected by flow reversal, our new correlation provides significant improvement. It can be used at dimensionless gas velocities as low as

0.2. Such a feature is especially desirable for modeling liquid loading related phenomena in natural gas producing wells.

Table 5.7—Multiphase flow parameters of 78 gas wells published by Oden and Jennings (1988).

Properties	Unit	Minimum	Maximum
Gas Rate	Mscf/d	460	27,400
Oil Rate	stb/d	0	1,300
Water Rate	stb/d	0	2,000
GOR	Mscf/stb	0	1,170
Gas Gravity	-	0.593	0.884
Oil Gravity	-	0.62	0.931
H2S	mol%	0	18.52
CO2	mol%	0	7.1
N2	mol%	0	4.45
Well Depth	ft	7,237	21,453
Tubing ID	inch	1.61	3.96
Surface Temperature	F	67	188
Bottomhole Temperature	F	168	322
Surface Pressure	psia	806	9,438
Bottomhole Pressure	psia	1,587	11,890

Validation Against Gas Wells Data

The ultimate goal of the new model is to capture the progression of overall liquid accumulation inside the well and assessing the flowing bottomhole pressure during condition prevailing the liquid loading phenomena. The gradual change of liquid-content then can be observed in advance, before yielding a significant negative impact on the well

productivity. It is advantageous for production engineers to have this crucial information, because early actions can be performed to prevent unfavorable situations.

Although the liquid-content model has been tested against extended experimental data set in the previous section, it is essential to verify it under producing gas well conditions. For fairness, published old-dated data from Oden and Jennings (1988) consisting of 78 vertical gas wells are used for this purpose. The notable multiphase parameters are shown in **Table 5.7**. The data are characterized by wide ranges of pressure, temperature, as well as liquid rate. Since temperature profiles are not available, we use linear interpolation. The gas and liquid rates were recorded at the surface. All of the wells were reported producing without artificial lift and not experiencing liquid loading.

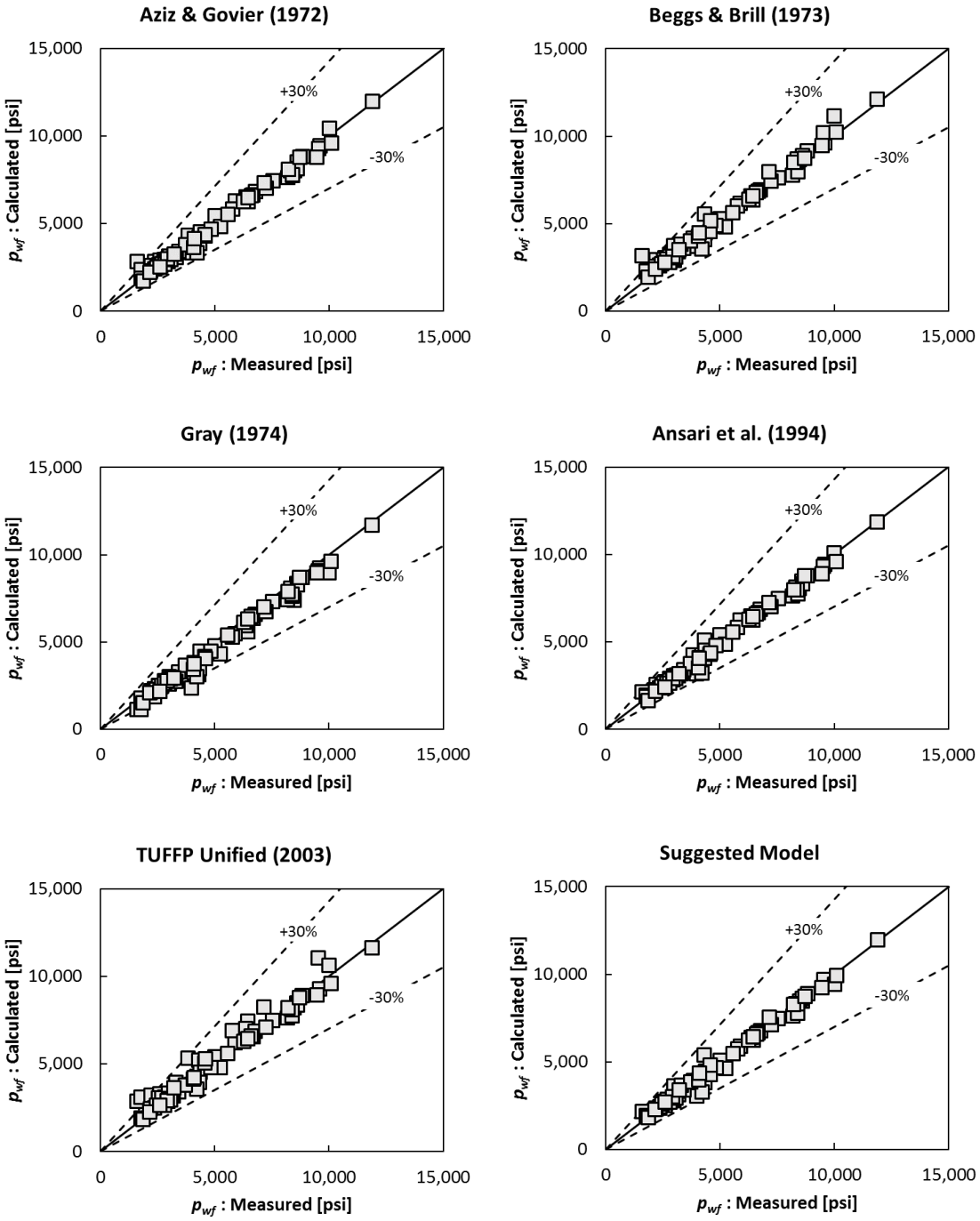

Fig. 5.9— Comparison of calculated and measured flowing bottomhole pressures using the data published by Oden and Jennings (1988).

The performance of the proposed method is illustrated in **Fig. 5.9** and **Table 5.8**, compared to the existing two-phase models. In general, all of the models predict the flowing bottomhole pressure, p_{wf}, in an acceptable manner. The suggested method yields RMS error close to 7% and hence performs as well as the Ansari et al. (1994) model. Moreover, the proposed model significantly improves the accuracy for the wells with gas rate, q_g, and total liquid rate, q_l, less than 1 MMscf/D and 50 stb/D, respectively. It is important to emphasize these lower gas and liquid rates because the chance of liquid loading occurrence is higher within these limits. These results also corroborate the applicability of the new method for cases where condensate is co-produced.

Table 5.8—Statistical comparisons of flowing bottomhole pressure based on published 78 gas wells data of Oden and Jennings (1988).

	$RMS\ error$ (%)		
	All 78 wells	$q_g < 1$ MMscf/D	$q_l < 50$ stb/D
Suggested Model (Chapter IV)	7.4	13.5	2.7
Aziz and Govier (1972)	11.3	31.0	8.7
Beggs and Brill (1973)	15.2	36.6	12.2
Gray (1974)	11.8	19.4	7.1
Ansari et al. (1994)	7.3	13.9	6.0
TUFFP Unified (Zhang et al. 2003a, b)	17.0	43.4	19.8

Conclusion

The new liquid content model has been verified against published experimental and field data sets, and its predictive capability was compared against several existing two-phase models. The existing flow pattern dependent models show difficulties in reproducing our 46-holdup measurements. Inconsistencies were observed around gas velocities near to flow regime transitions. This observation is in agreement with the findings of Yuan et al. (2013), Guner et al. (2015), and Skopich et al. (2015).

The gathered experimental data sets was partitioned into two. First, data points satisfying the condition of clearly annular flow or when the system is not affected by partial flow reversal. The suggested model reproduced these points within an acceptable accuracy although data sets cover various flow loop dimensions and flow rates. Second, data points that were affected by partial flow reversal, by means of flow regimes other than a clear annular flow. The new model performed even better than most of the existing correlations.

The new wellbore model gave an acceptable accuracy in predicting the flowing bottomhole pressure of gas wells not affected by liquid loading condition. Although the model emphasizes particular condition of partial flow reversal, it can be concluded that our model can also be used under normal operating conditions of producing gas wells. In other words, the new model is actually a two-phase wellbore model comparable to existing wellbore models/correlations.

CHAPTER VI

FIELD DIAGNOSTICS

Introduction

In this chapter, we present the application of the new wellbore model in analyzing and diagnosing liquid loading in gas wells. The following examples from Fayetteville shale involve 22 deviated gas wells. The well data consisted of surface gas and water production rates, tubing head pressure, p_{th}, operational history, and several flowing bottomhole pressure measurements. Condensate were not reported to be present in these 23 wells.

The notable well parameters are shown in **Table 6.1**. Several wells were reported already producing with artificial lift (such as plunger lift, gas lift, surface compression, or surfactants) to lessen the occurrence of liquid loading. It can be seen that artificial lifts have been implemented in all of the wells with average gas production of less than 500 Mscf/D.

Table 6.1—The 22 gas producing wells experiencing liquid loading.

Well Name	Producing Method	Average Gas Rate (Mscf/D)	Average Water Rate (bbl/D)	Producing Time (days)	Shut-in Time (days)
AH-1	FOAMER	207.3	1.7	2916	54
AH-2	PLUNGER	254.5	9.4	2534	303
AH-3	PLUNGER	262.1	22.5	2075	430
AH-4	GAS LIFT	276.2	3.3	2458	317
AH-5	COMPRESSION	413.2	5.7	1407	65
AH-6	PLUNGER	425.7	6.4	2657	73
BH-1	NATURAL FLOW	542.9	25.0	895	698
BH-2	FOAMER	653.6	31.6	862	31
BH-3	NATURAL FLOW	667.4	10.5	1453	46
BH-4	NATURAL FLOW	672.0	28.5	1210	588
BH-5	NATURAL FLOW	719.4	24.1	1187	124
BH-6	NATURAL FLOW	731.0	2.0	1481	88
BH-7	GAS LIFT	780.5	402.6	431	1191
BH-8	FOAMER	781.0	26.7	1186	5
BH-9	NATURAL FLOW	964.3	9.6	2287	88
BH-10	FOAMER	977.2	6.5	2293	60
BH-11	PLUNGER	988.2	13.7	1626	484
CH-1	FOAMER	1060.3	12.3	1953	548
CH-2	NATURAL FLOW	1074.1	26.0	1214	42
CH-3	NATURAL FLOW	1127.4	14.4	1106	186
CH-4	PLUNGER	1257.7	46.3	2007	106
CH-5	NATURAL FLOW	1732.1	74.5	613	53

The flowing bottomhole pressure was measured using the techniques for acoustic liquid level analysis (McCoy et al. 2009). First, a gas gun delivers high pressure wave down the well and the acoustic trace is recorded. The travel time of this wave provides indication of the quantity of liquid that is rest in the well (tubing or annulus) or the degree of uniformity of liquid distribution along the well. Distinguishable features of various flow regimes may be observable, especially when the gas rate is low enough which allows the development of bubbly or slug flow at the deeper part of the well. These flow regimes

contribute to a very high local liquid content and denote sharp fluctuations in acoustic feedback. The pressure gradient distributions in a flowing gas well then can be determined hence the approximate flowing bottomhole pressure.

In this chapter, the liquid loading diagnostic processes are first started with the effort to reproduce the reported flowing bottomhole pressure measurement results. We use the methods of Beggs and Brill (1973) and Gray (1974) in comparison with our model. These existing models were selected based on their wide acceptance in petroleum industry. Additionally, they represent flow-pattern-dependent and flow-pattern-independent correlations. The Beggs and Brill (1973) and Gray (1974) correlations are described in details in **Appendix C and D**, respectively.

Prediction of Flowing Bottomhole Pressure

In analyzing wellbore liquid content and pressure gradient in a gas well, one must consider the existence of a particular artificial method because the applied external forces and/or chemical will give change to the well behavior. For instance, dripping surfactant down the well will ultimately change the interfacial tension in two-phase system and hence liquid holdup and pressure gradient. Similarly occurred for the well with plunger or surface compression where system pressure is interrupted. However, most of the simplified two-phase models may not perform well under artificial lift conditions without introducing some correction factors. Traditionally, a correction factor is usually "hard-coded" in a liquid holdup correlation, by means of manipulating the original calculated holdup to obtain minimum error in p_{wf} difference. In this study we limit our analysis using

only original forms of two-phase correlations because the available bottomhole pressure data from acoustic measurement has greater uncertainty compared to permanent measuring device.

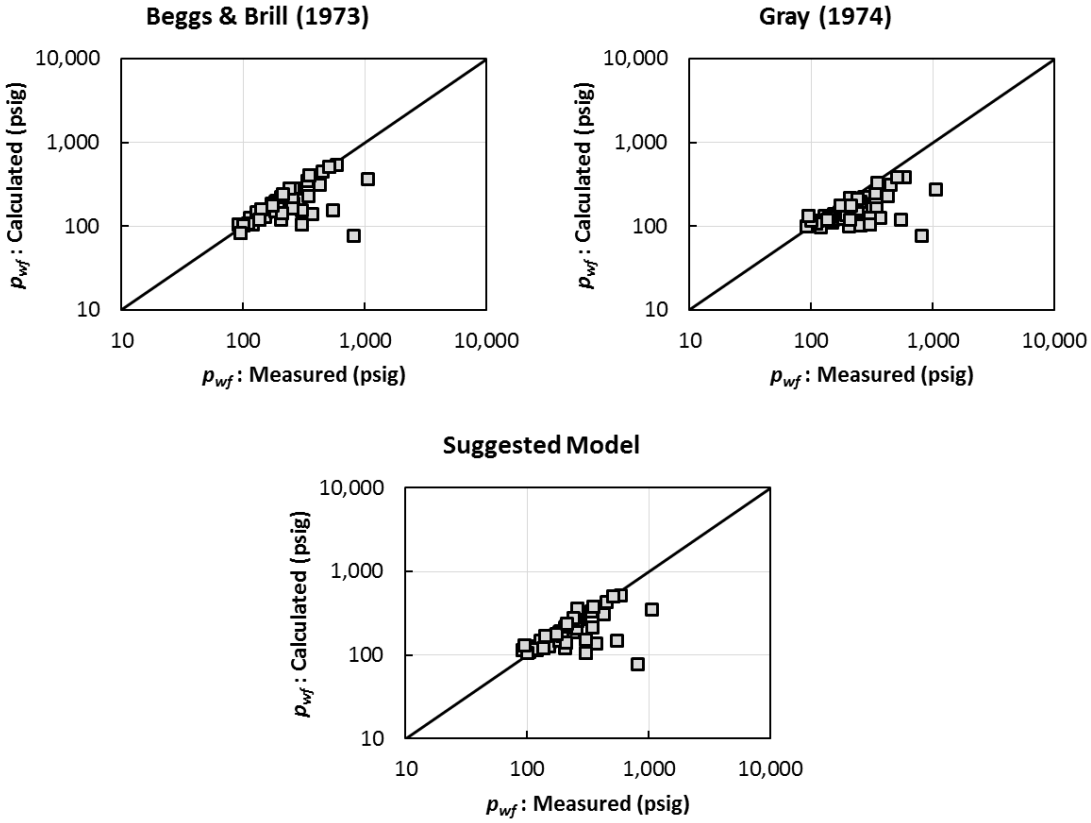

Fig. 6.1—Comparison of measured and calculated flowing bottomhole pressure for natural flow wells listed in Table 6.1.

The capability of our model in reproducing measured flowing bottomhole pressure in comparison with existing models for naturally flowing gas wells included in Table 6.1 and shown in **Fig. 6.1**. Similarly shown in **Fig. 6.2** for wells that have artificial lifts. We

only take in data points that fulfill our region of interests which mainly is the gas velocity of $u_g^* > 0.2$.

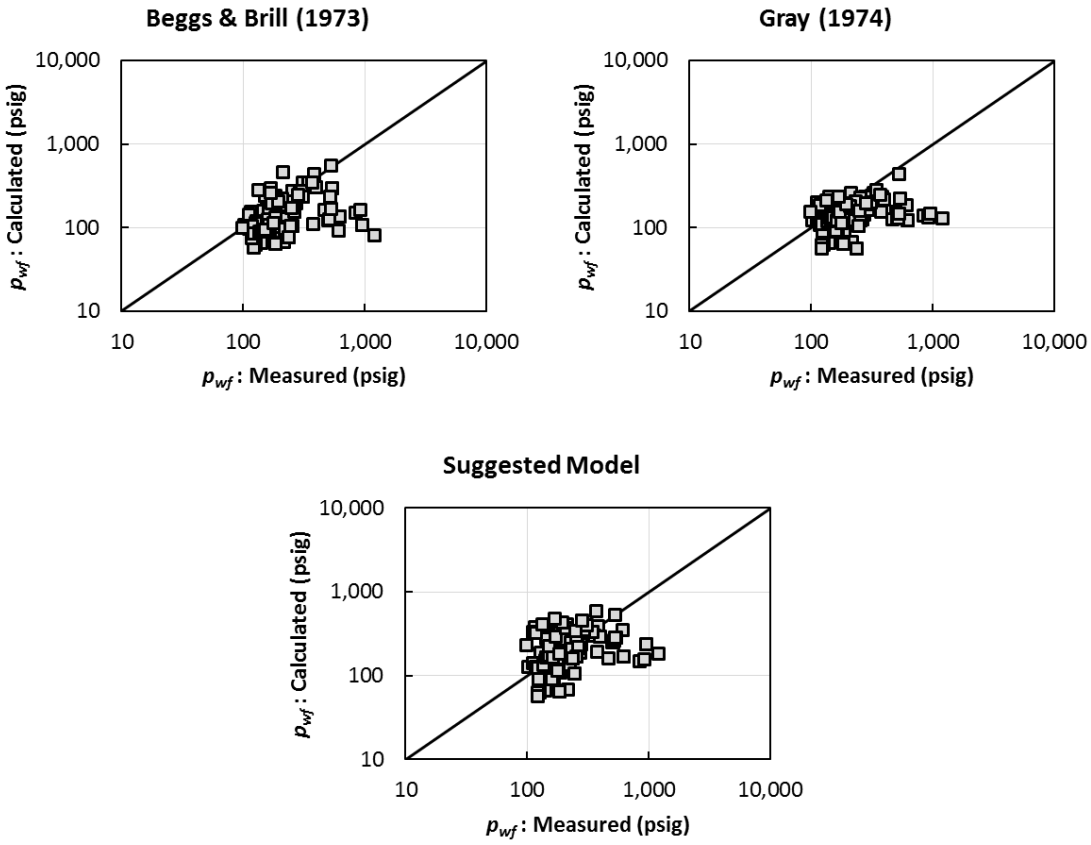

Fig. 6.2—Comparison of measured and calculated flowing bottomhole pressure for wells with artificial lifts listed in Table 6.1.

Statistical comparison is indicated in **Table 6.2**. It can be seen that without artificial lifts, all models are generally acceptable to be used to predict flowing bottomhole pressure. However, the question is whether these two-phase models provide realistic contributions from each pressure loss components. Additionally, the model must be able

to present the gradual increase of liquid content way before liquid loading symptoms become severe. Therefore, in the next sections we demonstrate the use of the new wellbore model in analyzing liquid loading situations and corresponding flowing bottomhole pressure behavior in gas wells producing without and with artificial lift.

Table 6.2—Statistical performance of two-phase correlations against 22 gas wells experiencing liquid loading described in Table 6.1.

	$Error^a$ (%)	RMS^b (%)
Natural Flow		
Proposed Model	-7.7	30.1
Beggs and Brill (1973)	-10.7	25.5
Gray (1974)	-23.6	58.2
Artificial Lifts		
Proposed Model	5.2	82.9
Beggs and Brill (1973)	-23.4	43.9
Gray (1974)	-26.6	77.2

$$^{a}Error = \frac{\left(p_{wf,\text{calc}} - p_{wf,\text{meas}}\right)}{p_{wf,\text{meas}}} \times 100\%$$

$$^{b}RMS = \sqrt{\frac{1}{n}\sum_{1}^{n}\left(\frac{\Delta p_{F,exp} - \Delta p_{F,calc}}{\Delta p_{F,exp}}\right)^2} \times 100\%$$

The proposed model also delivers more acceptable results compared to other models in the presence of artificial lift. Despite the expected higher RMS, the actual

relative error of 5% is a promising indication that the new model has no tendency to over-predict or under-predict the overall pressure loss.

Natural Flow Producers

In this section, we apply the new wellbore model for wells that can be categorized as low and high producers, but still flowing naturally. Two wells, namely BH-1 and CH-2, were selected to showcase these categories. The 30-day average initial gas production rates of well BH-1 and CH-2 were 1,564 and 4,278 Mscf/D, respectively, so we call the first well "low producer" and the second well "high producer". The rest of the wells, meanwhile, were already involved in the computation to confirm the consistency of the new model in reproducing flowing bottomhole pressure measurements.

Both sample wells were hydraulically fractured in numerous stages along the horizontal section. Liquid loading problems have been reported frequently and various remediation actions have been performed. The tubing in each well runs only through the vertical and deviated sections. The intersections between the horizontal segment and the vertical fractures give rise to complex multiphase flow phenomena. In this work, we focus only on flow inside the tubing because the flowing pressure at the bottom of the tubing has crucial effect on the production system. For simplicity, we call the pressure at the end of the tubing as "flowing bottomhole pressure".

Low Producer

In general, liquid loading problems occurred in this well because of operational reasons such as compressor troubles, artificial lift failures and the interference (frac hit) from hydraulic fracturing operation in neighboring wells. In general, liquid loading problems occurred in this well because of natural depletion. Liquid loading has been significantly impacting the overall productivity.

Well surveillance report indicates that during a 1593 day interval there were 698 downtime days, attributed to liquid loading. In a short period of time, one major liquid loading sequence may be followed by erratic production with multiple shut-in periods in between. This is particularly interesting, because the settled liquid during the first shut-in period was not properly removed or the technical issues were not completely resolved, and thus a higher bottomhole pressure was sustained afterwards. In order to restart the well properly, a minimum required pressure difference between reservoir and bottomhole must be attained.

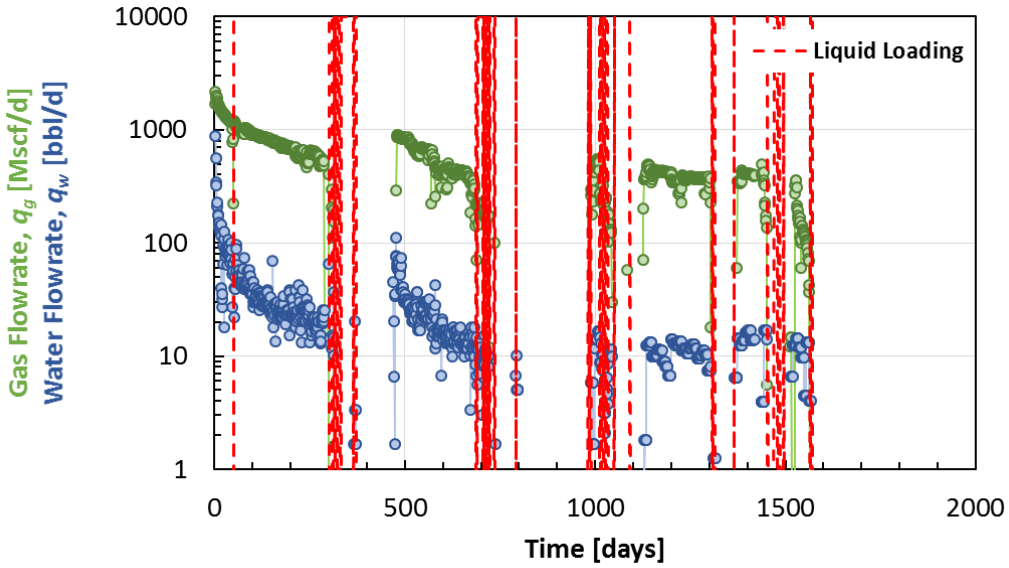

Fig. 6.3—Gas and water production rates and liquid loading sequences of well BH-1.

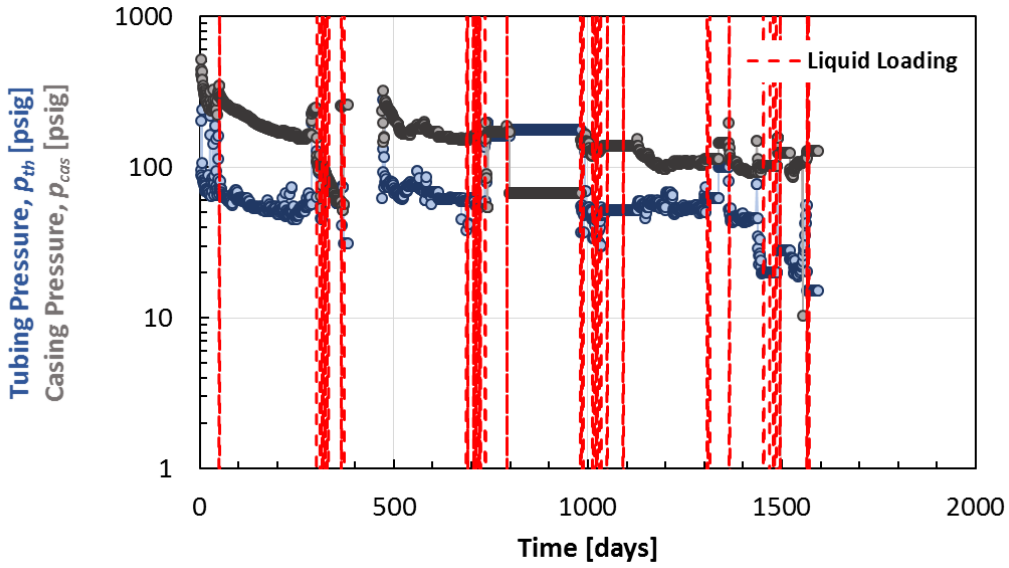

Fig. 6.4—Tubing and casing pressures and liquid loading sequences of well BH-1.

We simplified the historical data by identifying the starting points of major liquid loading cycles. In total, there were 6 major liquid loading cycles. The gas and water rates as well as the historical shut-in periods related to liquid loading are shown in **Fig. 6.3**. The tubing and casing pressures are indicated in **Fig. 6.4**. The description of various well parameters are summarized in **Table 6.3**.

Table 6.3—Well parameters for Well BH-1

Tubing head temperature, T_{th} (^{o}F)	110
Reservoir temperature, T_{res} (^{o}F)	131
Gas specific gravity, γ_g	0.58
Interfacial tension, σ (dyne/cm)	60
Water salinity, S (%)	5
End of tubing TVD (ft)	3650
End of tubing MD (ft)	4136
Tubing inner diameter (inch)	1.995

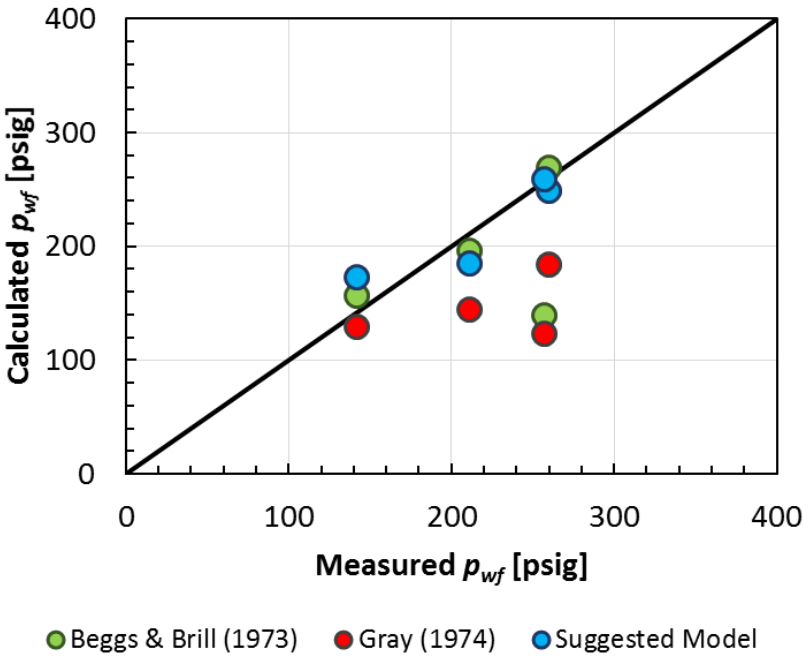

Fig. 6.5—Measured and calculated flowing bottomhole pressure for well BH-1.

The calculated p_{wf} using traditional model of Beggs and Brill (1973), Gray (1974), and the proposed model were compared against measurement results as shown in **Fig. 6.5**. However, a higher resolution in observing liquid-content and flowing bottomhole pressure was necessary in the vicinity of liquid loading cycles.

We dissected the time frames based on the occurrence of liquid loading into early, mid, and late periods. The progression of h_l and p_{wf} are shown in **Fig. 6.6**, where liquid-content presented here is the average liquid-content along the tubing. The slopes of h_l curves calculated using the proposed model are always positive when the well producing towards its liquid loading situations. This indicates consistent increase of h_l inside the tubing. As a consequence, the strongly related p_{wf} will also increase.

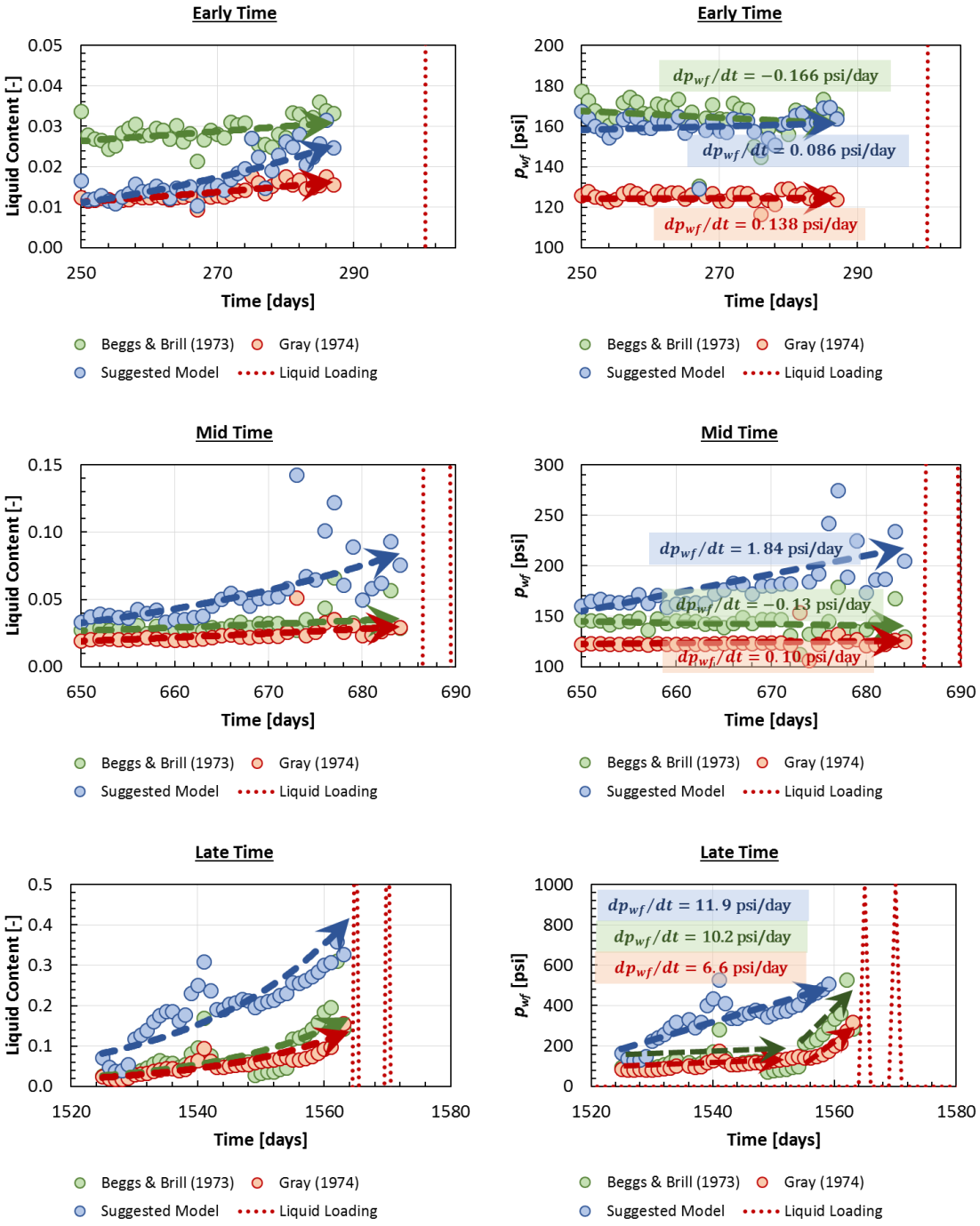

Fig 6.6—Progressions of liquid-content and flowing bottomhole pressure in well BH-1 before liquid loading occurrence.

It is seen in **Fig. 6.6** that all methods provide positive slopes of h_l curves. However, some discrepancies are observed in the p_{wf} curve, where the Beggs and Brill (1973) correlation yields negative slope in early-time and mid-time. It means that even when the Beggs and Brill (1973) correlation calculates a positive trend of h_l, the overall pressure drop in the tubing is still dominated by the frictional component. In the case of the suggested model, the h_l increases and the p_{wf} increases as well. This is the expected behavior, because we also detect a decrease in the observed gas production rate (explained by the decrease in available drawdown.)

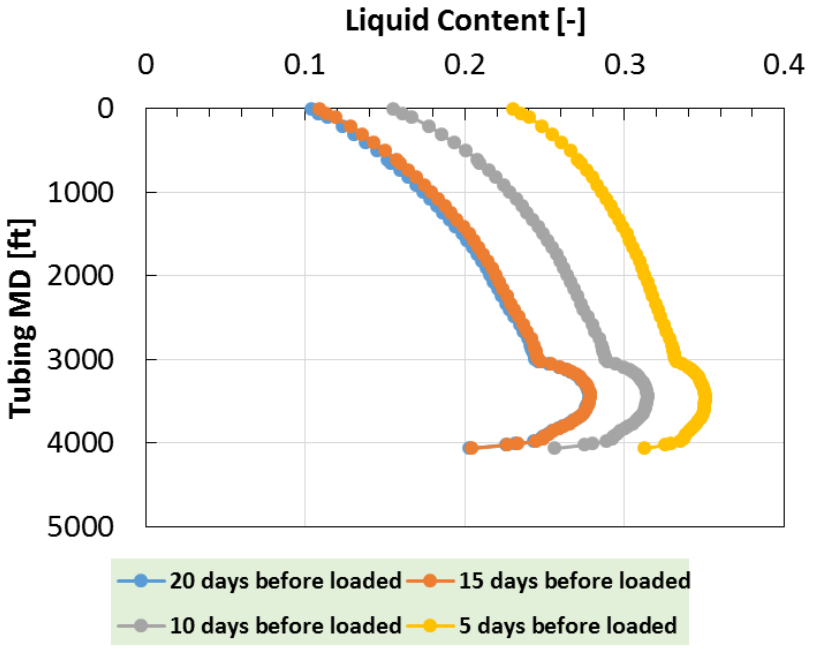

Fig 6.7—Liquid content profile from the tubing head to the end of tubing of well BH-1 before the occurrence of liquid loading (calculated using the suggested model).

The liquid content profile along the wellbore is illustrated in **Fig. 6.7**. The in-situ liquid content is actually increasing from the wellhead to the bottom of the wellbore except at some locations highly affected by well deviation. The difference between the minimum and maximum liquid content is as high as 250% where the maximum value is located at deviation angle of around 53 degree (see Chapter IV).

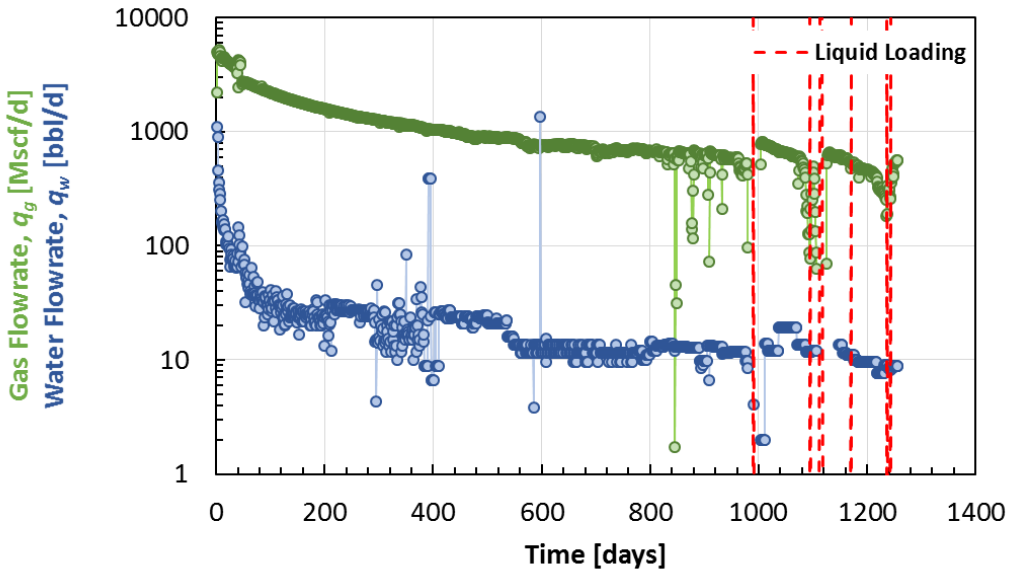

Fig. 6.8—Gas and water production rates and liquid loading sequences of well CH-2.

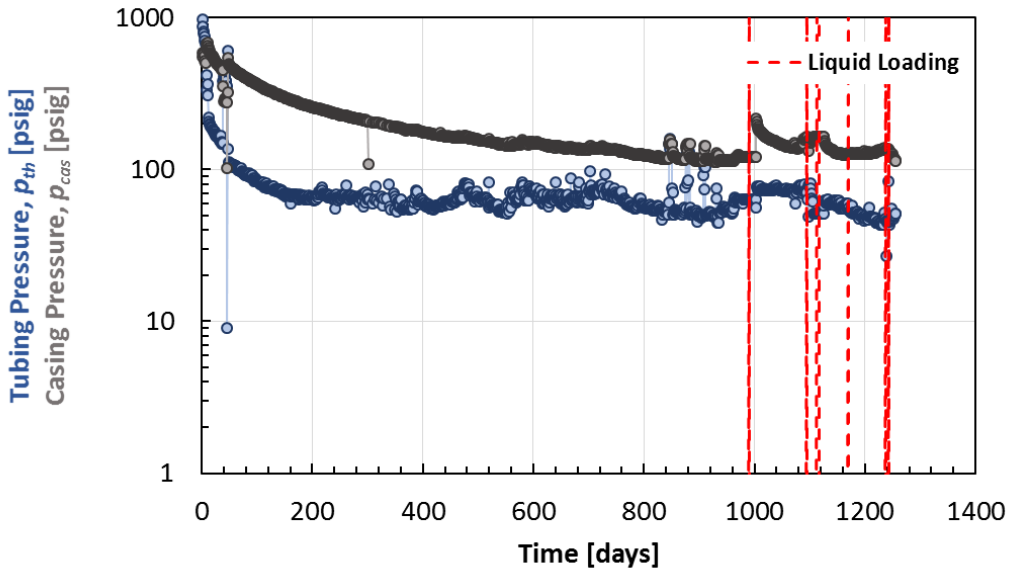

Fig. 6.9—Tubing and casing pressures and liquid loading sequences of well CH-2.

High Producer

The gas and water rates as well as liquid loading occurrences for CH-2 are shown in **Fig. 6.8**. Tubing and casing pressures are illustrated in **Fig. 6.9**. The description of various well parameters are summarized in **Table 6.4**. The main cause of liquid loading was the interference from hydraulic fracturing in a neighboring well on the 980-th day of production. The well experienced a production decline before the interference and then encountered a steeper decline followed by multiple liquid loading cycles. **Fig. 6.10** shows the comparison of calculated p_{wf} using various models against measurement results.

Table 6.4—Well parameters for Well CH-2

Tubing head temperature, T_{th} (°F)	113
Reservoir temperature, T_{res} (°F)	126
Gas specific gravity, γ_g	0.58
Interfacial tension, σ (dyne/cm)	60
Water salinity, S (%)	5
End of tubing TVD (ft)	3496
End of tubing MD (ft)	3986
Tubing inner diameter (inch)	1.995

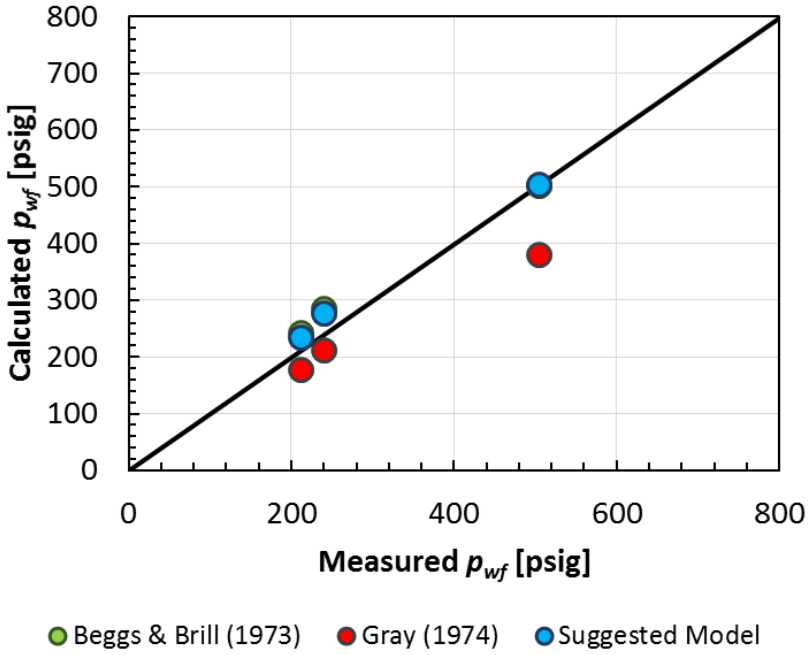

Fig. 6.10—Measured and calculated flowing bottomhole pressure for well CH-2.

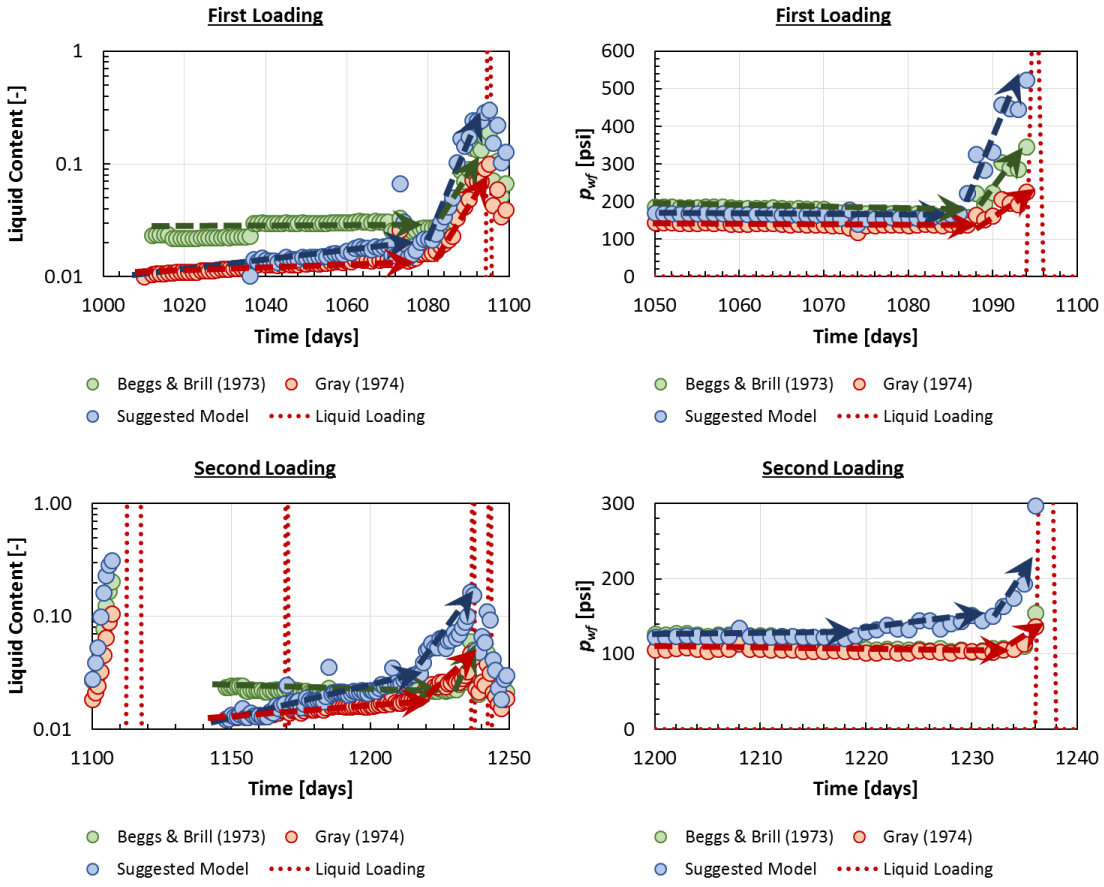

Fig. 6.11—Progressions of liquid-content and flowing bottomhole pressure in well CH-2 before liquid loading occurrence.

According to the production history, we divided liquid loading observations into two major cycles. The first cycle started on day 1012 after the well encountered fracturing interference and the second cycle began on day 1150. The progressions of h_l and p_{wf} are shown in **Fig. 6.11**. The positive slopes of h_l curves calculated by proposed model indicate that the liquid loading begins way before its symptoms become apparent from daily production. In the first cycle, the liquid-content is increasing right after the fracturing

interference. The slopes of h_l and p_{wf} curves are always positive and increasing substantially for 20 days before shut-in. Similar observations can also be made for the second cycle. As opposed to the proposed model, the method of Beggs and Brill (1973) shows negative slopes of p_{wf} for both cycles, although it provides a positive slope of h_l curve in the first cycle. The method of Gray (1974) provides positive slopes of h_l but for both cycles show negative slopes of p_{wf}.

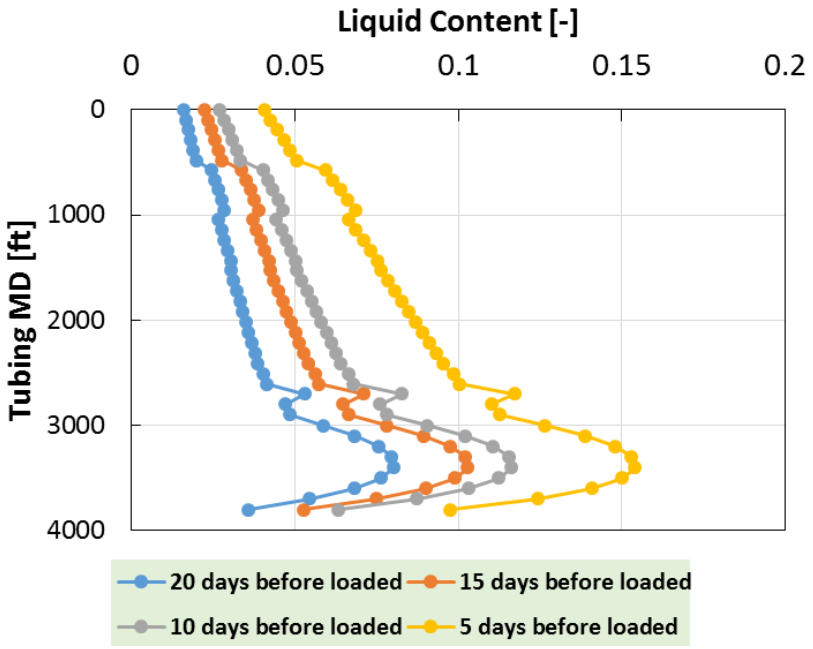

Fig 6.12—Liquid content profile from the tubing head to the end of tubing of well CH-2 before the occurrence of liquid loading (calculated using the suggested model).

It can be seen again in **Fig. 6.12** that the local liquid content along the wellbore is consistently increasing regardless the locations. The liquid content profile varies

significantly and the maximum is five times greater than the minimum. This extreme variation is of crucial significance in analyzing liquid loading. The use of critical velocity only at only one location (either at the wellhead or at the bottom of the well) seems to be unreliable under such circumstances.

The observations of liquid-content and flowing bottomhole pressure suggest that additional effort should be spent to prolong the life of these wells. Most of the time gravitational pressure loss caused by liquid-content dominates the system during liquid loading, and thus, velocity string may be a good candidate to lessen the liquid-content.

We emphasize that even when the observed surface water rate does not increase significantly, the new method can reveal the gradual liquid accumulation inside the well. It is more sensitive to the change in the observed gas rate. As opposed to the traditional models, the resulting liquid-content trend and the calculated bottomhole pressure trend are more consistent with each other and with the actual production rate. The individual contributions to the overall pressure gradient are represented in a more realistic way.

Artificial Lift Producer

An example of gas well with relatively low gas rate producing with the help of artificial lift is shown in **Fig. 6.13**. Well AH-6 has been producing for more than 7 years with average gas rate being around 426 Mscf/D. This well was interfered by hydraulic fracturing of a neighboring well on the 280-th day of production. Unlike well CH-2, well AH-6 was able to continue its production after the frac hit, despite a significant increase in water production that lasted for 4 months.

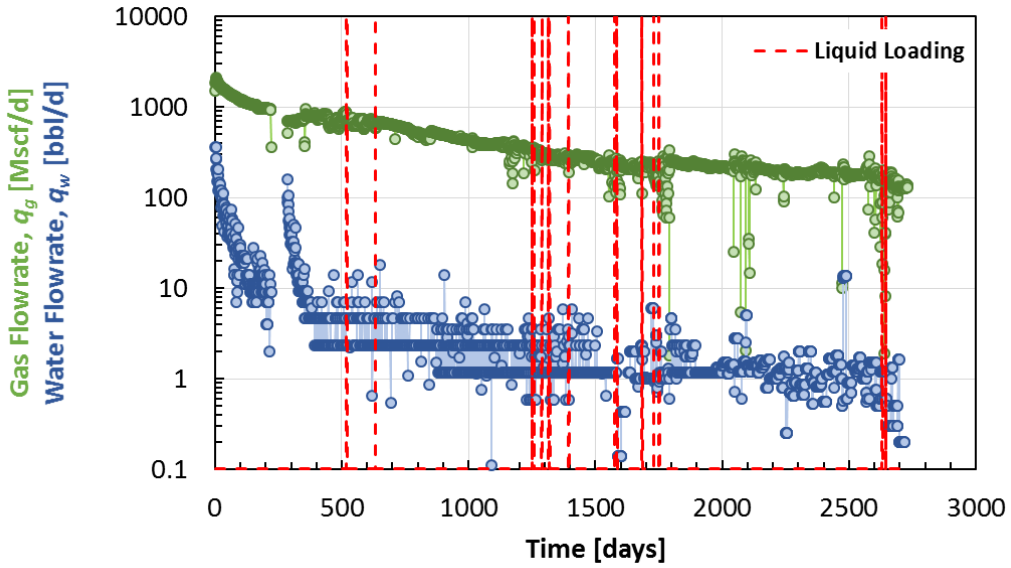

Fig. 6.13—Gas and water production rates and liquid loading sequences of well AH-6.

A better overall productivity of well AH-6 was partly due to the relatively small amount of co-produced liquids. After producing for 1000 days, the water rate was only about 2 to 4 bbl/D. However, liquid loading was still a major problem as gas production declined. Therefore, the operator decided to install a plunger lift to maintain the level of liquid content inside the wellbore. The plunger lift was installed on the 1781-th day of production when the production hovered around 200 Mscf/D. The results are quite satisfying as water production rate has been declining ever since.

In this section, the liquid content and flowing bottomhole pressure are diagnosed carefully by considering liquid loading events before and after the plunger lift installation. **Fig. 6.14** shows the responses in liquid content and bottomhole pressure as the well progresses into liquid loading situations.

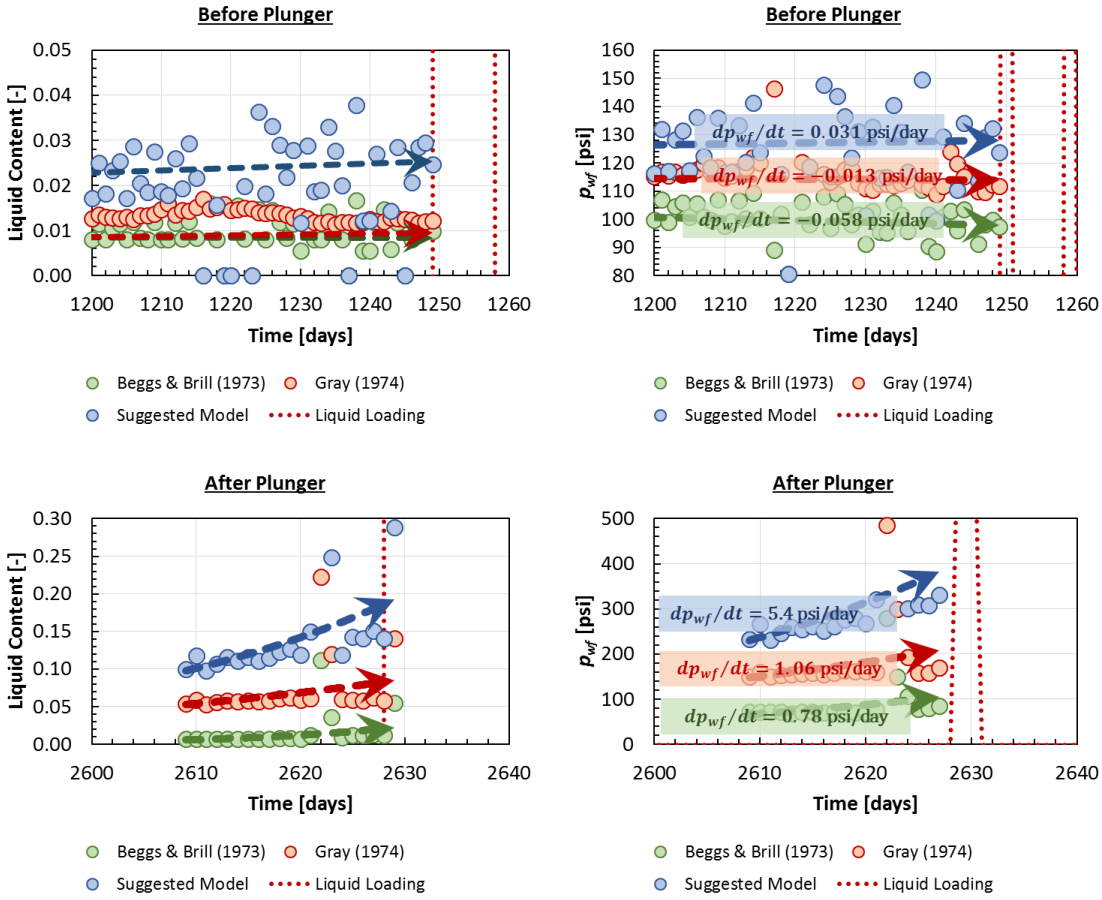

Fig 6.14—Progressions of liquid-content and flowing bottomhole pressure in well AH-6 before liquid loading occurrence.

For time periods before the installation of the plunger lift, the suggested model consistently provides continuously increasing trend of both liquid content and flowing bottomhole pressure. In contrast, the method of Beggs and Brill (1973) and Gray (1974) show inconsistent profiles of p_{wf}: while the liquid-content is slowly increasing it is not reflected on the p_{wf}.

After the installation of plunger lift, liquid loading was also occurring multiple times especially when the artificial lift system encountered mechanical problems. All models are able to deliver acceptable responses on h_l and p_{wf} profiles, but the suggested model provides more certain trends as the slope of h_l and p_{wf} are significantly higher compared to others.

Conclusion

The application of the new wellbore model in predicting overall liquid content and flowing bottomhole pressure in gas wells experiencing cyclical liquid loading conditions was presented. The liquid content and flowing bottomhole pressure was calculated sequentially from the wellhead to the bottom of the wellbore. The well was segmented into several sections, where the maximum allowable section length is equivalent to our flow loop length. Each section has its fluid flow properties hence pressure gradient.

First, the calculated bottomhole pressure was compared against the measured value which was the approximation from acoustic measuring device. The new model consistently reproduced measured pressure within acceptable accuracy for two cases: naturally flowing wells and gas wells with artificial lift system. A higher statistical error contributed by additional forces or chemicals employed in the well with artificial lift was expected in the first place.

Second, we analyzed liquid content and bottomhole pressure profiles over time. The new model consistently provided gradual increase of liquid content reflected on the upward trend of flowing bottomhole pressure way before the wells entered shut-in period

due to severe liquid loading situation. The new model also can be used to monitor the efficiency of artificial lift. Sudden increase in liquid content of an artificial lift well may also give indication of persistent mechanical problems.

CHAPTER VII

CONCLUSIONS AND FUTURE WORK

Conclusions

The complex liquid-loading phenomena (instability in the surface liquid rate, followed by instability in the surface gas rate, anomaly in casing-tubing pressure difference, possible re-injection into the formation, etc.) can be effectively diagnosed at early stages with the help of the developed model. There are two key predictors: First, the liquid-content inside the wellbore is steadily increasing. Second, the flowing bottomhole pressure starts to increase and the gas production rate declines steeper than justified by reservoir pressure decline. The liquid accumulation is a long and gradual process and the more obvious liquid loading symptoms occur only during the culmination of the process.

This work described the importance of the two-phase flow modeling for monitoring long term gas well production performance, specifically if the well encounters repetitive liquid loading situations. The developed approach is able to provide the early warning signs by projecting the gradual increase of wellbore liquid content. In its core lies a two-phase liquid hold-up correlation developed from our own experiments.

Based on the experiments in a large length to diameter ratio (L/D) facility, conducted around conditions when liquid loading allegedly occurred and very high in-situ holdup ratios can prevail, we introduced a new liquid content prediction method. The proposed correlation reproduced our own experimental data with good accuracy. Published experimental and gas wells data sets were also reproduced reasonably well.

The new method does not consider the onset of liquid loading as a single event in time. Rather, the model uses characteristic gas flow rate as a scaling variable in the correlation modeling the overall liquid content inside the wellbore. This feature makes it useful during normal producing conditions as well.. The proposed method is simple as it requires only the flow rates, densities, and tube diameter. Therefore, it is suitable to be used in day to day basis, and simultaneous analysis for many wells can be performed in a reasonable time. It is suggested that the application range is restricted to dimensionless gas velocities of $0.2 < u_g^* < 3.5$. Within that range, however, the method is flow-pattern independent. Using the proposed model, trends in liquid-content and flowing bottomhole pressure can be detected earlier and with more certainty than was previously possible.

We used the model to diagnose the historical liquid loading occurrences in selected shale gas wells. The new model was employed in flowing bottomhole pressure calculation and the results were reasonable within the application range. The accumulation of liquid content was consistently observed days or weeks before liquid loading symptoms became obvious. The strongly related flowing bottomhole pressure was also calculated and showed consistent behavior.

The critical gas rate concept is often used to select a particular artificial lift method for gas producing wells experiencing liquid loading. However, the implementation of liquid loading remediation method is likely to be late if the critical gas rate concept is used. In practice, artificial lift is installed most often when the well already encounters productivity loss. If artificial lift is not yet available, extended shut-in periods may be needed to de-liquefy the wellbore.

The new model offers hints to the underlying two-phase flow structure in the wellbore and can provide the necessary information earlier in time. Then the appropriate artificial lift method can be selected and implemented before the well undergoes severe production losses. Therefore, the gas-deliverability can be preserved and production loss can be minimized.

Future Work

Possible future applications of the developed model include (but are not restricted to) the following:

1. Collecting high frequency data from gas wells is becoming wide-spread. Supervisory Control and Data Acquisition (SCADA) is usually implemented in a "digital well". However, the available data are often under-utilized. The new wellbore model as an engineering tool that can be easily incorporated in a SCADA system, allowing early diagnosis and remediation of production disruptions.
2. Artificial lift systems, for example the commonly used plunger lift, can be analyzed and optimized with greater success if the new model is incorporated. The plunger intermittently uses the energy of the reservoir to carry the liquid to the surface. The round-trip frequency of the plunger should be selected in view of the anticipated liquid accumulation rate. The new model can be used to monitor the trend of liquid content in the wellbore, providing valuable information to determine the optimum plunger cycle.

3. While the developed model has promising potential, it should be checked and improved as more precise laboratory data become available with a wider range of parameters. In particular, more data are needed with liquids of various physical properties and under a wider range of pressures and temperatures.

REFERENCES

Alamu, M. B. 2012. Gas-Well Liquid Loading Probed with Advanced Instrumentation. (English). *SPE J.* **17** (1): 251-270. SPE-153724-PA. http://dx.doi.org/10.2118/153724-pa.

Alamu, M. B., Azzopardi, B. J. 2011. Simultaneous Investigation of Entrained Liquid Fraction, Liquid Film Thickness and Pressure Drop in Vertical Annular Flow. *Journal of Energy Resources Technology* **133** (2): 0231031-02310310. http://dx.doi.org/10.1115/1.4004265.

Anderson, G. H., Mantzouranis, B. G. 1960. Two-Phase (Gas—Liquid) Flow Phenomena—I Pressure Drop and Hold-up for Two-Phase Flow in Vertical Tubes. *Chem. Eng. Sci.* **12** (2): 109-126. http://dx.doi.org/10.1016/0009-2509(60)87004-2.

Ansari, A. M., Sylvester, N. D., Sarica, C. et al. 1994. A Comprehensive Mechanistic Model for Upward Two-Phase Flow in Wellbores. *SPE Prod & Fac* **9** (2): 143-151. SPE-20630-PA. http://dx.doi.org/10.2118/20630-PA.

Aziz, K., Govier, G. W. 1972. Pressure Drop in Wells Producing Oil and Gas. *J. Can. Pet. Technol.*: 38-48. PETSOC-72-03-04. http://dx.doi.org/10.2118/72-03-04.

Azzopardi, B. J. 2008. Flow Patterns: Does Gas/Solids Flow Pattern Correspond to Churn Flow in Gas/Liquid Flow. *Ind. Eng. Chem. Res.* **47** (20): 7934-7939. http://dx.doi.org/10.1021/ie800868b.

Azzopardi, B. J., Wren, E. 2004. What is Entrainment in Vertical Two-Phase Churn Flow? *Int. J. Multiphase Flow* **30** (1): 89-103. http://dx.doi.org/10.1016/j.ijmultiphaseflow.2003.11.001.

Barbosa Jr, J. R., Hewitt, G. F., König, G. et al. 2002. Liquid Entrainment, Droplet Concentration and Pressure Gradient at the Onset of Annular Flow in a Vertical Pipe. *Int. J. Multiphase Flow* **28** (6): 943 - 961. http://dx.doi.org/10.1016/S0301-9322(02)00003-4.

Beggs, D. H., Brill, J. P. 1973. A Study of Two-Phase Flow in Inclined Pipes. *J Pet Technol* **25** (5): 607-617. SPE-4007-PA. http://dx.doi.org/10.2118/4007-PA.

Belfroid, S., Schiferli, W., Alberts, G. et al. 2008. Prediction Onset and Dynamic Behaviour of Liquid Loading Gas Wells. Presented at the SPE Annual Technical Conference and Exhibition, Denver, Colorado, USA. 21-24 September. SPE-115567-MS. http://dx.doi.org/10.2118/115567-ms.

Bendiksen, K. H., Maines, D., Moe, R. et al. 1991. The Dynamic Two-Fluid Model Olga: Theory and Application. *SPE Prod Eng* **6** (2): 171-180. SPE-19451-PA. http://dx.doi.org/10.2118/19451-PA.

Brill, J. P., Beggs, H. D. 1974. *Two-Phase Flow in Pipes*. The Hague, INTERCOMP Course (Reprint).

Carr, N. L., Kobayashi, R., Burrows, D. B. 1954. Viscosity of Hydrocarbon Gases Under Pressure. *J Pet Technol* **6** (10): 47-55. SPE-297-G. http://dx.doi.org/10.2118/297-G.

Chisholm, D. 1973. Pressure Gradients Due to Friction During the Flow of Evaporating Two-Phase Mixtures in Smooth Tubes and Channels. *Int. J. Heat Mass Transfer* **16** (2): 347-358. http://dx.doi.org/10.1016/0017-9310(73)90063-X.

Chupin, G., Hu, B., Haugset, T. et al. 2007. Integrated Wellbore/Reservoir Model Predicts Flow Transients in Liquid-Loaded Gas Wells. Presented at the SPE Annual Technical Conference and Exhibition, Anaheim, California, USA. 11-14 November. SPE-110461-MS. http://dx.doi.org/10.2118/110461-ms.

Cioncolini, A., Thome, J. R. 2012. Void Fraction Prediction in Annular Two-Phase Flow. *Int. J. Multiphase Flow* **43** (0): 72-84. http://dx.doi.org/10.1016/j.ijmultiphaseflow.2012.03.003.

Coleman, S. B., Clay, H. B., McCurdy, D. G. et al. 1991. A New Look at Predicting Gas-Well Load-Up. *J Pet Technol* **43** (3): 329-333. SPE-20280-PA. http://dx.doi.org/10.2118/20280-PA.

Dix, G. E. 1971. Vapor Void Fractions for Forced Convection with Subcooled Boiling at Low Flow Rates, Ph.D. Thesis, University of California, Berkeley.

Dousi, N., Veeken, C. A. M., Currie, P. K. 2006. Numerical and Analytical Modeling of the Gas-Well Liquid-Loading Process. (English). *SPE Prod & Oper* **21** (4): 475-482. SPE-95282-PA. http://dx.doi.org/10.2118/95282-pa.

Dukler, A. E. 1960. Fluid Mechanics and Heat Transfer in Vertical Falling-Film Systems. *Chem. Eng. Prog. Symp. Ser.* **56** (30): 1-10.

El-Boher, A., Lesin, S., Unger, Y. et al. 1988. Experimental Studies of Liquid Metal Two-Phase Flows in Vertical Pipes. Presented at the Proceedings of the 1st

World Conference on Experimental Heat Transfer, Fluid Mechanics, and Thermodynamics, Dubrovnik, Yugoslavia.

Fernandez, J. J., Falcone, G., Teodoriu, C. 2010. Design of a High-Pressure Research Flow Loop for the Experimental Investigation of Liquid Loading in Gas Wells. (English). *SPE Proj Fac & Const* **5** (2): 76-88. http://dx.doi.org/10.2118/122786-pa.

Fiedler, S., Auracher, H. 2004. Experimental and Theoretical Investigation of Reflux Condensation in an Inclined Small Diameter Tube. *Int. J. Heat Mass Transfer* **47** (19–20): 4031-4043. http://dx.doi.org/10.1016/j.ijheatmasstransfer.2004.06.005.

Friedel, L. 1979. *Improved Friction Pressure Drop Correlations for Horizontal and Vertical Two-Phase Pipe Flow*. Ispra, Italy: European Two-phase Group Meeting (Reprint).

Godbole, P. V., Tang, C. C., Ghajar, A. J. 2011. Comparison of Void Fraction Correlations for Different Flow Patterns in Upward Vertical Two-Phase Flow. *Heat Transfer Engineering* **32** (10): 843-860. http://dx.doi.org/10.1080/01457632.2011.548285.

Gool, F. R. V., Currie, P. K. 2008. An Improved Model for the Liquid-Loading Process in Gas Wells. (English). *SPE Prod & Oper* **23** (4): 458-463. SPE-106699-PA. http://dx.doi.org/10.2118/106699-pa.

Gray, H. E. 1974. Vertical Flow Correlations in Gas Wells. In *User Manual for Api 14b, Subsurface Controlled Safety Valve Sizing*, Appendix B.

Greskovich, E. J., Cooper, W. T. 1975. Correlation and Prediction of Gas-Liquid Holdups in Inclined Upflows. *AlChE J.* **21** (6): 1189-1192. http://dx.doi.org/10.1002/aic.690210619.

Guner, M., Pereyra, E., Sarica, C. et al. 2015. An Experimental Study of Low Liquid Loading in Inclined Pipes from 90^0 to 45^0. Presented at the SPE Production and Operations Symposium, Oklahoma City, Oklahoma, USA 1-5 March. SPE-173631-MS. http://dx.doi.org/10.2118/173631-MS.

Guo, B., Ghalambor, A., Xu, C. 2006. A Systematic Approach to Predicting Liquid Loading in Gas Wells. (English). *SPE Prod & Oper* **21** (1): 81-88. SPE-94081-PA. http://dx.doi.org/10.2118/94081-pa.

Hall-Taylor, G. F., H., P. M. C., L. 1963. The Motion and Frequency of Large Disturbance Waves in Annular Two-Phase Flow of Air-Water Mixtures. *Chem. Eng. Sci.* **18** (8): 537-552. http://dx.doi.org/10.1016/0009-2509(63)85014-9.

Hewitt, G. F. 1961. Analysis of Annular Two-Phase Flow: Application of the Dukler Analysis to Vertical Upward Flow in a Tube, Atomic Energy Research Establishment, Harwell, Berkshire.

Hewitt, G. F. 2012. Churn and Wispy Annular Flow Regimes in Vertical Gas–Liquid Flows. *Energy & Fuels* **26** (7): 4067-4077. http://dx.doi.org/10.1021/ef3002422.

Hewitt, G. F., Roberts, D. N. 1969. Studies of Two-Phase Flow Patterns by Simultaneous X-Ray and Flash Photography, Atomic Energy Research Establishment, Harwell, Berkshire.

Hu, B., Veeken, C. A. M., Yusuf, R. et al. 2010. Use of Wellbore-Reservoir Coupled Dynamic Simulation to Evaluate the Cycling Capability of Liquid-Loaded Gas Wells. Presented at the SPE Annual Technical Conference and Exhibition, Florence, Italy. 19-22 September. SPE-134948-MS. http://dx.doi.org/10.2118/134948-ms.

Kaji, R., Azzopardi, B. J. 2010. The Effect of Pipe Diameter on the Structure of Gas/Liquid Flow in Vertical Pipes. *Int. J. Multiphase Flow* **36** (4): 303-313. http://dx.doi.org/10.1016/j.ijmultiphaseflow.2009.11.010.

Lea, J. F., Nickens, H. V. 2004. Solving Gas-Well Liquid-Loading Problems. (English). *SPE Journal of Petroleum Technology* **56** (4): 30-36. http://dx.doi.org/10.2118/72092-ms.

Lea, J. F., Nickens, H. V., Wells, M. 2003. *Gas Well Deliquification - Solution to Gas Well Liquid Loading Problems*. Houston, Texas: Gulf Professional Publishing (Reprint).

Levy, S. 1999. *Two-Phase Flow in Complex Systems*. New York, John Wiley Sons (Reprint).

Li, J., Almudairis, F., Zhang, H.-q. 2014. Prediction of Critical Gas Velocity of Liquid Unloading for Entire Well Deviation. Presented at the International Petroleum Technology Conference, Kuala Lumpur, Malaysia. 10-12 December. IPTC-17846-MS. http://dx.doi.org/10.2523/IPTC-17846-MS.

Limpasurat, A., Valko, P. P., Falcone, G. 2015. A New Concept of Wellbore-Boundary Condition for Modeling Liquid Loading in Gas Wells. *SPE J.* **20** (3): 550 - 564. SPE-166199-PA. http://dx.doi.org/10.2118/166199-PA.

Liu, L. 2014. The Phenomenon of Negative Frictional Pressure Drop in Vertical Two-Phase Flow. *Int. J. Heat Fluid Flow* **45** (1): 72-80. http://dx.doi.org/10.1016/j.ijheatfluidflow.2013.12.003.

Lockhart, R. W., Martinelli, R. C. 1949. Proposed Correlation of Data for Isothermal Two-Phase, Two-Component Flow in Pipes. *Chem. Eng. Prog.* **45**: 39-48.

Lumban-Gaol, A., Valkó, P. P. 2014. Liquid Holdup Correlation for Conditions Affected by Partial Flow Reversal. *Int. J. Multiphase Flow* **67** (0): 149-159. http://dx.doi.org/10.1016/j.ijmultiphaseflow.2014.08.014.

Luo, S., Kelkar, M., Pereyra, E. et al. 2014. A New Comprehensive Model for Predicting Liquid Loading in Gas Wells. *SPE Prod & Oper* **29** (4): 337-349. SPE-172501-PA. http://dx.doi.org/10.2118/172501-PA.

McCain, W. D., Jr. 1991. Reservoir-Fluid Property Correlations-State of the Art (Includes Associated Papers 23583 and 23594). **6** (2): 266-272. SPE-18571-PA. http://dx.doi.org/10.2118/18571-PA.

McCoy, J. N., Rowlan, O. L., Podio, A. 2009. Acoustic Liquid Level Testing of Gas Wells. Presented at the SPE Production and Operations Symposium, Oklahoma City, Oklahoma. 4-8 April. SPE-120643-MS. http://dx.doi.org/10.2118/120643-MS.

Müller-Steinhagen, H., Heck, K. 1986. A Simple Friction Pressure Drop Correlation for Two-Phase Flow in Pipes. *Chemical Engineering and Processing: Process Intensification* **20** (6): 297-308. http://dx.doi.org/10.1016/0255-2701(86)80008-3.

Nguyen, V. T., Spedding, P. L. 1977. Holdup in Two-Phase, Gas-Liquid Flow—Ii: Experimental Results. *Chem. Eng. Sci.* **32** (9): 1015-1021. http://dx.doi.org/10.1016/0009-2509(77)80139-5.

Nosseir, M. A., Darwich, T. A., Sayyouh, M. H. et al. 2000. A New Approach for Accurate Prediction of Loading in Gas Wells under Different Flowing Conditions. *SPE Prod & Oper* **15** (4): 241-246. SPE-66540-PA. http://dx.doi.org/10.2118/66540-PA.

Oddie, G., Shi, H., Durlofsky, L. J. et al. 2003. Experimental Study of Two and Three Phase Flows in Large Diameter Inclined Pipes. *Int. J. Multiphase Flow* **29** (4): 527-558. http://dx.doi.org/10.1016/S0301-9322(03)00015-6.

Oden, R. D., Jennings, J. W. 1988. Modification of the Cullender and Smith Equation for More Accurate Bottomhole Pressure Calculations in Gas Wells. Presented at the SPE Permian Basin Oil and Gas Recovery Conference, Midland, Texas. 10-11 March. SPE-17306-MS. http://10.2118/17306-MS.

Owen, D. G. 1986. An Experimental and Theoretical Analysis of Equilibrium Annular Flows, Ph.D. Thesis. University of Birmingham, UK.

Shi, J., Sun, Z., Li, X. 2016. Analytical Models for Liquid Loading in Multifractured Horizontal Gas Wells. **21** (2): 471-487. SPE-2014-1922861-PA. http://dx.doi.org/10.2118/2014-1922861-PA.

Skopich, A., Pereyra, E., Sarica, C. et al. 2015. Pipe-Diameter Effect on Liquid Loading in Vertical Gas Wells. *SPE Prod & Oper* **30** (2): 164-176. SPE-164477-PA. http://dx.doi.org/10.2118/164477-PA.

Sutton, R. P., Cox, S. A., Lea, J. F. et al. 2010. Guidelines for the Proper Application of Critical Velocity Calculations. *SPE Prod & Oper* **25** (2): 182 - 194. SPE-120625-PA. http://dx.doi.org/10.2118/120625-PA.

Taitel, Y., Bornea, D., Dukler, A. E. 1980. Modelling Flow Pattern Transitions for Steady Upward Gas-Liquid Flow in Vertical Tubes. *AlChE J.* **26** (3): 345-354. http://dx.doi.org/10.1002/aic.690260304.

Turner, R. G., Hubbard, M. G., Dukler, A. E. 1969. Analysis and Prediction of Minimum Flow Rate for the Continuous Removal of Liquids from Gas Wells. *J Pet Technol* **21** (11): 1475-1482. SPE-2198-PA. http://dx.doi.org/10.2118/2198-PA.

van't Westende, J. M. C., Kemp, H. K., Belt, R. J. et al. 2007. On the Role of Droplets in Cocurrent Annular and Churn-Annular Pipe Flow. *Int. J. Multiphase Flow* **33** (6): 595-615. http://dx.doi.org/10.1016/j.ijmultiphaseflow.2006.12.006.

Veeken, C. A. M., Belfroid, S. P. C. 2011. New Perspective on Gas-Well Liquid Loading and Unloading. (English). *SPE Prod & Oper* **26** (4): 343-356. SPE-134483-PA. http://dx.doi.org/10.2118/134483-pa.

Wallis, G. B. 1969. *One-Dimensional Two-Phase Flow*. New York, McGraw-Hill (Reprint).

Waltrich, P. J. 2012. Onset and Subsequent Transient Phenomena of Liquid Loading in Gas Wells: Experimental Investigation Using a Large Scale Flow Loop, Ph.D. Thesis, Texas A&M University, College Station, Texas.

Waltrich, P. J., Falcone, G., Barbosa Jr, J. R. 2013. Axial Development of Annular, Churn and Slug Flows in a Long Vertical Tube. *Int. J. Multiphase Flow* **57** (0): 38-48. http://dx.doi.org/10.1016/j.ijmultiphaseflow.2013.06.008.

Woldesemayat, M. A., Ghajar, A. J. 2007a. Comparison of Void Fraction Correlations for Different Flow Patterns in Horizontal and Upward Inclined Pipes. *Int. J. Multiphase Flow* **33** (4): 347 - 370. http://dx.doi.org/10.1016/j.ijmultiphaseflow.2006.09.004.

Woldesemayat, M. A., Ghajar, A. J. 2007b. Comparison of Void Fraction Correlations for Different Flow Patterns in Horizontal and Upward Inclined Pipes. *Int. J. Multiphase Flow* **33** (4): 347-370. http://dx.doi.org/10.1016/j.ijmultiphaseflow.2006.09.004.

Yuan, G., Pereyra, E., Sarica, C. et al. 2013. An Experimental Study on Liquid Loading of Vertical and Deviated Gas Wells. Presented at the SPE Production and Operations Symposium, Oklahoma City, Oklahoma, USA. 23-26 March. SPE-164516-MS. http://dx.doi.org/10.2118/164516-MS.

Zabaras, G., Dukler, A. E., Moalem-Maron, D. 1986. Vertical Upward Cocurrent Gas-Liquid Annular Flow. *AlChE J.* **32** (5): 829-843. http://dx.doi.org/10.1002/aic.690320513.

Zhang, H.-Q., Wang, Q., Sarica, C. et al. 2003a. Unified Model for Gas-Liquid Pipe Flow Via Slug Dynamics—Part 1: Model Development. *Journal of Energy Resources Technology* **125** (4): 266-273. http://dx.doi.org/10.1115/1.1615246.

Zhang, H.-Q., Wang, Q., Sarica, C. et al. 2003b. Unified Model for Gas-Liquid Pipe Flow Via Slug Dynamics—Part 2: Model Validation. *Journal of Energy Resources Technology* **125** (4): 274-283. http://dx.doi.org/10.1115/1.1615618.

Zhou, D., Yuan, H. 2010. A New Model for Predicting Gas-Well Liquid Loading. (English). *SPE Prod & Oper* **25** (2): 172-181. SPE-120580-PA. http://dx.doi.org/10.2118/120580-pa.

APPENDIX A

EXPERIMENTAL MEASUREMENT RESULTS

# of Test	Pressure [kPa] at z/D					ρ_g [kg/m³] at z/D					u_{sg} [m/s] at z/D					u_{sl} [m/s]	h_l [-]
	18	189	419	671	817	18	189	419	671	817	18	189	419	671	817		
1	119.2	115.8	111.6	108.0	105.6	1.39	1.35	1.30	1.26	1.23	22.3	23.0	23.8	24.6	25.2	0.0045	0.006
2	115.7	112.5	108.9	105.8	103.8	1.35	1.32	1.27	1.24	1.21	19.2	19.8	20.4	21.1	21.5	0.0045	0.010
3	115.9	112.4	108.7	105.3	103.2	1.36	1.31	1.27	1.23	1.21	16.6	17.1	17.7	18.3	18.7	0.0045	0.017
4	117.4	113.3	109.2	105.4	102.9	1.37	1.32	1.28	1.23	1.20	14.9	15.5	16.0	16.6	17.0	0.0045	0.024
5	120.1	115.2	110.3	105.6	102.8	1.40	1.35	1.29	1.24	1.20	13.1	13.7	14.3	14.9	15.3	0.0045	0.034
6	125.5	118.9	112.4	106.3	102.6	1.47	1.39	1.31	1.24	1.20	11.2	11.8	12.5	13.2	13.7	0.0045	0.051
7	139.8	129.8	119.1	108.5	102.6	1.63	1.52	1.39	1.27	1.20	8.1	8.7	9.5	10.4	11.0	0.0045	0.086
8	148.7	136.8	123.7	110.5	103.1	1.74	1.60	1.45	1.29	1.20	6.5	7.1	7.9	8.8	9.4	0.0044	0.108
9	164.7	148.8	131.4	113.7	103.9	1.93	1.74	1.54	1.33	1.21	4.4	4.9	5.6	6.4	7.0	0.0046	0.155
10	186.2	164.7	141.1	117.5	104.6	2.18	1.93	1.65	1.37	1.22	2.5	2.9	3.3	4.0	4.5	0.0045	0.227
11	117.4	114.6	109.9	106.4	104.7	1.37	1.34	1.28	1.24	1.22	19.5	20.0	20.9	21.6	21.9	0.0060	0.012
12	117.3	114.3	109.5	105.8	104.1	1.37	1.34	1.28	1.24	1.22	17.1	17.6	18.3	19.0	19.3	0.0060	0.017
13	118.5	115.0	109.9	105.8	103.8	1.38	1.34	1.28	1.24	1.21	15.2	15.6	16.4	17.0	17.3	0.0060	0.024
14	119.3	114.8	110.2	105.9	103.0	1.39	1.34	1.29	1.24	1.20	14.4	14.9	15.6	16.2	16.6	0.0061	0.028
15	122.7	118.0	111.5	106.2	103.6	1.43	1.38	1.30	1.24	1.21	12.5	13.0	13.8	14.5	14.8	0.0060	0.040
16	123.8	118.8	112.0	106.4	103.6	1.45	1.39	1.31	1.24	1.21	12.2	12.7	13.5	14.2	14.5	0.0063	0.047
17	129.4	122.8	114.3	107.0	103.6	1.51	1.44	1.34	1.25	1.21	10.6	11.2	12.0	12.8	13.2	0.0060	0.059
18	136.6	128.3	117.7	108.3	103.6	1.60	1.50	1.38	1.27	1.21	9.1	9.7	10.5	11.5	12.0	0.0060	0.076
19	137.4	129.0	118.2	108.5	103.7	1.61	1.51	1.38	1.27	1.21	8.9	9.5	10.4	11.3	11.8	0.0061	0.080
20	139.0	129.5	119.0	108.8	103.0	1.63	1.51	1.39	1.27	1.20	8.5	9.2	10.0	10.9	11.5	0.0060	0.087

# of Test	Pressure [kPa] at z/D					ρ_g [kg/m³] at z/D					u_{sg} [m/s] at z/D					u_{sl} [m/s]	h_l [-]
	18	189	419	671	817	18	189	419	671	817	18	189	419	671	817		
21	143.7	133.2	121.3	109.6	103.1	1.68	1.56	1.42	1.28	1.21	7.6	8.3	9.1	10.0	10.7	0.0060	0.096
22	144.5	134.4	121.7	109.9	103.8	1.69	1.57	1.42	1.28	1.21	7.6	8.2	9.0	10.0	10.6	0.0061	0.098
23	153.3	141.3	126.2	111.7	104.4	1.79	1.65	1.47	1.31	1.22	6.0	6.5	7.3	8.2	8.8	0.0061	0.120
24	168.1	151.7	133.1	114.6	104.4	1.97	1.77	1.56	1.34	1.22	4.1	4.6	5.2	6.1	6.6	0.0060	0.166
25	184.2	164.2	140.5	117.4	105.5	2.15	1.92	1.64	1.37	1.23	2.6	2.9	3.4	4.1	4.6	0.0062	0.227
26	199.5	174.7	146.9	119.9	105.1	2.33	2.04	1.72	1.40	1.23	1.7	1.9	2.3	2.8	3.2	0.0062	0.271
27	138.5	132.2	123.2	113.5	109.9	1.62	1.54	1.44	1.33	1.28	22.1	23.2	24.8	27.0	27.9	0.0309	0.011
28	133.9	128.0	119.8	111.3	107.8	1.57	1.50	1.40	1.30	1.26	19.5	20.4	21.8	23.5	24.2	0.0309	0.018
29	130.3	124.4	116.7	109.0	105.6	1.52	1.45	1.36	1.27	1.23	17.0	17.8	19.0	20.4	21.0	0.0310	0.029
30	130.1	124.1	116.5	108.8	105.4	1.52	1.45	1.36	1.27	1.23	16.3	17.1	18.2	19.5	20.2	0.0310	0.032
31	131.6	124.8	116.6	108.3	104.8	1.54	1.46	1.36	1.27	1.22	13.9	14.7	15.7	16.9	17.5	0.0311	0.045
32	136.3	128.0	118.3	108.3	104.5	1.59	1.50	1.38	1.27	1.22	11.6	12.3	13.3	14.6	15.1	0.0306	0.064
33	139.1	131.0	119.7	108.5	105.2	1.63	1.53	1.40	1.27	1.23	10.8	11.5	12.5	13.8	14.3	0.0307	0.070
34	144.8	135.0	122.1	108.8	105.2	1.69	1.58	1.43	1.27	1.23	9.3	9.9	11.0	12.3	12.8	0.0298	0.092
35	150.2	138.9	124.7	109.2	105.1	1.76	1.62	1.46	1.28	1.23	8.2	8.8	9.8	11.2	11.7	0.0309	0.103
36	160.0	146.5	129.5	110.2	105.3	1.87	1.71	1.51	1.29	1.23	6.4	7.0	7.9	9.3	9.7	0.0304	0.129
37	172.5	156.1	135.7	111.5	105.7	2.02	1.82	1.59	1.30	1.24	4.6	5.0	5.8	7.1	7.4	0.0308	0.167
38	149.8	140.3	130.4	116.8	111.8	1.75	1.64	1.52	1.37	1.31	21.3	22.8	24.5	27.3	28.6	0.0603	0.018
39	145.5	136.3	126.7	114.4	109.4	1.70	1.59	1.48	1.34	1.28	19.3	20.6	22.2	24.5	25.6	0.0611	0.022
40	142.4	133.3	124.1	112.5	107.6	1.66	1.56	1.45	1.32	1.26	17.1	18.2	19.6	21.6	22.6	0.0603	0.031
41	141.2	131.7	122.4	110.8	105.7	1.65	1.54	1.43	1.29	1.24	15.5	16.6	17.9	19.8	20.7	0.0618	0.045
42	141.9	131.8	122.0	110.1	104.9	1.66	1.54	1.43	1.29	1.23	13.6	14.6	15.8	17.5	18.3	0.0601	0.058
43	144.3	133.3	122.8	110.0	104.6	1.69	1.56	1.44	1.29	1.22	12.2	13.2	14.3	16.0	16.8	0.0604	0.069
44	150.9	138.0	125.6	110.1	104.3	1.76	1.61	1.47	1.29	1.22	9.8	10.7	11.7	13.4	14.1	0.0614	0.095
45	157.5	142.8	128.4	110.5	104.2	1.84	1.67	1.50	1.29	1.22	8.0	8.8	9.8	11.4	12.1	0.0612	0.116
46	164.2	147.9	131.5	110.9	104.3	1.92	1.73	1.54	1.30	1.22	6.7	7.4	8.4	9.9	10.6	0.0607	0.133

APPENDIX B

FORMULA FOR CALCULATION OF FLUID PROPERTIES

This appendix describes correlations used for fluid properties calculation applied in the wellbore model.

Gas Properties

Gas Density

The gas density is calculated by considering real gas behavior as follows:

$$\rho_g = \frac{pMW_g}{zRT} \tag{B-2}$$

where p is the pressure; MW_g is the molecular weight of gas which commonly formulated as $MW_g = \gamma_g MW_a$ where γ_g is the gas gravity and MW_a is molecular weight of air; z is the gas compressibility factor; R is the universal gas constant; and T is the temperature.

The z-factor can be calculated using some existing correlations. For a simplicity, we use an explicit correlation developed by Brill and Beggs (1974). In general, this correlation requires only gas gravity (γ_g), molecular fractions of N_2, CO_2, and H_2S $(y_{N_2}, y_{CO_2}, y_{H_2S})$, as well as pressure (p) and temperature (T).

The derivation of their correlation is as follows:

$$p_{pc} = 678 - 50\left(\gamma_g - 0.5\right) - 206.7y_{N_2} + 440y_{CO_2} + 606.7y_{H_2S} \quad \text{(B-3)}$$

$$T_{pc} = 326 + 315.7\left(\gamma_g - 0.5\right) - 240y_{N_2} - 83.3y_{CO_2} + 133.3y_{H_2S} \quad \text{(B-4)}$$

$$p_{pr} = p/p_{pc} \quad \text{(B-5)}$$

$$T_{pr} = T/T_{pc} \quad \text{(B-6)}$$

$$A_0 = 1.39\left(T_{pr} - 0.92\right)^{0.5} - 0.36T_{pr} - 0.1 \quad \text{(B-7)}$$

$$B_0 = \left(0.62 - 0.23T_{pr}\right)p_{pr} + \left(\frac{0.066}{\left(T_{pr} - 0.86\right)} - 0.037\right)p_{pr}^2 + 0.32\frac{p_{pr}^2}{10^{E_0}} \quad \text{(B-8)}$$

$$C_0 = 0.132 - 0.32\log T_{pr} \quad \text{(B-9)}$$

$$E_0 = 9\left(T_{pr} - 1\right) \quad \text{(B-10)}$$

$$F_0 = 0.3106 - 0.49T_{pr} + 0.1824T_{pr}^2 \quad \text{(B-11)}$$

$$D_0 = 10^{F_0} \quad \text{(B-12)}$$

$$z = A_0 + (1 - A_0)e^{-B_0} + C_0{p_{pr}}^{D_0} \quad \text{(B-13)}$$

where p is in psi and T is in R.

Gas Viscosity

Gas viscosity is determined using the correlation of (Carr et al. 1954). The gas viscosity at temperature and atmospheric pressure is calculated first, given as:

$$\mu_1 = \mu_{1HC} + \mu_{1N_2} + \mu_{1CO_2} + \mu_{1H_2S} \quad \text{(B-14)}$$

where

$$\mu_{1HC} = 8.188\times10^{-3} - 6.15 \times 10^{-3} \log \gamma_g + \left(1.709 \times 10^{-5} - 2.062 \times 10^{-6}\gamma_g\right)T \quad \text{(B-15)}$$

$$\mu_{1N_2} = \left[9.59 \times 10^{-3} + 8.48 \times 10^{-3}\, log\, \gamma_g\right] y_{N_2} \quad \text{(B-16)}$$

$$\mu_{1CO_2} = \left[6.24 \times 10^{-3} + 9.08 \times 10^{-3}\, log\, \gamma_g\right] y_{CO_2} \quad \text{(B-17)}$$

$$\mu_{1H_2S} = \left[3.73 \times 10^{-3} + 8.49 \times 10^{-3}\, log\, \gamma_g\right] y_{H_2S} \quad \text{(B-18)}$$

The reduce viscosity then calculated as a function of pseudo-reduced pressure and temperature:

$$\mu_r = a_0 + a_1 p_{pr} + a_2 p_{pr}^2 + a_3 p_{pr}^3 + T_{pr}\left(a_4 + a_5 p_{pr} + a_6 p_{pr}^2 + a_7 p_{pr}^3\right) + T_{pr}^2\left(a_8 + a_9 p_{pr} + a_{10} p_{pr}^2 + a_{11} p_{pr}^3\right) + +T_{pr}^3\left(a_{12} + a_{13} p_{pr} + a_{14} p_{pr}^2 + a_{15} p_{pr}^3\right) \quad \text{(B-19)}$$

where a_0 through a_{15} are listed in Table B-1. Therefore, gas viscosity in centipoise (cp) is evaluated as follows:

$$\mu_g = \frac{\mu_1}{T_{pr}} e^{-\mu_r} \quad \text{(B-20)}$$

Table B-1—Viscosity correlation constants of (Carr et al. 1954).

a_0	-2.426	a_6	0.3603	a_{12}	0.08393
a_1	2.97	a_7	-0.01044	a_{13}	-0.1864
a_2	-0.2862	a_8	-0.7933	a_{14}	0.02033
a_3	0.008054	a_9	1.396	a_{15}	-0.0006095
a_4	2.808	a_{10}	-0.1491		
a_5	-3.498	a_{11}	0.00441		

Water Properties

Water properties including density, formation volume factor, and viscosity are calculated using correlations provided by (McCain 1991).

Water Density

The density of formation water is calculated at standard conditions as a function of salinity:

$$\rho_w = 62.368 + 0.438603S + 1.60074 \times 10^{-3}S^2 \quad \text{(B-21)}$$

where is S is the salinity in percentage of weight. The density at a certain condition is calculated by dividing density at standard conditions by formation volume factor (FVF), B_w, for pressure and temperature of interest.

Water FVF

The expression to calculate water FVF is given as:

$$B_w = \left(1 + \Delta V_{wp}\right)(1 + \Delta V_{wT}) \tag{B-22}$$

where

$$\Delta V_{wT} = -1.0001 \times 10^{-2} + 1.33391 \times 10^{-4} T + 5.50654 \times 10^{-7} T^2 \tag{B-23}$$

$$\begin{aligned} \Delta V_{wp} = {} & -1.95301 \times 10^{-9} pT - 1.72834 \times 10^{-13} p^2 T \\ & -3.58922 \times 10^{-7} p - 2.25341 \times 10^{-10} p^2 \end{aligned} \tag{B-24}$$

Pressure (p) and temperature (T) are in psi and F, respectively.

Water Viscosity

First, the water viscosity has to be estimated at reservoir temperature and atmospheric pressure:

$$\mu_{w1} = AT^{-B} \tag{B-25}$$

where

$$A = 109.574 - 8.40564S + 0.313314S^2 + 8.72213 \times 10^{-3} S^3 \tag{B-26}$$

and

$$\begin{aligned} B = {} & 1.2166 - 2.63951 \times 10^{-2} S + 6.79461 \times 10^{-4} S^2 \\ & +5.47119 \times 10^{-5} S^3 - 1.55586 \times 10^{-6} S^4 \end{aligned} \tag{B-27}$$

The water viscosity at 1 atm then can be adjusted to pressure of interest:

$$\mu_w = \mu_{w1}(0.9994 + 4.0295 \times 10^{-5} p + 3.1062 \times 10^{-9} p^2) \qquad \text{(B-28)}$$

APPENDIX C

BEGGS AND BRILL CORRELATION

Beggs and Brill (1973) conducted two-phase flow experiments in inclined pipes. They proposed an empirical correlation where the basis laid on the flow regime identification if the pipe were horizontal. The liquid holdup for a particular pipe inclination was correlated to the holdup in horizontal pipe. Therefore, they introduced a correction function to take into account the effect of pipe inclination.

First, local liquid fraction must be calculated as follows:

$$\lambda_l = \frac{u_{sl}}{u_m} \tag{C-1}$$

where λ_l is the local liquid fraction, u_{sl} is the superficial liquid velocity, and u_m is the mixture velocity $(u_m = u_{sg} + u_{sl})$. Then dimensionless variables must be computed in order to predict the prevailing flow regime.

$$N_{FR} = \frac{u_m^2}{gD} \tag{C-2}$$

$$L_1 = 316\lambda_l^{0.302} \tag{C-3}$$

$$L_2 = 0.0009252\lambda_l^{-2.4684} \tag{C-4}$$

$$L_3 = 0.10\lambda_l^{-1.4516} \tag{C-5}$$

$$L_4 = 0.5\lambda_l^{-6.738} \tag{C-6}$$

The flow regime determination follows the criterions described in **Table C-1**.

Table C-1—Flow pattern determination of Beggs and Brill (1973).

Flow Pattern	Rules
Segregated	$\lambda_l < 0.01$ and $N_{FR} < L_1$ or $\lambda_l \geq 0.01$ and $N_{FR} < L_2$
Transition	$\lambda_l \geq 0.01$ and $L_2 < N_{FR} \leq L_3$
Intermittent	$0.01 \leq \lambda_l < 0.4$ and $L_3 < N_{FR} \leq L_1$ or $\lambda_l > 0.4$ and $L_3 < N_{FR} \leq L_4$
Distributed	$\lambda_l < 0.4$ and $N_{FR} \geq L_1$ or $\lambda_l \geq 0.4$ and $N_{FR} > L_4$

The liquid holdup is expressed as:

$$h_l = h_{l0}\psi \tag{C-7}$$

$$h_{l0} = \frac{a\lambda_l^b}{N_{FR}^c} \tag{C-8}$$

where h_{l0} is the liquid holdup for horizontal pipe. ψ is the correction accounting pipe inclination angle, given as

$$\psi = 1 + C[\sin(1.8\theta) - 0.333\sin^3(1.8\theta)] \tag{C-929}$$

$$C = (1-\lambda_l)\ln\left(d\lambda_l^e N_{vl}^f N_{FR}^g\right) \tag{C-10}$$

where coefficients $a, b, c, d, e, f,$ and g are given in **Table C-2**, depending on the underlying flow pattern.

Table C.2—Holdup constants of Beggs and Brill (1973).

Flow Pattern	a	b	c	d	e	f	g
Segregated	0.98	0.4846	0.0868	0.011	-3.768	3.539	-1.614
Intermittent	0.845	0.5351	0.0173	2.96	0.305	-0.4473	0.0978
Distributed	1.065	0.5824	0.0609	No correction, $C = 0,\ \psi = 1$			

If the flow regime is transition then the holdup is expressed as an interpolating function using the segregated and intermittent terms:

$$h_l = A y_{l(\text{segregated})} + B y_{l(\text{intermittent})} \tag{C-11}$$

Where

$$A = \frac{L_3 - N_{FR}}{L_3 - L_2} \tag{C-12}$$

And

$$B = 1 - A \tag{C-13}$$

Therefore, the pressure gradient due to potential energy change can be calculated as:

$$\left(\frac{dp}{dz}\right)_{PE} = g \times \left[\rho_l h_l + \rho_g (1 - h_l)\right] \tag{C-14}$$

The mixture density and viscosity are determined by weighing in the local phases fractions:

$$\rho_m = \rho_l \lambda_l + \rho_g \lambda_g \tag{C-15}$$

$$\mu_m = \mu_l \lambda_l + \mu_g \lambda_g \tag{C-16}$$

The two-phase friction factor is expressed as

$$f_{tp} = f_n e^S \tag{C-17}$$

Where

$$S = \begin{cases} \ln(2.2x - 1.2) & if \ \ 1 < x < 1.2 \\ \dfrac{\ln(x)}{-0.0523 + 3.182\ln(x) - 0.8725[\ln(x)]^2 + 0.01853[\ln(x)]^4} & \end{cases} \tag{C-18}$$

And

$$x = \frac{\lambda_l}{y_l^2} \tag{C-19}$$

The no-slip friction factor can be computed using explicit Chen equation involving Reynolds number as follows:

$$f_n = \frac{1}{-4\log\left[\frac{k_e/D}{3.7065} - \frac{5.0452}{N_{Re}}\log\left[\frac{(k_e/D)^{1.1098}}{2.8257} + \left(\frac{7.149}{N_{Re}}\right)^{0.8981}\right]\right]} \tag{C-20}$$

$$N_{Re} = \frac{\rho_m u_m D}{\mu_m} \tag{C-21}$$

and frictional pressure gradient can be evaluated as:

$$\left(\frac{dp}{dz}\right)_F = \frac{2\, f_{tp} \rho_m u_m^2}{D} \tag{C-22}$$

APPENDIX D

GRAY CORRELATION

Gray (1974) proposed an empirical correlation to calculate two-phase pressure drop in gas wells. The correlation was derived from gas well data sets consisting of 108 wells which were producing some liquids. In general, the correlation is suitable for vertical gas well with where the superficial gas velocity is below 15 m/s, tubing size is below 90 mm, and volumetric gas liquid ratio (GLR) is below 280 Sm^3/Sm^3. The flow is treated as single phase where the parameters considered are the phase velocity and properties, tube size, and gas liquid ratio.

First, local liquid fraction must be calculated as follows:

$$\lambda_l = \frac{u_{sl}}{u_m} \tag{D-1}$$

where λ_l is the local liquid fraction, u_{sl} is the superficial liquid velocity, and u_m is the mixture velocity $\left(u_m = u_{sg} + u_{sl}\right)$. The mixture density and viscosity are determined by weighing in the local phases fractions:

$$\rho_m = \rho_l \lambda_l + \rho_g \lambda_g \tag{D-2}$$

$$\mu_m = \mu_l \lambda_l + \mu_g \lambda_g \tag{D-3}$$

where ρ_m is the in-situ mixture density and μ_m is the in-situ mixture viscosity; ρ_g and ρ_l are gas and liquid densities, respectively; and μ_g and μ_l are gas and liquid viscosities, respectively.

Gray correlation uses three dimensionless parameters related to density differences, surface tension, and the ratio of the superficial liquid to gas velocities to calculate the holdup and hence the hydrostatic pressure drop. The three dimensionless variables are expressed as:

$$N_1 = \frac{\rho_m^2 \times u_m^4}{g \times \sigma \times (\rho_l - \rho_g)} \tag{D-4}$$

$$N_2 = \frac{g \times D^2(\rho_l - \rho_g)}{\sigma} \tag{D-5}$$

$$N_3 = 0.0184\left[1 - 0.0554 \times \ln\left(1 + \frac{730R_v}{R_v + 1}\right)\right] \tag{D-6}$$

where R_v is the ratio of superficial liquid to gas velocities (u_{sl}/u_{sg}). D is the tubing diameter, g is the gravitational constant, and σ is the two-phase interfacial tension.

The liquid holdup then can be calculated using the following expression:

$$h_l = 1 - (1 - \lambda_l)(1 - \mathrm{e}^{f_l}) \tag{D-7}$$

$$f_l = -2.314\left(N_1\left(\frac{205}{N_2} + 1\right)\right)^{N_3} \tag{D-8}$$

where f_l is a holdup correction factor. Therefore, the pressure gradient due to gravitation can be calculated as:

$$\left(\frac{dp}{dz}\right)_{PE} = g \times \left[\rho_l h_l + \rho_g(1 - h_l)\right] \tag{D-9}$$

Pressure loss due to friction is expressed as a change in the effective pipe wall roughness dependent on the liquid to gas ratio.

$$k_e = \begin{cases} \dfrac{0.852 \times \sigma}{\rho_m u_m^2} & if \;\; R_V > 0.7 \\ k + R_V \left(\dfrac{\dfrac{12.92738 \times \sigma}{\rho_m u_m^2} - k}{0.007} \right) & if \;\; R_V < 0.7 \end{cases} \tag{D-10}$$

where k is the absolute pipe roughness. The Reynolds number is used to determine friction factor:

$$N_{Re} = \frac{\rho_m u_m D}{\mu_m} \tag{D-11}$$

The friction factor then can be computed using explicit Chen equation as follows:

$$f_f = \frac{1}{-4 \log\left[\frac{k_e/D}{3.7065} - \frac{5.0452}{N_{Re}} \log\left[\frac{(k_e/D)^{1.1098}}{2.8257} + \left(\frac{7.149}{N_{Re}}\right)^{0.8981}\right]\right]} \tag{D-12}$$

and frictional pressure gradient can be evaluated as:

$$\left(\frac{dp}{dz}\right)_F = \frac{2\, f_f \rho_m u_m^2}{D} \tag{D-13}$$